Delft University of Technology

Structural response of a composite material upon a wave impact

Giovanni Trabace

TU Delft Delft University of Technology

MARIN

Structural response of a composite material upon a wave impact

by

Giovanni Trabace

to obtain the degree of Master of Science
at the Delft University of Technology,
to be defended publicly on Thursday January 30, 2020 at 09:00.

Student number:	4751248	
Thesis committee:	Prof. Dr. ir. M.L. Kaminski,	TU Delft
	ir. R.W. Bos,	TU Delft
	Dr. ir. H. Bogaert,	MARIN
	Dr. ir. B. Hofland,	TU Delft
	Dr. C.L. Walters,	TU Delft

Abstract

This master thesis shows a study of the waves propagation phenomena inside a layered structure such as the MarkIII cargo containment system (CCS), widely used for the transport of the liquefied natural gas overseas. As a consequence of the wave impacts that take place inside the LNG tanks, strain waves start propagating, reflecting and transmitting at the interfaces which compose the layered structure. The aim of the thesis is to better understand how the propagation of strain waves inside a material resolves the discontinuity between liquid and structure at the moment of the impact, and how the theory of strain waves propagation can be applied to a theoretical model in order to define the deformation of the structure.

Acknowledgement

The thesis presented in this document could not have been performed without the support of many people. First of all, I would like to thank my supervisor at the Marine Research Institute Netherlands (MARIN) Hannes Bogaert for the numerous discussions, advises and insights given to me during these nine months, for treating me with respect, providing me all possible support and help I needed, giving to me the chance to expand my knowledge, and encouraging me to accomplish and improve my results. I would like to thank Joris van den Berg for helping me and correcting some mathematical aspects of the thesis during my internship at MARIN. I would also like to thank Prof. Mirek Kaminski and my supervisor of TU Delft Reinier Bos because they have always been available to help me, and open to the discussions, and for giving to me the chance to extend my academic knowledge.

I would also like to thank my old sister and my old brother for the advises received and because they have been two examples for me, my international friends for making me feel home, my Italian friends for always being on my side although the distance, TU Delft University for welcoming me when I arrived in the Netherlands, and MARIN for the kindness and help received during my nine months of internship.

Finally, I would like to express my deep gratitude to my parents who understood from the first instant how much important education was for me, and for supporting me in every single choice, every single day.

Contents

Chapter 1

Introduction

Ships and offshore structures are continuously subjected to waves and harsh environmental conditions in open sea and in the oceans causing the occurrence of many severe wave impacts against a ship structure or the decks of a floating platform. Waves can be assumed as pressure forces acting on the exposed surfaces. In order to design a safe structure and to guarantee the longest lifetime possible, standard regulations and international requirements must be respected. It might be advantageous to analyse metocean data, namely a collection of data and information including uncertainty about weather conditions, that can be useful to predict the environmental phenomena, and therefore, the external loads that can act on the structure. In addition, it is important to investigate on the behaviour of the structure immediately after an impact takes place, in order to understand how the external loads are relevant for the integrity of the structure.

There are several situations that relate a wave impact to the structure, and not all of them concern ocean waves and the external environment; an example is represented by the LNG carriers which are tank ships employed in the transportation of liquefied natural gas (LNG). The use of LNG carriers is rapidly growing as it represents an alternative way to transport natural gas through pipelines. The LNG is a natural gas which has been cooled down to around $-162°C$, and therefore, condensed into a liquid that has a volume 600 times smaller. This allows to transfer it overseas through LNG carriers. These ships are equipped with cargo containment systems (CCSs) that minimize the heat transfer limiting the LNG evaporation, and maximize the cargo capacity. When a tank is partially filled surface waves take place inside it and impact its walls (sloshing impact). Below, it is shown the sloshing inside the dock of an amphibious warfare ship of the Royal Netherlands Navy.

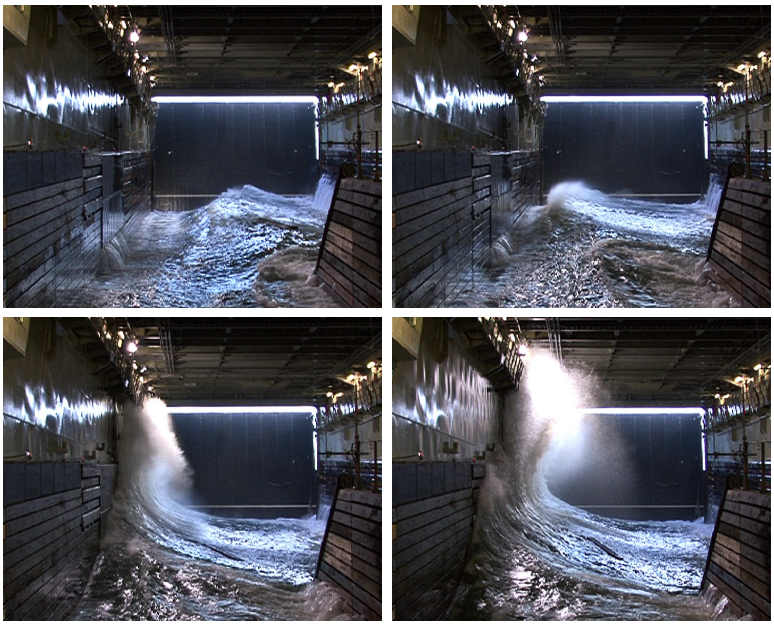

Figure 1.1: Sloshing inside the dock of an amphibious warfare ship of the Royal Netherlands Navy during trials conducted by MARIN. [1]

This thesis is part of the SLING research project. The aim of the SLING is to improve the experimental basis of the sloshing tests and the corresponding approach to scale the measured pressures. Sloshing model tests are used to define the design loads for LNG tanks. The SLING project disentangles the physics involved in the sloshing impacts in the LNG tanks. It focuses on the multiphase dynamics, the variability of the impact loads, and the structural response through several experiments, numerical simulations and theoretical models. The thesis investigates the first instant of a wave impact process, namely when the first contact between liquid and structure takes place. Specifically, it analyses the physical phenomena that develop inside the structure immediately after the first contact between wave and wall, and provides a simplified layered model linked to the physics of the waves propagation in the structure. The aim of the simplified model is to be used in the liquid impact simulator that is under development in the SLING research project. The liquid impact simulator is a collection of theoretical models to describe the impact of a wave and the corresponding structural response. It will be used to evaluate the effects of the inappropriate scaled properties of liquid and gas in sloshing model tests on the multiphase dynamics involved in the sloshing impacts and on the variability of the impact loads. The effects are quantified in terms of structural response.

1.1 Research Questions

In the field of wave impacts against a structure, it is important to focus on different types of phenomena that take place during the process. Let consider a wave approaching a structure (composite structure) shown in Figure 1.2.

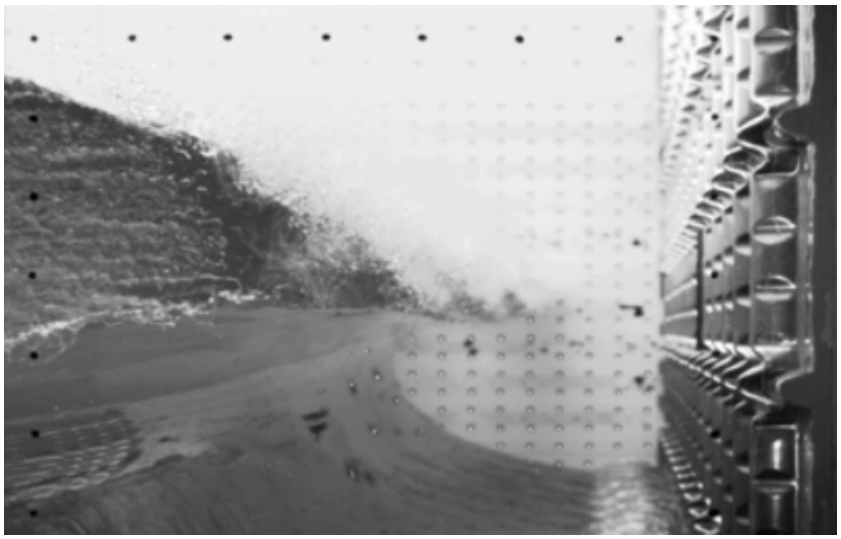

Figure 1.2: Wave approaching the structure. [1]

At first, as the wave gets close to the wall, there is a [**1**] transfer of liquid momentum to gas momentum; the escaping gas shears the free surface causing the [**2**] development of free-surface instabilities which are considered the main source of variability of the local pressures; the gas between liquid and structure is compressed because it cannot [**3**] escape quickly enough and because it is [**4**] entrapped; a [**5**] phase transition is involved because LNG is in thermo-dynamical equilibrium with its vapour, and the compression of vapour induces condensation, therefore expansion leads to evaporation; consequently, there is a [**6**] change in the liquid momentum because the liquid is forced to sharply turn in front of the wall; then, the [**7**] liquid is compressed as it hits the wall; immediately after the impact, there is the propagation of a pressure wave from the contact point in the liquid at the speed of sound; at the moment of the contact, the structure is involved. The wall is covered with a containment system that is composed of several materials; its flexibility influences the loads, and the energy content of the load is distributed through the structure [**8**]. The following list summarises the process of the wave impact:

1 Transfer of liquid momentum to gas momentum

2 Development of free surface instabilities

3 Compression of escaping gas

4 Compression of entrapped gas

5 Phase transition

6 Change of liquid momentum

7 Compression of liquid

8 Propagation of time-space distributed loads through composite structure

As mentioned, at the moment of the first contact between liquid and structure, there is the [$*$] propagation of a pressure wave from the contact point through the liquid, but also the [$**$] *propagation of a strain wave* from the contact point through the structure. Both pressure wave and strain wave have the purpose to decrease the discontinuity between liquid and structure at the moment of the direct impact; the propagation of pressure wave is part of [**7**] whereas the propagation of strain wave in the material is part of [**8**] because it affects the layered structure.

Figure 1.3 shows locally the exact moment of impact when [$*$] and [$**$] occur, namely when pressure wave in the liquid and strain wave in the structure start propagating.

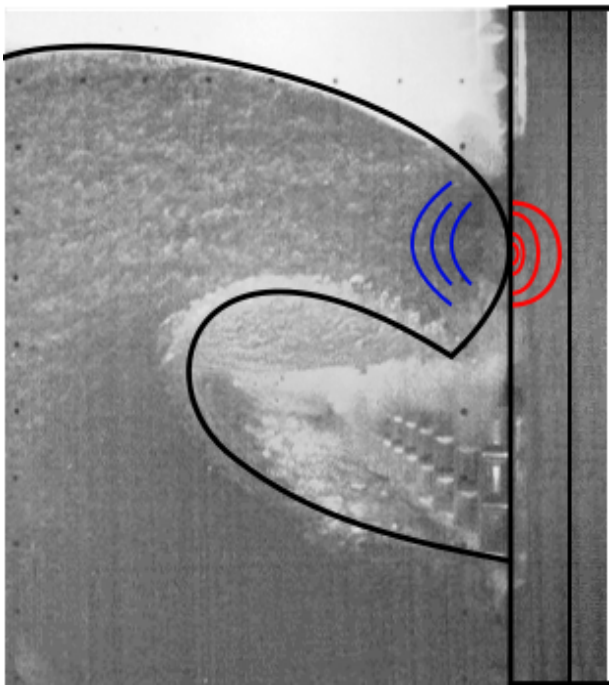

Figure 1.3: Development of pressure wave (blue) in the liquid and strain wave (red) in the structure.

The aim of the thesis is to better understand how the propagation of strain waves through the structure resolves the discontinuity between liquid and structure; for this reason, the first research question is defined:

Q1. How do strain waves propagate through the structure upon a liquid impact?

In order to provide a theoretical model that matches with the physical description of the strain waves, the second research question is defined:

Q2. How can the theory of the strain waves propagation be applied to a theoretical model?

An appropriate answer to the research questions **Q1.** and **Q2.** is a physical description of the strain waves propagation inside a layered material, and a simplified

theoretical model that can provide the deformation of the layered material in terms of these waves.

1.2 Research Approach

The research approach used for this project concerned four important parts that represent the structure of the project:

- Layered Structure Part
- Hydrodynamic Part
- Waves Propagation Part
- Theoretical Model Part

The layered structure part concerns the material used for the physical and mathematical investigation; the hydrodynamic part is related to the external process, namely the physical phenomena that take place in the liquid; the waves propagation part concerns the internal process, that is to say, the analysis of the wave propagation phenomena inside the layered structure; the last part concerns a simplified theoretical model used to get the deformations. From the beginning it was believed that a well understanding of the physics behind the problem could help to describe and to build a suitable theoretical layered model. Figure 1.4 shows the initial problem from which the entire project was developed; at the beginning no model was chosen, neither general information about propagating waves into a material was known nor an external force was defined.

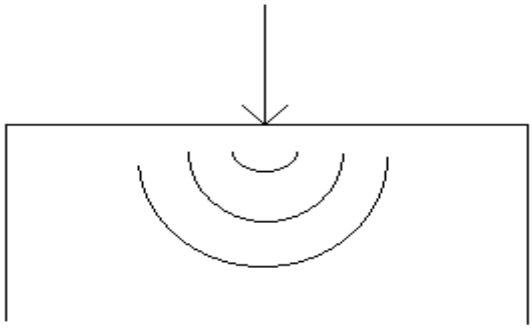

Figure 1.4: Initial problem.

The first step of this project was to study the external process, in particular what happened to the liquid before the contact with the structure. Consequently, attention was focused on the theory of the wave motion inside elastic solids, analysing different types of waves such as plane waves, spherical waves, surface waves (Rayleigh

and Love waves). From the beginning it was believed that each type of wave could be associated to a potential which has a particular mathematical expression according to the type of wave. Defining the expression of the potentials meant to find both deformations and stresses in the material because both of them depend on the first and second derivatives of the potentials. The study of the hydrodynamic part made clear that the external load changed in both space and time (the spreading of the wave crest along the wall surface increased the contact area over time). The waves developed in the structure immediately after the first impact were assumed spherical, which means the disturbance propagated radially from the source located on the free surface. The MarkIII CCS was selected in its original configuration; after studying the mechanism of wave propagation phenomena (which means the generation of reflected and transmitted waves at the interfaces) in a material composed by few layers, the first simplifications to the original model were made; they had the purpose to decrease the number of interfaces and consequently, the number of layers. The waves propagation and the theoretical model parts were build gradually and at the same time, that is to say, whenever a new element was added to the physics, then it was applied to the theoretical model. It led to difficult equations involving both compression and distortion potentials for spherical waves. In addition, it was understood that each change in the external load caused new wave propagation phenomena inside the structure. Due to the complexity of the entire problem, it was decided to simplify it by considering a 1D-problem.

In the 1D-problem only the generation and propagation of compression plane waves were considered. The reason of starting from a 3D-case with both compression and distortion spherical waves propagating in many layers concerned the aim of describing the theoretical model in terms of physics; in other words, physics and maths of the theoretical model had to match each other.

Figure 1.5 shows the exact moment when a wave crest impacts against the structure. As can be seen, the hydrodynamics concerns the external process, in particular all physical phenomena that take place inside the liquid before the impact, at the moment of the impact and also after the direct impact of the wave crest; it can be considered the starting point and the reason why the internal process takes place. The internal process is related to the wave propagation phenomena that occur in the layers composing the model; the last two parts are related to the generation and propagation of waves inside, and both of them are affected by the hydrodynamics. Figure 1.6 shows a schematic representation of the approach. Notice that changes of the model were made based on the waves propagation part and on the theoretical model part. As it will be seen, the interaction between hydrodynamics and waves propagation parts (in red) will be related to the generation of different waves inside the layered material due to the changes of the external force, whereas the interaction between hydrodynamics and theoretical model parts (in blue) concerns the presence of the external force in the mathematical equations.

Notice that Figure 1.5 shows the exact moment of the impact of the wave crest against a wall for a particular type of impact, the gas pocket impact [1].

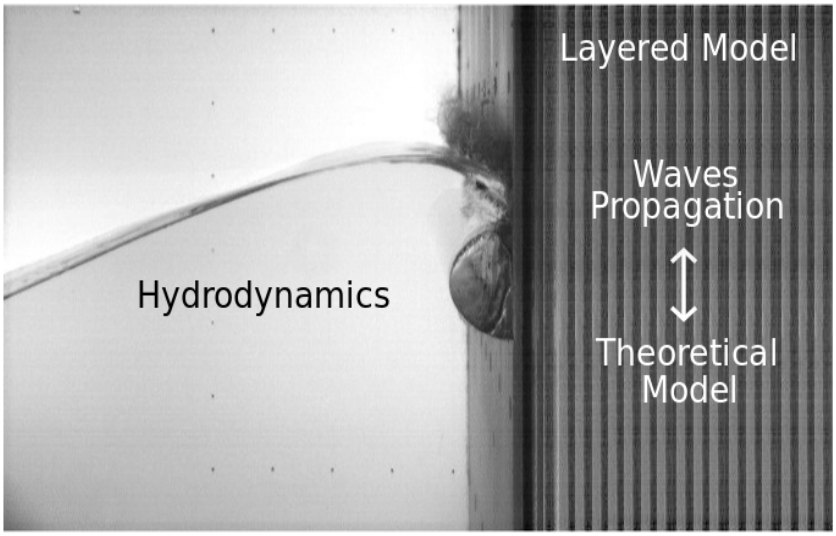

Figure 1.5: Research approach for the process of the wave impact against a structure.

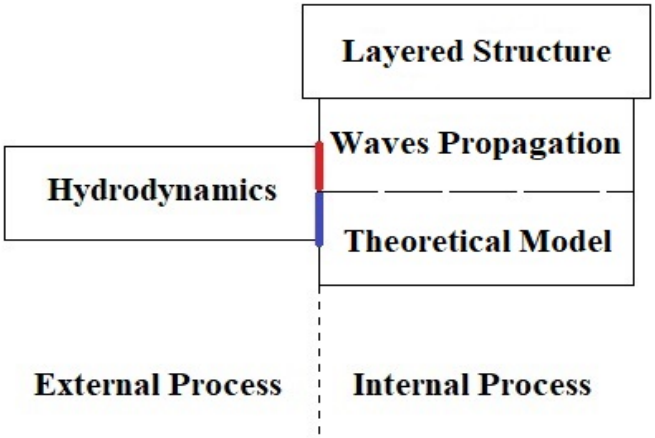

Figure 1.6: Schematic representation of the research approach.

1.3 Outline of the Thesis

The overall structure of the thesis takes the form of six chapters. This current chapter is the introduction to the project and has the purpose to give an initial idea of the topic; in addition, it shows the reason, the research questions, and the research approach of the project. Chapter 2 presents the original and the simplified structure and introduces some theoretical concepts. Chapter 3 first describes the wave impacts, then analyses how the changes in the liquid affect the structure, finally defines the external force acting on the free surface. Chapter 4 represents the physics of the problem: at first the concept of waves propagation inside a material is introduced, then compression and distortion waves are distinguished; it follows the analysis of the wave propagation phenomena inside the simplified model, and consequently different models are presented in order to involve all waves propagation

phenomena that occur inside; finally the concepts of wave shape and potentials are discussed. Chapter 5 first explains the method used and, then presents a specific case, the three-layered model; consequently, a more generalized case, a n-layered model, is formulated. Finally, Chapter 6 presents the conclusions and provides some recommendations for future works.

Chapter 2

Layered Structure

2.1 Introduction

The purpose of this chapter is to introduce the structure that will be used for this thesis. Due to the complexity of the problem, some simplifications will be done in order to make easier the evaluation of some aspects of this thesis, such as the global wave propagation phenomena which will be analysed in Chapter 4. Section 2.2 will introduce the real structure, whereas Section 2.3 will show the same structure with some simplifications. The concepts of *loading area*, *out-of-loading area*, *source* and *spreading area* will be introduced in Section 2.4.

2.2 MarkIII CCS

The structure chosen for this project is the MarkIII CCS (Cargo Containment System). Since the goal of this thesis is to define the deformation of a layered structure, this type of model can be suitable for this project. The MarkIII (Figure 2.1) is one of the most common membrane-type LNG insulation employed for the LNG carriers. Membrane CCSs are widely used for large seagoing LNG carriers because the hull space is utilized most efficiently, therefore the cargo capacity is maximized, and the heat transfer is minimized.

As can be seen in Figure 2.2, there are two levels: a primary level composed by a top plywood and a primary RPUF (Reinforced Poly-Urethane Foam), and a secondary level composed by a Rigid Secondary Barrier foil (RSB), a secondary RPUF and a back plywood; all components can be clearly seen in Figure 2.3. All layers are bounded together in workshop with PU glue.

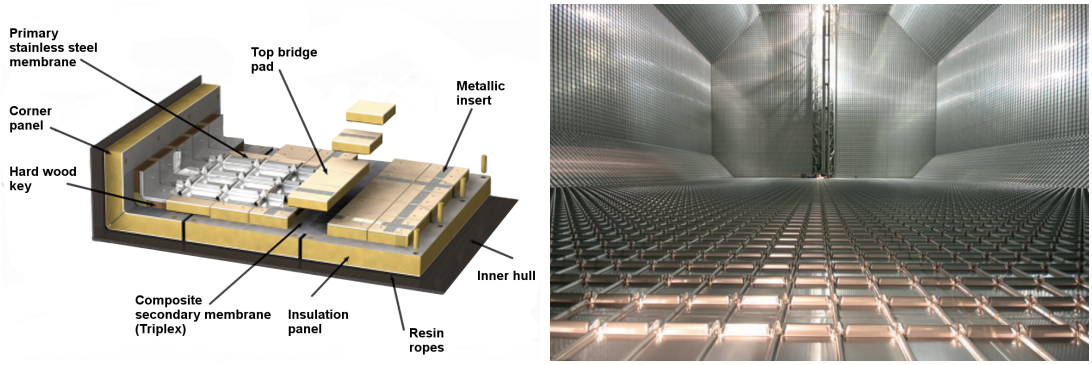

Figure 2.1: Membrane CCS. Courtesy GGT and Lloyds Register. [1]

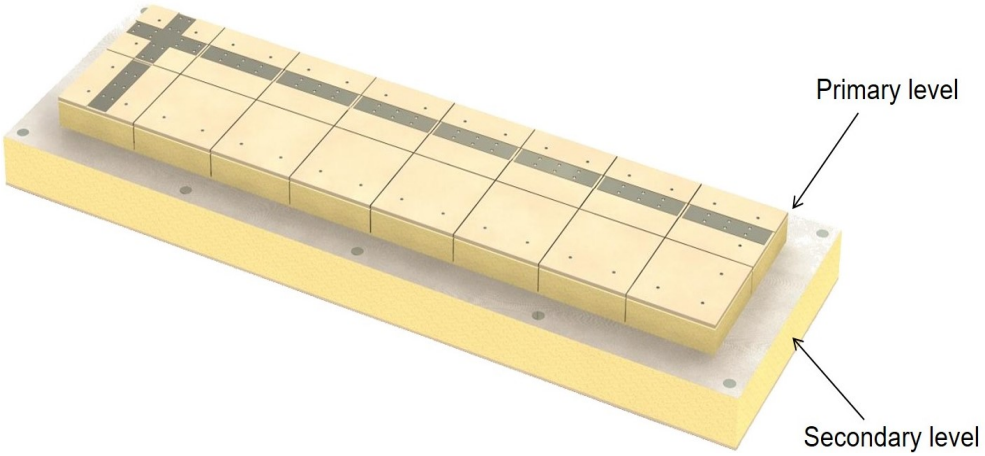

Figure 2.2: Primary level and secondary level of the MarkIII. [2]

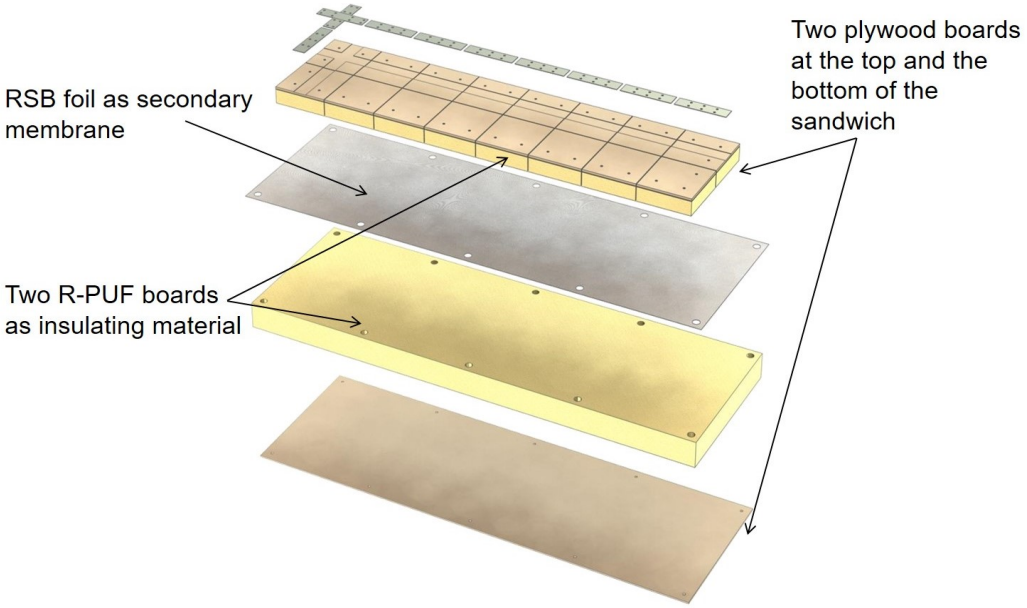

Figure 2.3: Components of the MarkIII. [2]

Figure 2.4 shows a portion of the cross section of the MarkIII; it is possible to see that the RSB (3), the secondary RPUF (4) and the back plywood (5) are continuous and longer than the primary RPUF (2) and the top plywood (1) which are discontinuous and they are approximately 940 mm long each, and repeat eight times over a typical panel as can be seen in Figures 2.2 and 2.3. Notice that there are resin ropes (6) which connect the structure to the steel plate (inner hull) (7).

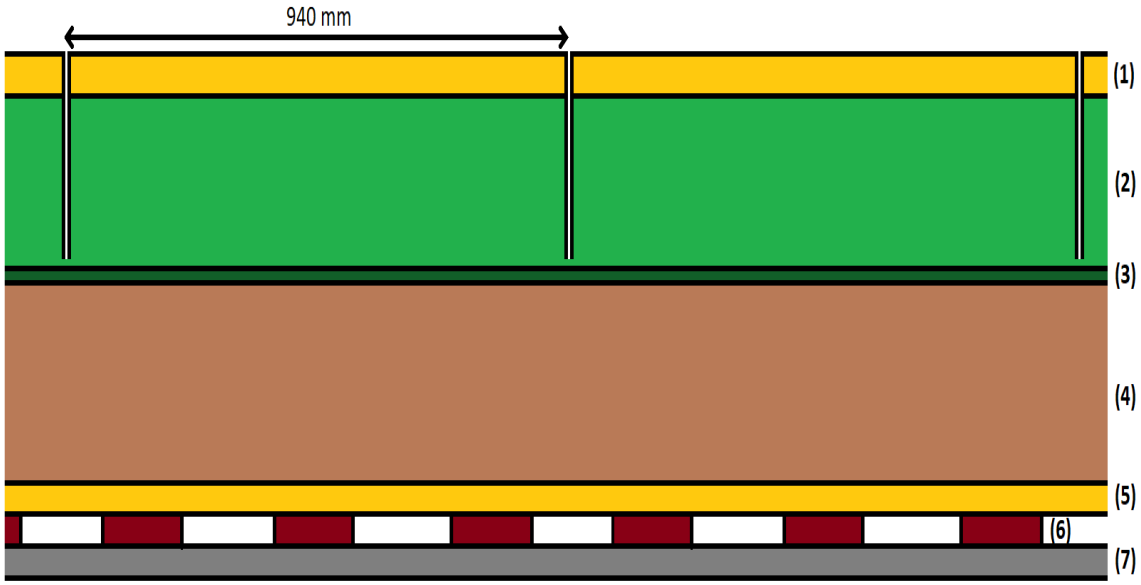

Figure 2.4: Portion of the cross section of the MarkIII.

2.3 Simplified MarkIII CCS

The first simplification to the structure shown in Figure 2.4 is to consider the horizontal length of the RSB, secondary RPUF and back plywood the same as the length of the top plywood and the primary RPUF (**S0**):

S0. All layers which compose the MarkIII structure have the same horizontal length.

Based on Figure 2.5 it is possible to apply more additional simplifications.

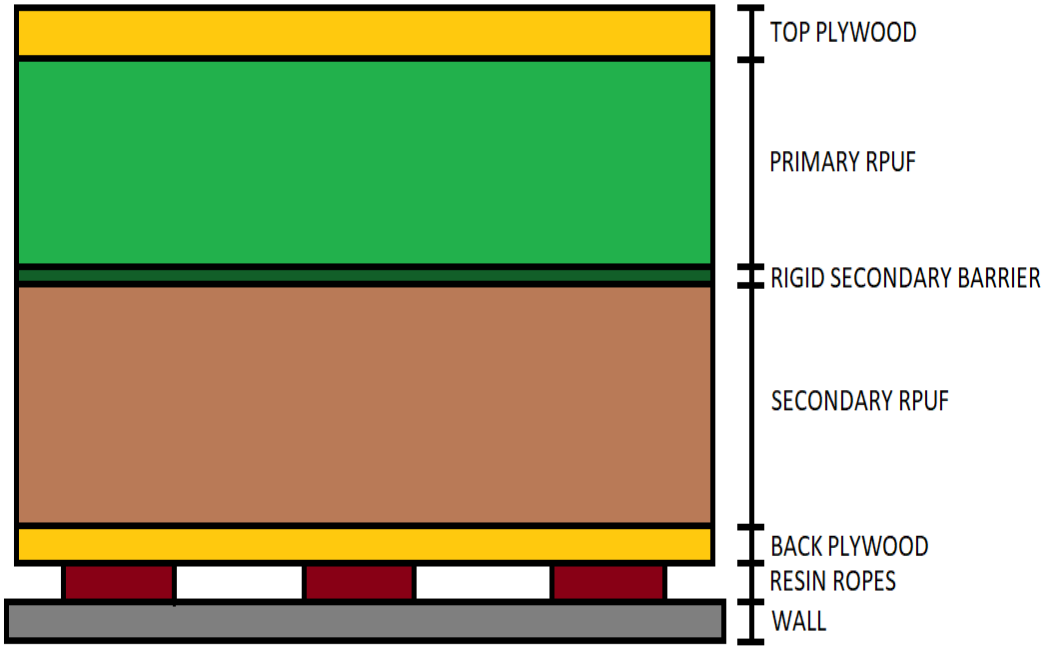

Figure 2.5: MarkIII CCS structure considered (with simplification **S0**).

In the simplified structure, only four layers are considered: top plywood (L1), primary RPUF (L2), secondary RPUF (L3), and back plywood (L4). It is assumed that they are in contact each other. Comparing the simplified model with the real model, three additional simplifications are made:

S1. The thickness of the Rigid Secondary Barrier (RSB) is neglected, and no wave is assumed to travel inside.

S2. The resin ropes are removed; it is assumed the direct contact between the back plywood and the wall.

S3. It is assumed that the top plywood and the back plywood have the same thickness.

S1 is made in order to decrease the number of layers of the model and simplify the wave propagation phenomena for the entire structure; the RSB represents an interface that divides the primary RPUF and the secondary RPUF, and it is supposed the RSB is subjected to bending. **S2** is also made in order to simplify the wave propagation phenomena and avoid the presence of the resin rope corners (points in blue, Figure 2.6). Furthermore, **S3** assumes that the first and the fourth layer have the same thickness. In the real model, the top plywood has a thickness of 12 mm, whereas the back plywood has a thickness of 9 mm. Since the difference is very small, it is possible to assume the same value of 12 mm for both layers.

To better understand simplification **S2**, it is possible to see Figure 2.6. The blue points are located in the bottom plywood (L4) close to the corners of the resin rope. In terms of stresses, there is a combination of vertical traction/compression,

bending, shear in this zone, and an equivalent stress called *Von Mises stress* is used for the analysis at these locations. In terms of propagation phenomena, it is not well known how the incident waves reflect and propagate at the corners. At these locations, it is believed that the incident waves are subjected to some deviations at the moment of reflection. Due to the complexity of the phenomena, the resin ropes are removed.

Notice that simplification **S3** has been added after evaluating the global wave propagation phenomena for the entire structure (analysed in Chapter 4). It will be possible to consider the same reflection and transmission phenomena for L1 and L4 because of the same material characteristics and the same thickness. By considering the same thickness for L1 and L4, it is possible to assume the same propagation-times ($t_{\alpha_1} = t_{\alpha_4}, t_{\beta_1} = t_{\beta_4}$).

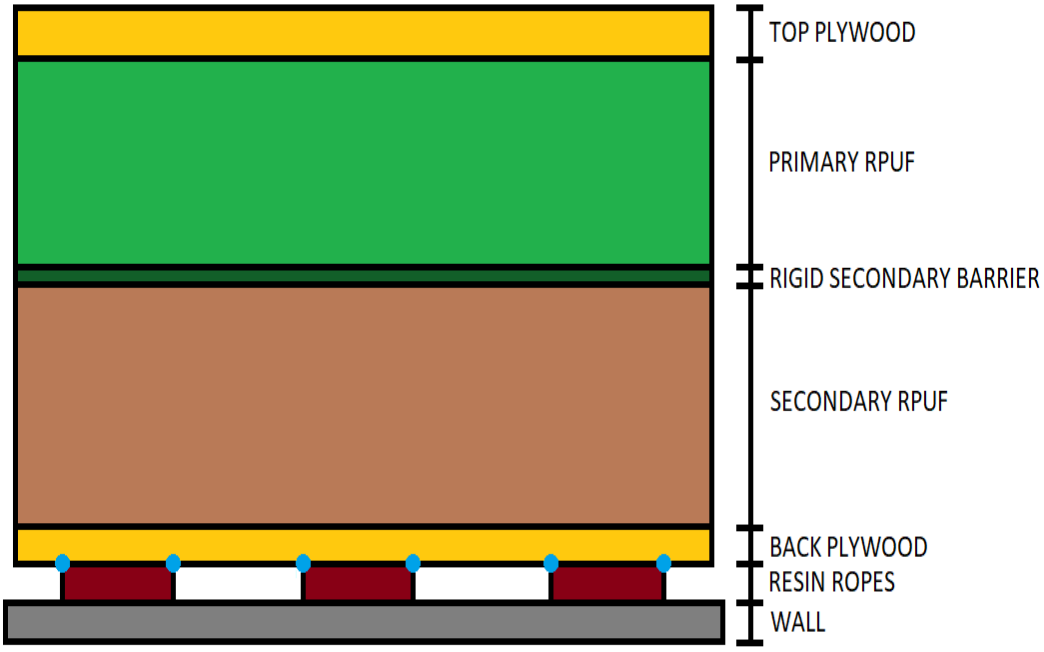

Figure 2.6: MarkIII CCS with blue points located in the bottom plywood close to the resin rope corners.

Figure 2.7 shows the MarkIII CCS with simplifications.

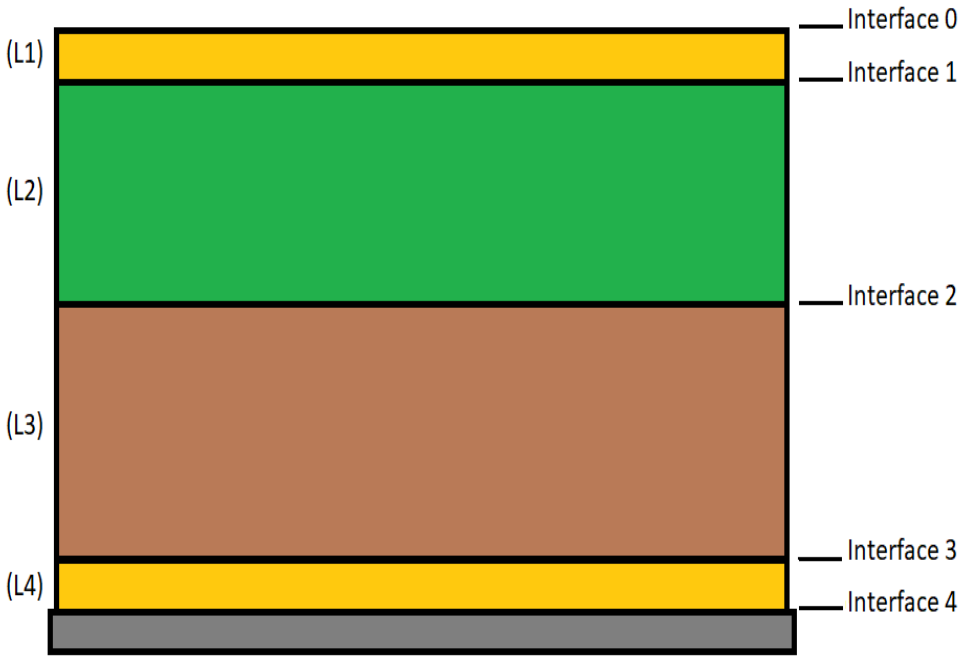

Figure 2.7: MarkIII CCS structure (with simplifications)

As can be seen, there are four layers and five interfaces where the wave propagation phenomena will take place. Notice that interface 0 is a free boundary, whereas interface 4 connects the back plywood to the wall.

The following table shows the material characteristics and the dimensions of each layer of the simplified model that will be used for computing the wave propagation velocities. Notice that L1 and L4 have the same material characteristics and same dimensions (**S3**), whereas L2 and L3 have same material characteristics but thickness. In addition, H represents the thickness, namely the vertical distance, whereas L represents the length of the layers. Thermal effects and viscosity effects are not considered.

Layers	ρ	ν	E	H	L
	kg/m^3	-	MPa	m	m
Top plywood	710	0.17	8900	0.012	0.340
Primary RPUF	120	0.18	84	0.089	0.340
Secondary RPUF	120	0.18	84	0.160	0.340
Back plywood	710	0.17	8900	0.012	0.340

Table 2.1: Material characteristics and dimensions [3]

2.4 Additional Concepts

It is important to define some additional concepts related to the simplified model that will be used in the next chapters. It is relevant to distinguish between *loading area* and *out-of-loading area*, give the definitions of *source* and *spreading area*. Notice that in this chapter, the spreading area will be analysed only qualitatively.

The *loading area*, also called *impact area*, is defined as the region of the model that is directly affected by the external impact; in other words, it is the area of the structure where waves propagate immediately after the contact between an external load and the surface of the structure. It is assumed the loading area is located at the center of the structure as can be seen in Figure 2.8 (identified by the dark blue area).

The *out-of-loading areas*, also called *out-of-impact areas*, represent all the surrounding regions of the loading area which will feel the effect of the external impact after a certain amount of time. Notice that this distinction between loading area and out-of-loading area is based on the concept of wave propagation; it takes some time before that the regions located far from the impact point feel the effects of the disturbance. Waves will propagate inside the material, from the source to the surrounding regions, during this amount of time. The out-of-impact areas are represented by the light blue regions surrounding the loading area in Figure 2.8.

The *source* is the origin from which the disturbance starts propagating radially. Theoretically, it is assumed that the external load acts at the centre of the model. In Figure 2.8, the source is represented by the red point located at the centre of the impact area and on the free surface of the top plywood (L1).

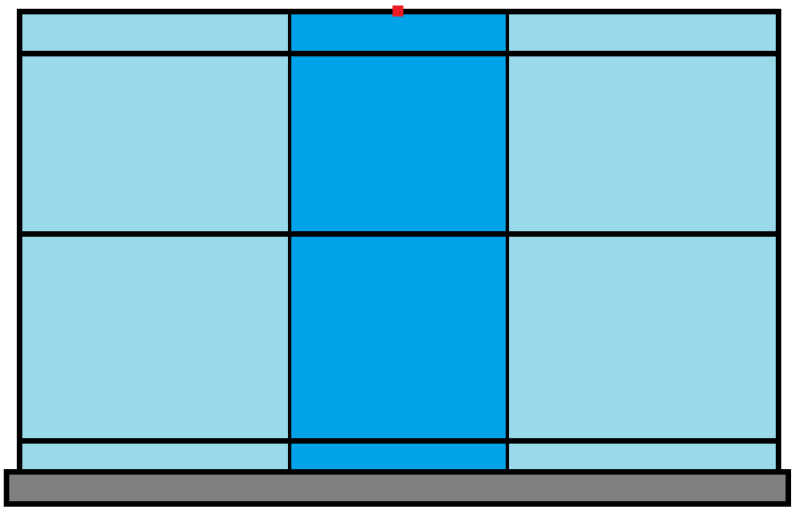

Figure 2.8: Loading area (dark blue), out-of-loading area (light blue), source (red point)

Furthermore, another important difference between loading area and out-of-loading area is the type of waves that propagate inside. Spherical waves will develop and

travel inside the loading area as consequence of the direct impact, whereas longitudinal (sinusoidal) waves will propagate in the out-of-loading area.

2.4.1 Spreading Area

It is relevant to add the concept of *spreading area*. Before explaining what the spreading area means, let consider a co-ordinate system (O, r, z), with the origin at the centre of the impact area, coincident with the source; it is possible to assume that the (semi)-horizontal dimension of the spreading area r can reach a maximum length of R. When $r > R$ the disturbance is not in the spreading area anymore but it continues to propagate through the out-of-impact areas. Then, in that case, the disturbance will not propagate in terms of strain waves but in terms of longitudinal waves.

The expression *spreading area* identifies the region inside the structure where the wave propagation phenomena take place, namely where the strain waves travel, and are reflected and transmitted at the interfaces; in other words, it is the area where the disturbance spreads out. It might seem that the concepts of *loading area* and *spreading area* coincide, but the main difference is the time-dependence that characterizes the spreading area. As can be seen in Figure 2.9, the spreading area, identified in green, changes with time t. When the external force is a point load (Figure 2.9), then the spreading area increases in both horizontal and vertical directions, that is to say, both of them are a function of time t. If the wave fronts are assumed perfectly spherical, then the rate of change (the increase) in both horizontal and vertical directions is the same: $r(t) = h(t)$ because the spreading is radial. If it is assumed that the vertical dimension of the region where strain waves propagate is larger than the horizontal one, the increase of the spreading area occurs only in the vertical dimension (when $r(t) > R$). When the first wave reaches the last interface (I4) at $t = t_{f'}$, then the spreading area will coincide with the loading area.

The increase of the spreading area, will depend on the propagation velocities of the waves that are generated and travel through the material. The spreading area can be defined as follows:

$$S(t) = \begin{cases} 2r(t) \cdot h(t), & if \quad 0 < h(t) < h_4 \ \ and \ \ 0 < r(t) < R \\ 2r \cdot h(t), & if \quad 0 < h(t) < h_4 \ \ and \ \ r(t) > R \end{cases} \tag{2.1}$$

where h_4 is the vertical distance of the last interface (I4) from the origin located on the free surface.

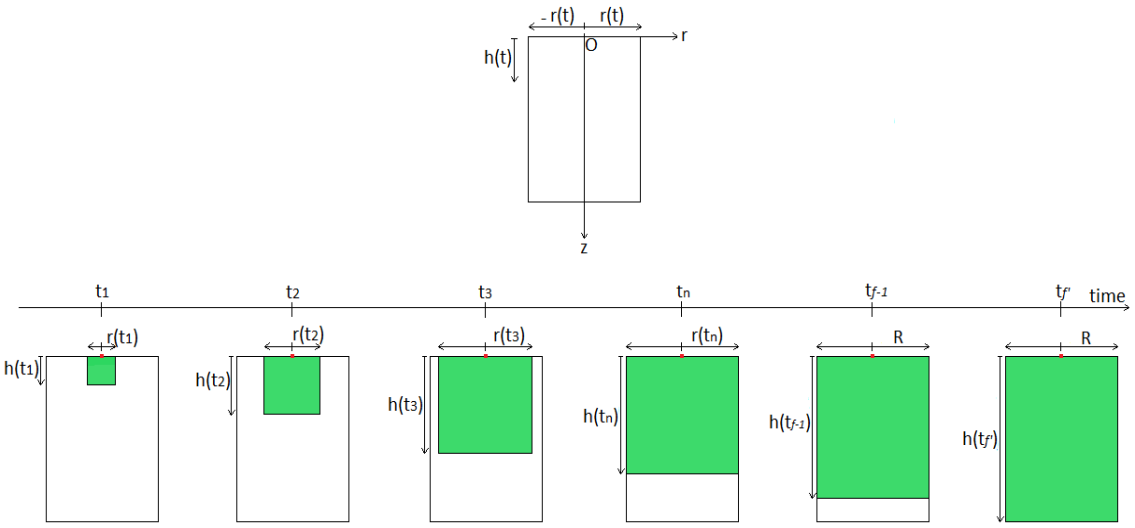

Figure 2.9: Qualitative change of the spreading area (in green) after an external load (red point) impinges on the surface.

Notice that Figure 2.9 describes qualitatively the change of the spreading area over time. The concept of spreading area will be analysed again in Chapter 4.

2.5 Conclusions

The purpose of this chapter was to introduce the layered structure which will be used in the next chapters. Since this thesis is part of the SLING research project that focuses on the sloshing impacts in the LNG tanks, the markIII CCS was selected in its original configuration (Figure 2.4). After studying the wave propagation phenomena that take place at the interface between two media the following simplifications were made:

S0. All layers which compose the MarkIII structure have the same horizontal length.

S1. The thickness of the Rigid Secondary Barrier (RSB) is neglected, and no wave is assumed to travel inside.

S2. The resin ropes are removed; it is assumed the direct contact between the back plywood and the wall.

S3. It is assumed that the top plywood and the back plywood have the same thickness.

Based on layered structure shown in Figure 2.7 the concepts of source, impact area, out-of-impact area and spreading area were defined.

Chapter 3

Hydrodynamics

3.1 Introduction

The term *impact* is very often related to the concept of *abruptness*, and since it involves a lot of processes and everyday life events such as automobile accidents, game of billiard, but also molecular collision, tidal waves, ocean waves or air blast against a structure, the word *impact* is related with a numerous range of different fields as psychology, meteorology, physics and especially engineering.

From a physical point of view, an *impact* can be defined as the process involved in the collision of two or more objects. The collision can also occur between two bodies of different 'nature' such as a liquid mass and a structure. The reaction to the collision between liquid and structure (structural response) is more complicated than that between two solid bodies, and the behaviour to this new abrupt event which changes the current state of equilibrium of the structure will differ. During the impact process between two objects, some forces will be created at the beginning of the collision, and consequently they will be removed as soon as the contact ceases to exist. During the direct impact between two objects, the energy transfer processes are also involved, and part of the energy is also dissipated from the system.

Although the contact force disappears after the separation of the two objects interested in the phenomenon, the impact force continues to exist as waves that propagate inside the material.

This thesis is mainly based on the structural part, but some analysis about the wave impact needs to be done. This chapter represents the hydrodynamic part of the problem and its purpose is to understand how the external phenomena affect the internal process, and to provide an external force that can be responsible of the wave propagation phenomena inside the material immediately after the impact. In other words, the hydrodynamic part can be considered as the starting point of this project. This chapter starts with Section 3.2 where the Elementary Loading Processes (ELPs) are introduced; Section 3.2.2 summarises the main types of wave impacts against a wall; particular attention is given to the gas pocket impact and the regions inside the structure that are affected by the impact liquid and the entrapped

gas. A distinction between pressure waves and strain waves in the liquid and in the structure, respectively, is also presented; Section 3.3 formulates the external force that hits the structure.

3.2 Wave Impacts

The case of an impact wave against a structure is different and more complicated than the impact phenomena that generally occur between two (solid) bodies of the same 'nature'. The main issue of the wave impact problems is the variation of the contact area with respect to the time and the behaviour of the liquid before, after, and at the moment of the collision with another object. Since a liquid mass is not a rigid body but a fluid which is free to move, it is going to spread out along the exposed surface of the structure. Generally, in the other types of impacts, with some exceptions, the loading area remains the same during the process or in the worst scenario, it can increase or decrease, but the change of the contact area is predictable. In the wave impacts, there are not only additional portions of water which hit the structure, but also, as will be seen, a gas pocket which acts as a load, entrapped between liquid and structure, and some instabilities in the fluid that need to be taken into account.

Therefore, in the case of a wave impact there are loads of different *nature*, and an unpredictable change in space and time of the external force.

3.2.1 Elementary Loading Processes

The impact loads against a structure, as for instance a wall, are caused by three processes called *Elementary Loading Processes*, also identified as ELPs which are the basic elements of the impact loads:

ELP1. Direct impact

ELP2. Building jet

ELP3. Compression of escaping or entrapping gas.

ELP1 concerns the abrupt stop of the liquid when it directly impacts the structure. It is related to the compression of the liquid. **ELP2** concerns the sharp turn of the liquid when it is forced along the structure, thus building up a jet, and therefore, it is related to the change of the liquid momentum. **ELP3** concerns the compression of the gas when it is escaping or is entrapped. Each ELP has its own pressure signature and their combination provides the pressure map defined as the time-space distribution of the impact loads.

The load induced by the ELP1 depends on the impact velocity, the extension of the impact area, the shape of liquid around the impact area, the density and compressibility of liquid, whereas the load induced by ELP2 depends on the velocity component of the liquid normal to the structure and the angle between the liquid

surface and the structure. In the case of ELP3, the induced load depends on the speed of sound of the gas, and, therefore, compressibility and density of the gas. [1] The pressure maps which are the time-space distributions of the impact loads, can be considered as the combination of all ELPs or just the result of one ELP. In Section 3.2.3 a particular type of wave impact will be analysed and it will be shown the combination of all elementary loading processes.

3.2.2 Types of Wave Impacts

In the analysis of the waves that impact against a structure, it is possible to distinguish between four types of wave impacts acting on a flat wall. In this section, the same distinction done in [1] is taken into account: the wave impacts differ each other according to the location of the focal point with respect to the wall; indeed, it is possible to have a change in wave shape by modifying the focal point location. It is possible to distinguish between *broken wave impact*, *slosh impact*, *flip-through impact* and *gas pocket impact* (that will be analysed in detail in Section 3.2.3).

A *broken wave impact* occurs when the overturning wave crest hits the free surface entrapping a gas pocket; then, the wave front hits the wall and deflects upward. This type of impact takes place when the focal point is located far in front of the wall. If the focal point is located behind the wall, then a *slosh impact* takes place. In this case, the wave does not break, and the trough moves upward as the crest gets close to the structure. As can be seen in the pictures of Figure 3.2, there is no direct impinging of the wave crest because the trough reaches earlier than the wave crest the impact zone. In case the focal point is near the wall, both wave crest and wave trough converge towards a small area at the wall; in this case a *flip-through impact* occurs. Furthermore, if the focal point is located closer to the wall, then a *gas pocket impact* takes place. Differently from the broken wave impact, in this case the wave front hits directly the wall; as the wave front approaches the wall, it starts overturning and, at the same time, the wave trough moves upward. The consequence is an entrapping of gas pocket between the forward moving wave front, the upward moving trough and the structure. The gas pocket will change its shape as it will move upward. The following figures show the different wave impacts mentioned above. For each case, it is possible to notice the wave that approaches the wall; the time step is 30 ms. It will be possible to notice an interaction between the forward moving wave front and the upward moving wave trough.

In Figure 3.1 it is possible to see the exact instant when the wave crest hits the free surface before the impact against the wall. Figure 3.2 shows the shape of the wave that approaches the wall for a slosh impact; the trough increases its speed upward preventing any impact of the crest. Figure 3.3 represents Test L031 [1] and shows the wave shape for the flip-through impact; it can be considered a limit case between the slosh impact and the gas pocket impact.

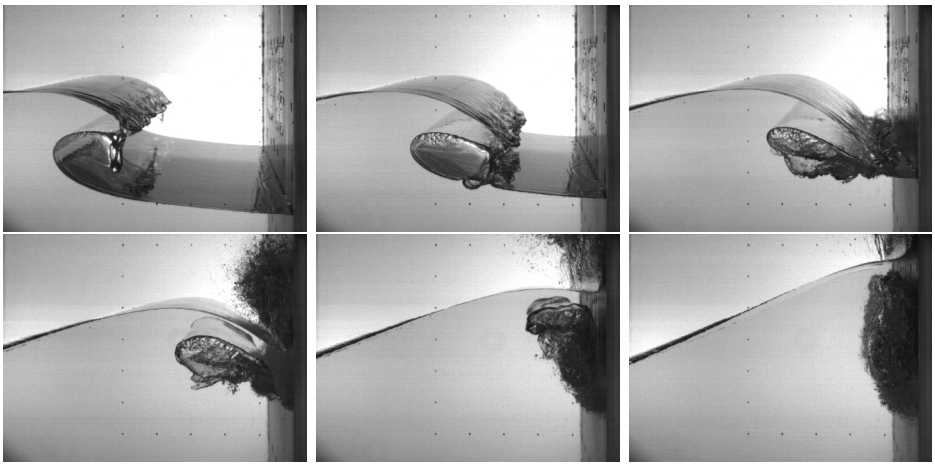

Figure 3.1: Broken wave impact: wave shape in front of the flat wall. Test L076. [1]

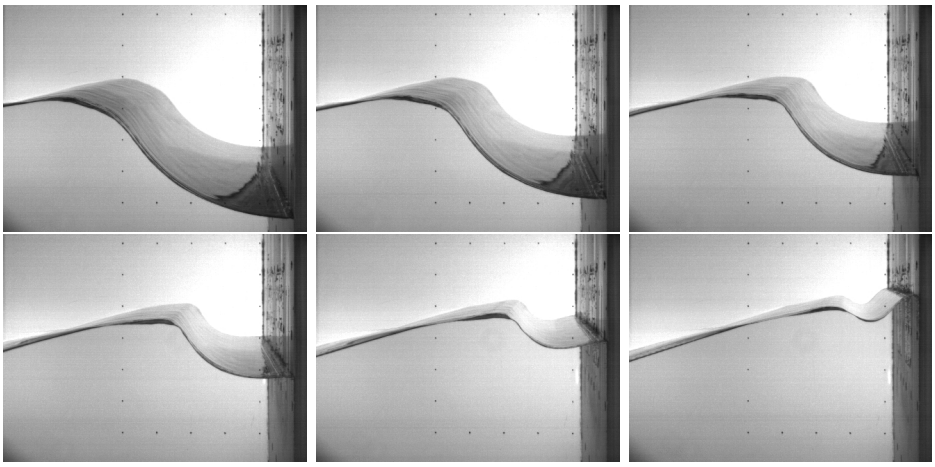

Figure 3.2: Slosh impact: wave shape in front of the flat wall. Test L082. [1]

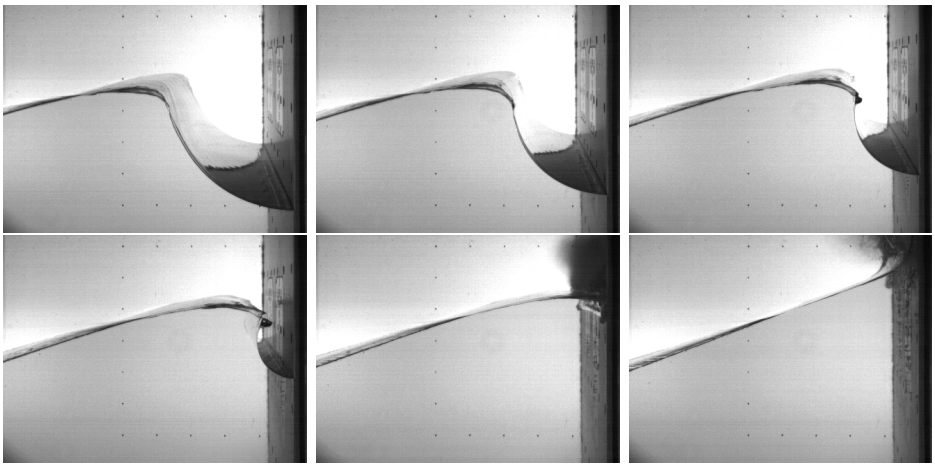

Figure 3.3: Flip-through impact: wave shape in front of the flat wall. Test L031. [1]

3.2.3 Gas Pocket Impact

In the case of a gas pocket impact, the focal point is located closer to the wall. As can be seen in the pictures of Figure 3.4, the wave crest starts overturning and the wave trough moves upward along the wall with an increase of speed as it gets close to the wall. In the fourth picture (first figure in the second row), it is shown the exact moment when a wave crest hits the wall; notice that a gas pocket is entrapped between the wall, the forward moving wave front and the upward moving trough.

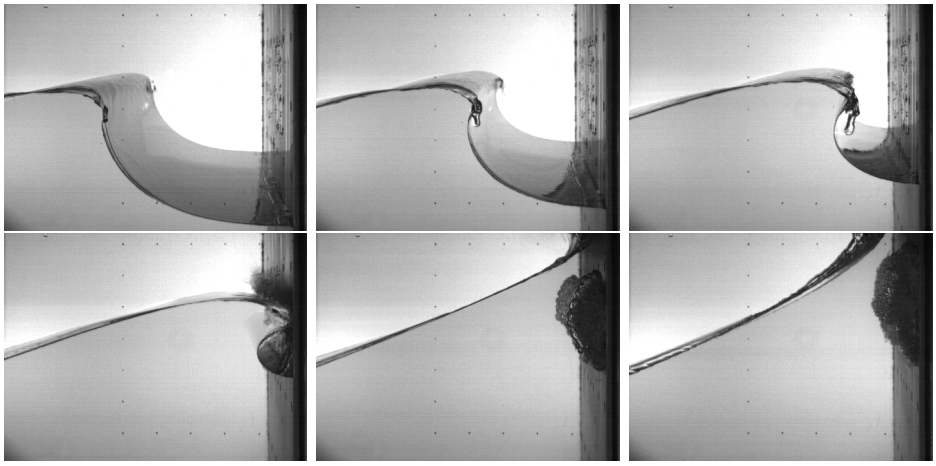

Figure 3.4: Gas pocket impact: wave shape in front of the flat wall. Time step 30 ms. Test L070. [1]

The fourth picture in Figure 3.4 represents the *starting point* of this thesis: the propagation of waves inside the structure takes place at the exact moment when the wave crest impacts against the free surface of the layered model, as shown in the introduction.

In order to fully understand what happens to both liquid and structure, some sketches have been included in this section, and they are shown below. As mentioned before, the purpose of the hydrodynamic part is both to provide a reasonable external force and to understand what is the connection between the external and internal processes, namely how the external phenomena affect the internal phenomena, before, after, and at the moment of the impact.

Figures 3.5-3.10 are a schematic representation of the gas pocket impact, and they show how the impact process that changes at each instant of time affects the internal regions of the structure; the wave approaching the structure is represented on the left, whereas the structure with inner regions is shown on the right. Notice that in each figure, different regions are highlighted according to the changes that occur outside the structure; this is the main meaning of Figures 3.5-3.10. Chapter 4 will investigate the physical phenomena that take place in the red region, the area of the structure affected by the direct impact of the wave crest (ELP1).

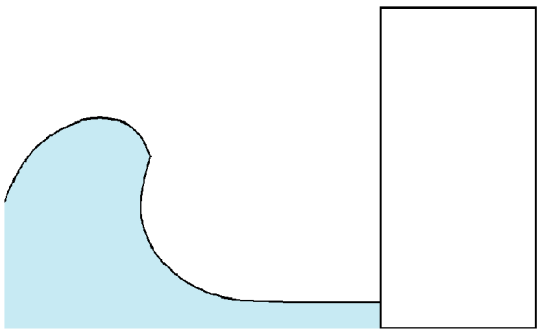

Figure 3.5: Wave shape in front of the wall, with a focal point located closer to the wall.

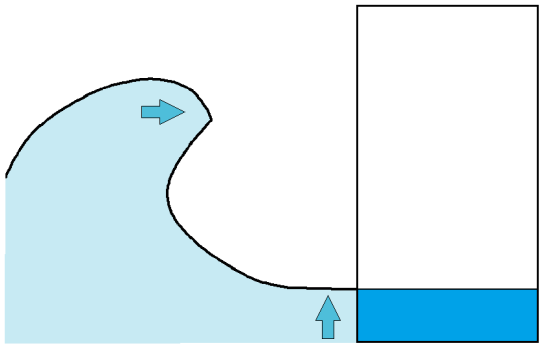

Figure 3.6: Wave approaching the structure with an overturning of the wave crest, at $t = t_0$.

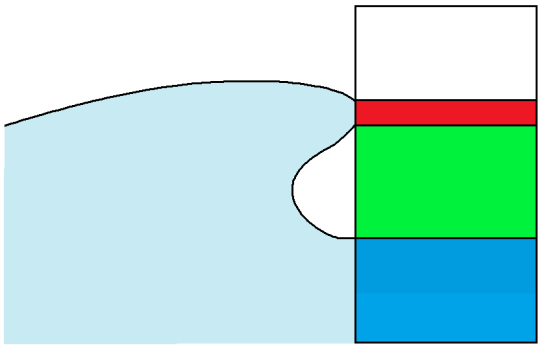

Figure 3.7: Direct impact of the wave crest and entrapping of a gas pocket, at $t = t_1$.

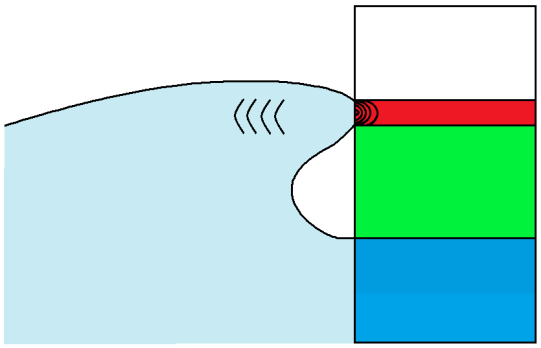

Figure 3.8: Pressure waves in the fluid and strain waves in the impact area, at $t = t_1$.

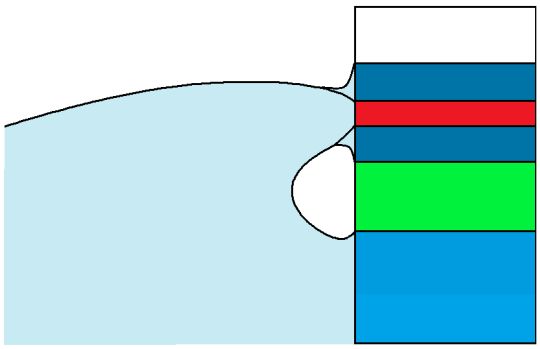

Figure 3.9: Spreading out of the wave along the wall and change of the entrapped gas pocket shape, at $t = t_2$.

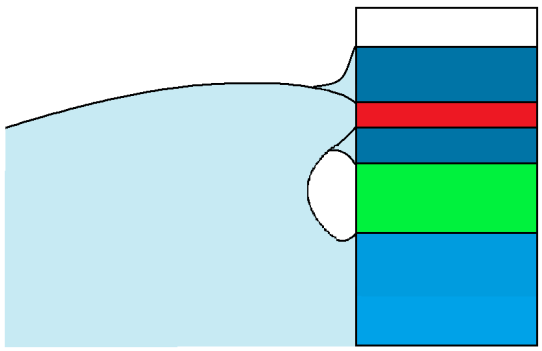

Figure 3.10: Spreading out of the wave along the wall and change of the gas pocket shape, at $t = t_3$.

Each picture shown above, is a summary of a part of the process before a new change takes place. In Figure 3.5 it is shown a wave shape in front of a wall, and the focal point is located closer to the wall; no region inside the structure experiences any change; in Figure 3.6 it is shown the same wave that is getting closer to the wall: the wave crest starts overturning and the wave trough starts moving upward along the wall with an increase of speed as the wave crest gets closer and closer to the wall; the two arrows show the direction in which the wave crest and trough are moving. It is important to specify that the wave trough is not forced to modify its shape as long as the distance between the wave crest and the wall remains large. The region inside the structure (blue) in contact with the moving wave trough is subjected to a pressure from the outside. Notice that this blue region is going to increase as time goes on because the wave trough is moving upward. In Figure 3.7 it is shown the exact moment of the impact (ELP1), namely when the wave crest hits the wall; it is assumed that the impact of the wave crest occurs at the instant $t = t_1$, and the flow is forced to abruptly stop due to the presence of the wall. Everything occurs before the direct impact takes place before the instant t_1. There is also an entrapping of the gas pocket between the wall, and the wave crest and trough. The region affected by the entrapped gas pocket is shown in green. The flow experiences a compression; indeed, in order to adapt quickly to this new situation, there is the propagation of a *pressure wave* (also called *shock wave*) through the liquid. While pressure waves propagate in the flow, another type of wave propagates in the structure: *strain waves*. Figure 3.8 that shows both pressure waves and strain waves will be analysed in detail later. After the impact of the wave crest takes place, the wave starts spreading along the wall as can be seen in Figure 3.9; this causes additional load in the regions (dark blue) around the impact area (in red). The flow is forced to make a sharp turn, building up a vertical jet (ELP2). In addition, the entrapped gas pocket (ELP3) moved upward and changes its shape (Figure 3.10).

In summary, the gas pocket impact is characterised by:

- approach of the wave crest
- overturning of the wave crest
- upward movement of the wave trough along the wall
- direct impact of the wave crest on the wall (ELP1)
- development of pressure waves in the flow and strain waves in the structure
- entrapping of the gas pocket between flow and structure (ELP3)
- spreading of the wave along the wall and building of a vertical jet (ELP2)
- change in the shape of the gas pocket moving upward

From the Figures 3.5-3.10 and the list above, it is possible to notice that there is a combination of all three ELPs in the gas pocket impact. Figure 3.11 shows a schematic representation of this combination for the case of the gas pocket impact. At the beginning of the process there is a compression of the gas (ELP3) due to the wave that is moving from the left toward the wall; then, when the wave reaches the structure, the direct impact of the wave crest (ELP1) occurs; therefore, the

gas pocket is entrapped between liquid and structure (ELP3), and the building jet (ELP2) takes place.

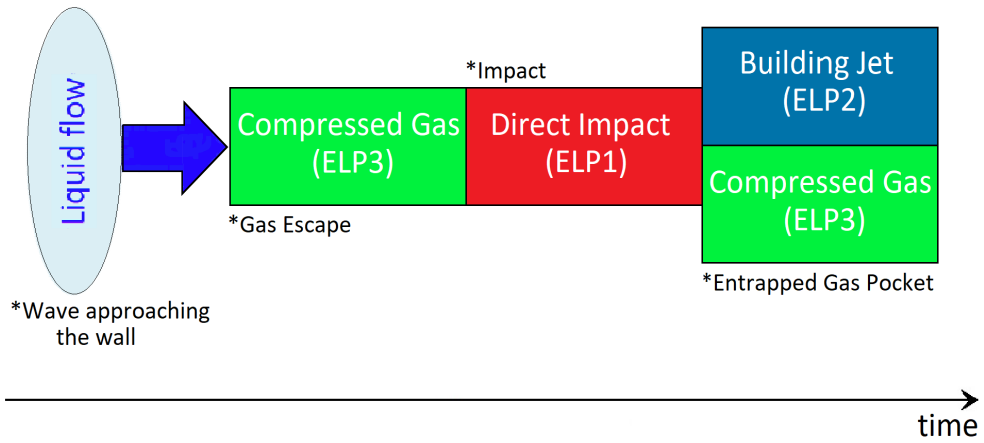

Figure 3.11: Schematic representation of the combination of ELPs for the gas pocket impact case. [4]

The schematic representation of the combination of ELPs can be modified adding the load from the trough that starts from the beginning when the wave crest begins approaching the wall.

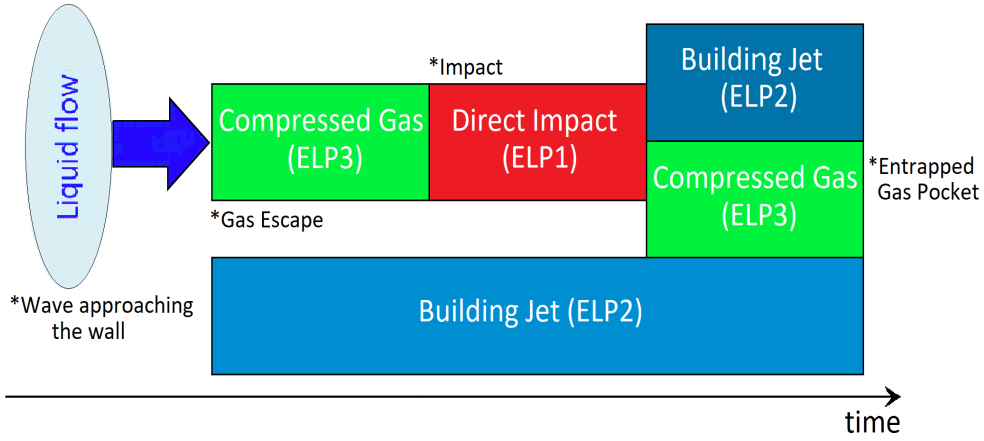

Figure 3.12: Schematic representation (modified) of the combination of ELPs for the gas pocket impact case. [4]

It is important to specify that in the process of the wave impact against a structure several physical phenomena are involved, such as transfer of momentum between liquid and gas, development of free surface instabilities, compression of escaping gas and entrapped gas, phase transition, change of liquid momentum, compression of liquid, fluid structure interaction, and propagation of time-space distributed loads through composite structure.

Specifically, as the wave gets close to the wall, the distance between wave and wall decreases, and there is a transfer of liquid momentum to gas momentum; the escaping gas shears the free surface causing the development of free-surface instabilities which are considered the main source of variability of the local pressures; since the gas between liquid and structure cannot escape quickly enough, it is compressed and it is entrapped; a phase transition is involved because LNG is in thermo-dynamical equilibrium with its vapour, and the compression of vapour induces condensation, therefore expansion leads to evaporation; consequently, there is a change in the liquid momentum because the liquid is forced to sharply turn in front of the wall; then, the liquid is compressed as it hits the wall; due to the discontinuity of the velocity between liquid and wall at the contact point, there is the propagation of a pressure wave from the contact point in the liquid at the speed of sound; at the moment of the contact, the structure is involved and since it is a composed of several layers, its flexibility influences the loads, and the energy content of the load is distributed through the structure.

3.2.4 Instabilities

As mentioned in the previous section, the escaping gas causes some free surface instabilities, known as Kelvin-Helmholtz instabilities, that degenerate into protrusions and then fragment. Figures 3.5-3.10 shown in Section 3.2.3 depict the process of the gas pocket impact in a simplified way. The impact wave crest seems to have a defined and uniform shape that overturns as it gets close to the wall and only changes completely its shape when ELP1 takes place at $t = t_1$. In the reality, the process is more complicated and the shape of the wave crest is characterized by a lot of instabilities caused by the escaping gas that shears the wave surface. In the pictures of Figure 3.13, it is shown the escaping gas between wave and wall (for the Test L109 [1]).

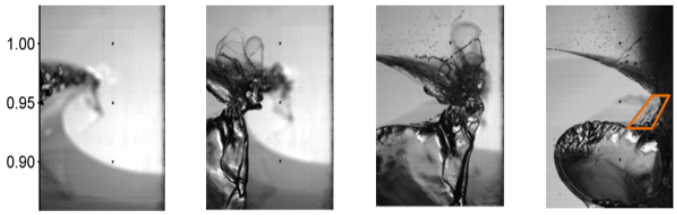

Figure 3.13: Escaping gas between the liquid and the wall for test L109. Time step is 15 ms. [1]

Figure 3.14-3.15 show how the presence of instabilities affects the load along the surface; the loading area is larger due to the presence of the instabilities.

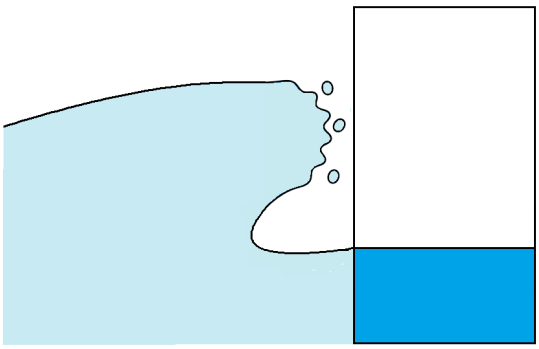

Figure 3.14: Wave crest approaching the wall with the presence of instabilities before the impact.

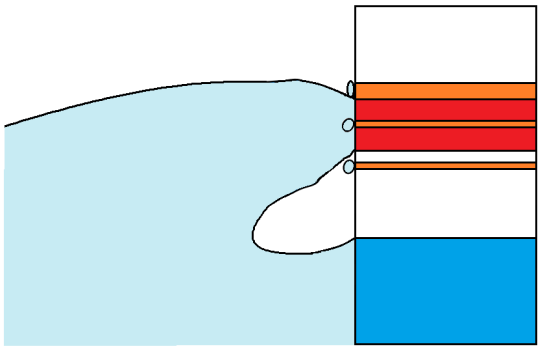

Figure 3.15: Wave crest at moment of impact, with instabilities that increase the impact area.

In this thesis, no instabilities will be taken into account; the external process will be assumed simplified and the incoming wave crest will be approximated by a spherical shape (see Section 3.3), but it is important to know that the presence of these instabilities increases the distribution of the pressure over a larger surface area; it means that more regions of the structure will be affected by the external impact.

3.2.5 Pressure Waves and Strain Waves

As mentioned before, at the moment of the direct impact of the wave crest (ELP1), there is the generation and consequently the propagation of two types of waves: pressure waves in the liquid and strain waves in the structure, as can be seen in Figure 3.16. Strain waves are generated and travel in the impact area (red region), and will be analysed in detail in Chapter 4.

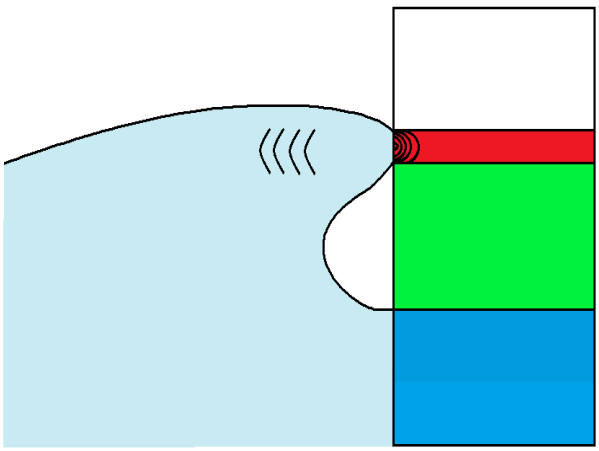

Figure 3.16: Development of pressure waves in the fluid and strain waves in the impact area at the moment of the direct impact $t = t_1$.

At the moment of the impact, both flow and structure need to adapt quickly to this new situation (represented by the impact). The flow adapts through the propagation of a pressure wave (shock wave), at the speed of sound, in the liquid, and it reduces the velocity of the flow around the contact point; the structure adapts through the propagation of strain waves in the impact area, and they increase the velocity of the structure around the contact point. Both pressure waves and strain waves help to decrease the discontinuity between liquid and structure at the moment of the direct impact. The generation and propagation of waves inside the structure can be considered a direct consequence of the external wave impact which acts like a disturbance modifying the current state of equilibrium of the structure.

If C is the contact point between liquid and structure, then a first cylindrical pressure wavelet is emitted from C. At each instant the spreading liquid edge will emit a wavelet (Huygens Principle). As it will be seen in the next section, there are two contact points which will move with opposite velocities $\overrightarrow{V_C(t)}$ and $-\overrightarrow{V_C(t)}$; the velocity of the contact point will decrease from ∞ that corresponds to the instant of time in which the contact between structure and liquid has not occurred yet.

It is important to specify that the regions in the Figure 3.16 change continuously with the time in terms of size, and it only represents the situation for an instant of time.

3.3 External Force and Contact Point

After evaluating the relationship between the external process and the internal process, it needs to define an external force. The external impact needs to be expressed as a force (pressure force). The complexity of the problem is mainly due to the variation of the force in both space and time. The external load can be considered as a pressure force and therefore, the contact area changes with time; this change can be seen in Figures 3.7-3.10 in which the impact surface increases as the wave starts spreading along the wall. In this section, the velocity of the contact point and the external force will be introduced.

Velocity of the contact point $V_C(t)$ and critical time t_{cr}

The first contact between the liquid and the structure occurs when ELP1 takes place, namely at $t = t_1$. It is assumed that there is neither instability nor gas, and a spherical shape is used to approximate the wave crest with an impact velocity perpendicular to the wall as can be seen in Figure 3.17.

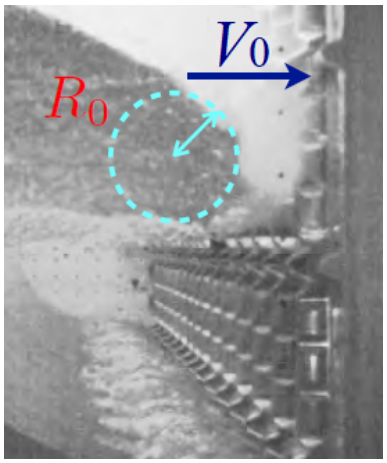

Figure 3.17: Radius of curvature R and impact velocity V_0 normal to the wall. [5]

In Figure 3.18 the approximated spherical wave with radius R and the impact velocity V_0 is shown, whereas in Figure 3.19 it is shown the pressure wave that is going to propagate in the liquid and the velocity of two contact points that are moving with oppose direction $\overrightarrow{V_C(t)}$ and $-\overrightarrow{V_C(t)}$. [6] [7]

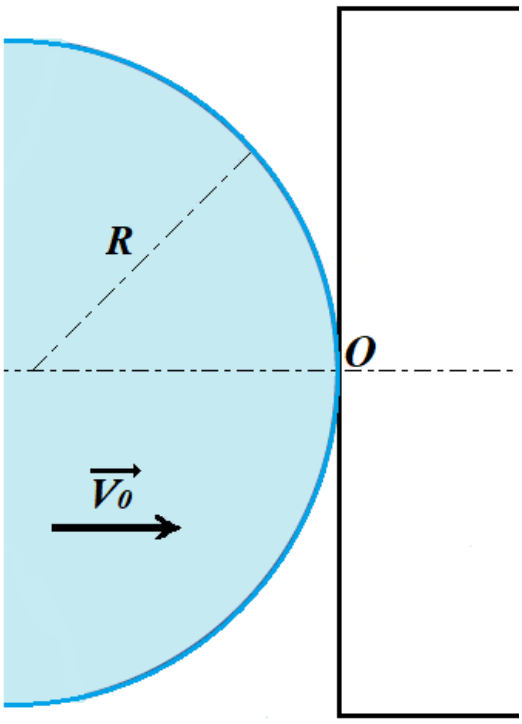

Figure 3.18: Approximated spherical shape of the impact wave, with radius of curvature R and impact velocity V_0.

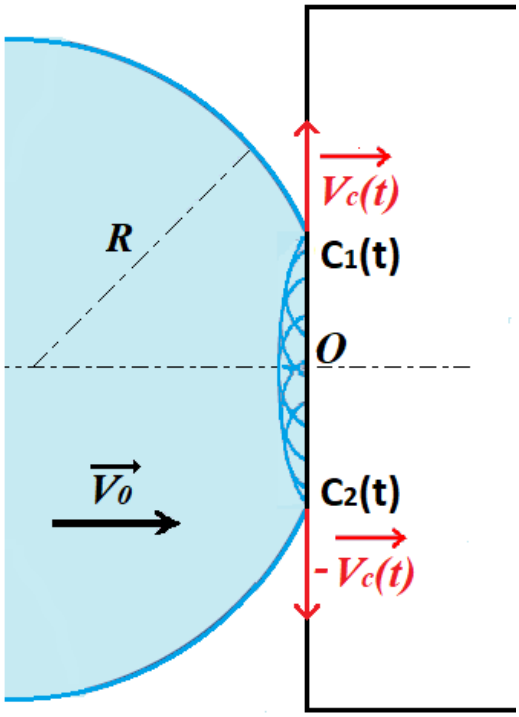

Figure 3.19: Velocity of the contact point $V_C(t)$ and propagation of pressure waves.

If C identifies the contact point, then its location is defined as follows:

$$r_c(t) = R\sqrt{1 - \left(1 - \frac{V_0 t}{R}\right)^2} \tag{3.1}$$

The first derivative respect to time will give the velocity of the contact point:

$$V_c(t) = \dot{r_c}\,(t) = \frac{V_0}{\sqrt{\frac{1}{\left(1-\frac{V_0 t}{R}\right)^2} - 1}} \tag{3.2}$$

During the process, the velocity of the contact point will decrease from ∞ to c which is the velocity of the contact point corresponding to $t = t_{cr}$. Thus, it results:

$$V_C(0) = \infty \qquad if \quad t = 0$$

$$V_C(t_{cr}) = c \qquad if \quad t = t_{cr}$$

At $t = 0$ there is no contact between liquid and structure. Notice that t_{cr} is the critical time defined as:

$$t_{cr} = \frac{R}{V_0}\left(1 - \frac{1}{\sqrt{1 + \left(\frac{V_0}{c}\right)^2}}\right) \approx \frac{R V_0}{2c^2} \tag{3.3}$$

In order to find some numerical values of $V_c(t)$, consider the following case:

$R \approx 90\ mm$

$V_0 \approx 7\ m/s$

$c = 1500\ m/s$

By using equation 3.3, then it results:

$$t_{cr} = 1.4 \cdot 10^{-7}\ s$$

The velocity of the contact point will assume values between ∞ and $t_{cr} = 1.4 \cdot 10^{-7} s$.

The graph in Figure 3.20 shows the relationship between the velocity of the contact point and time. Notice that $V_C(t)$ decreases from ∞ to $c = 1500\ m/s$ corresponding at $t = t_{cr}$.

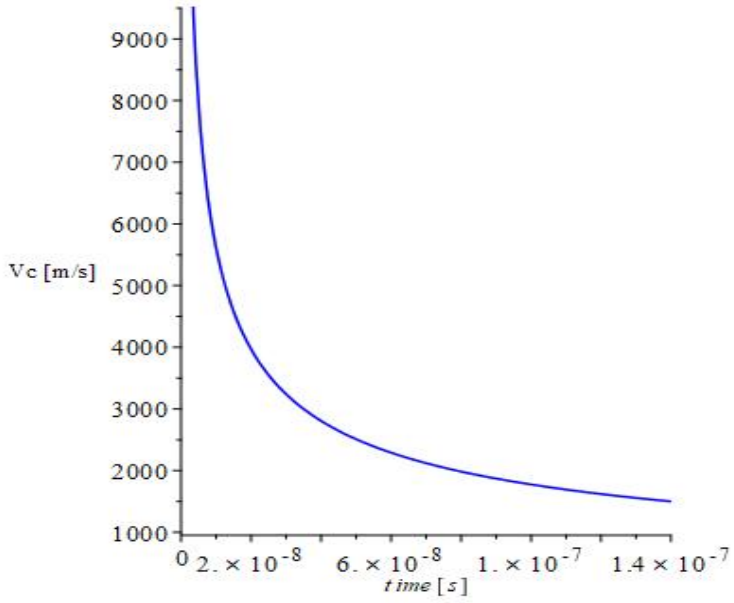

Figure 3.20: Velocity of the contact point with respect to time, in the interval $[0; t_{cr}]$

Pressure force $F(t)$

As mentioned before, the external force is expressed as a pressure force; then, it follows:

$$F(t) = \int p(t, A)\, dA \tag{3.4}$$

where $p(t, A)$ is the pressure map, and A is the contact area.

If the contact area is simply approximated to a rectangular shape, then, at each instant of time, more portions of the free surface will be in contact with the liquid.

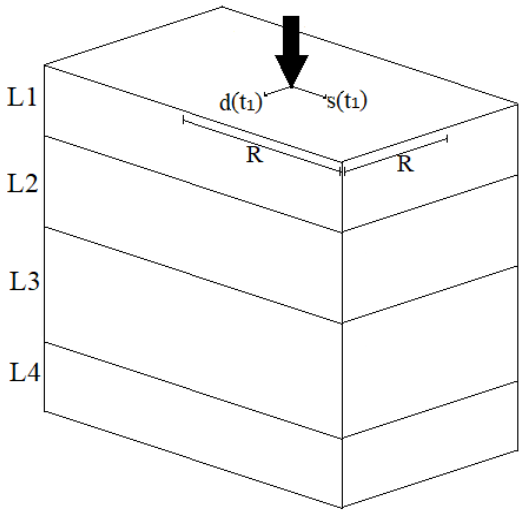

Figure 3.21: Layered structure with an external force acting on the free surface at the first instant $t = t_1$ of the impact.

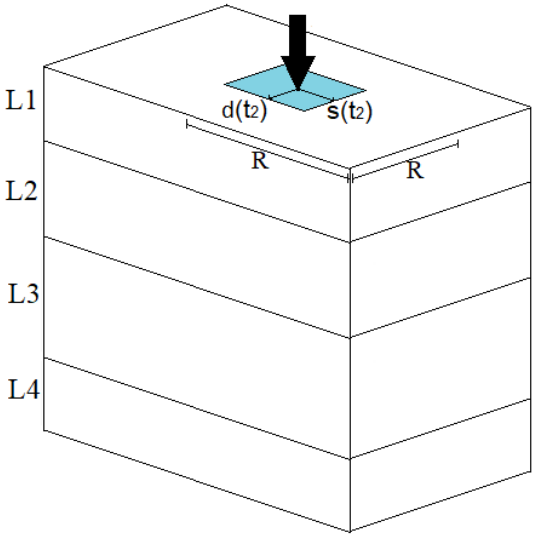

Figure 3.22: Impact area at $t = t_2$.

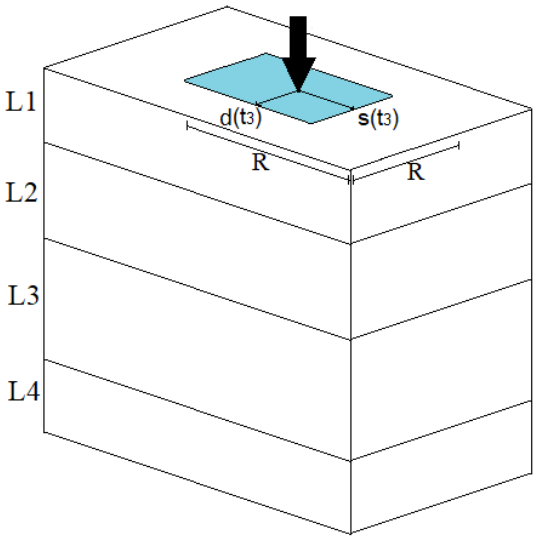

Figure 3.23: Impact area at $t = t_3$.

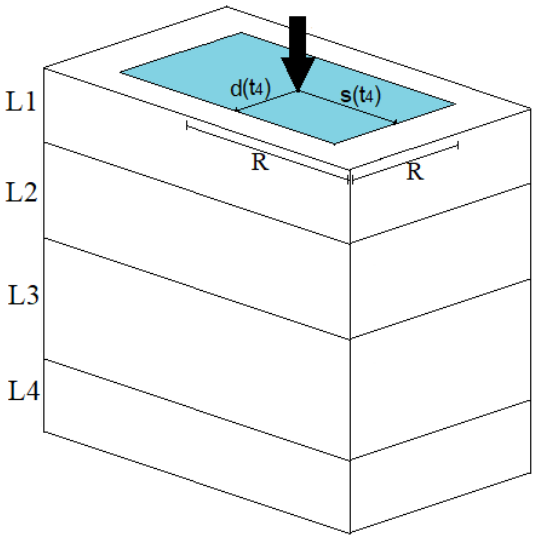

Figure 3.24: Impact area at $t = t_4$.

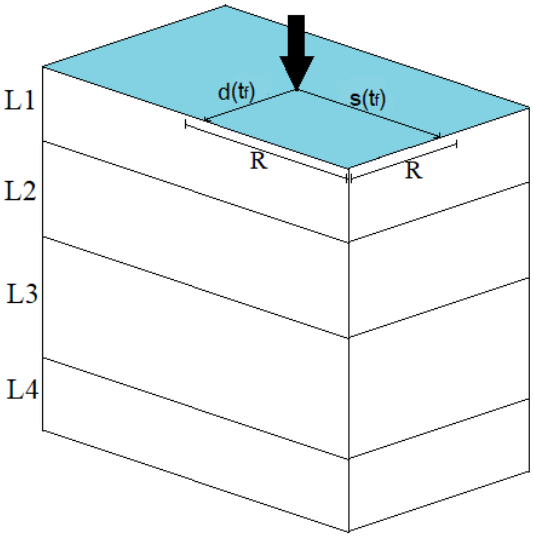

Figure 3.25: Impact area at $t = t_f$.

The external process is limited to the critical time, meaning that it takes place between:

$$0\ s < t < 1.4 \cdot 10^{-7}\ s$$

Figures 3.21-3.25 show the entire structure, and the impact area that changes at each instant of time. As can be seen, the contact area (in light blue) increases over time, and it is represented in a simplified form; indeed, the wave starts spreading out on the free surface at $t = t_1$, and the process comes to an end at $t = t_f$. In the reality, it is highly difficult to predict the increase of the impact area because,

as mentioned in the previous sections, it needs to take into account the presence of discontinuities which distribute pressure over a larger area.

In the next chapter, it will be seen that each change in the external force will be responsible of the generation of a different incident wave; in that case, different values of the external force, corresponding to different consequent instants of time will be used to show the different shape of the wave fronts. Thus, the external force can also be expressed as follows:

$$F_{tot} = \sum_{i=1}^{n} F_i(t) \tag{3.5}$$

3.4 Conclusions

From this chapter it is possible to conclude that there is a strong relationship between the external and internal process.

As mentioned before, the purpose of this chapter was to provide an understandable explanation about what happens outside the structure and therefore, provide a simplified external force to be used in the equations for expressing the deformation of the structure. In Section 3.2 the Elementary Loading Processes (ELPs) have been taken into account and different types of wave impacts have been described in order to understand which process could be suitable for this project. Therefore, the gas pocket impact has been considered because the direct impact of the wave crest (ELP1) is clearly involved. It has been seen that every change in the liquid affected different regions inside the structure (Figures 3.5-3.10). The instabilities have been also mentioned in order to clarify that their presence makes more complicated the entire process because they distribute pressure over a larger surface. In addition, both strain waves and pressure waves play an important role at the moment of the impact because they decrease the discontinuity between liquid and structure. In Section 3.3 the notions of velocity of the contact point, critical time have been introduced together with the external force.

This chapter represented the starting point of this project and the reason why the wave propagation phenomena are analysed. The generation and development of waves inside the layered material is a direct consequence of the external load acting on the surface of the layered structure. Next chapter will analyse the wave propagation phenomena in the impact area.

Chapter 4

Waves Propagation

4.1 Introduction

The concept of *waves propagation* is mainly based on the transmission or *spreading* of a sharply applied, localized disturbance in a medium. There are several examples of wave propagation phenomena both in many fields of the physics, such as in seismology with the propagation of tremors in the earth, in acoustics with the propagation of sound in air, or in electromagnetism with the propagation of electric and magnetic field, and in many everyday life events, such as the spreading of ripples on a pond of water. The waves can propagate in the air, gas, water, and solid media.

The interest in the wave propagation phenomena began with Pythagoras that studied the origin of musical sounds and the vibrations of strings. From the XVI century with Galileo Galilei that the science about wave propagation and vibrations developed rapidly. The first studies were more observational than quantitative and very often concerned water waves and acoustic waves due to the associations with wave motion.

The concept of *waves propagation* inside the media is frequently used to explain why the effects of a local force are also felt in the surrounding regions of the impact area of the body or the structure interested in the contact with an external load.

Assuming that the waves propagation takes place in a medium or in several media which are in contact each other, both reflection and transmission phenomena at the interfaces and particles motion need to be analysed in order to have a wider knowledge and information about the deformation occurring inside the material. Indeed, the physical basis for the propagation of a disturbance lies on the interaction of the discrete atoms of the solids, even if the medium is considered as continuous both in solid and fluid mechanics.

The interest in wave propagation phenomena also increased throughout the history due to its numerous applications, especially in engineering. Since earthquakes generate waves and tremors that propagate both inside and on the surface of earth, these waves have been useful until now to expand the knowledge about the interior of the earth or to identify the presence of oil and gas. Studying wave propagation

phenomena, making use of ultrasonics, gives the opportunity to detect the presence of potential defects inside materials. Furthermore, in the field of civil, offshore engineering and marine technology, wave propagation phenomena are mainly studied in order to investigate the response of a structure subjected to a blast load or an impact. They are also analysed in the field of material science to study the crack propagation or the interaction of dynamic stress fields with existing cracks, voids, or inclusions in the materials.

This chapter can be considered the core of this thesis and its purpose is to explain and provide a reasonable physical explanation of the wave propagation phenomena that take place inside the material due to an external load. Section 4.2 introduces the concept of the wave propagation phenomena inside a material; Section 4.3 presents two types of waves that travel in the simplified structure; the main difference between these two waves will be based on their propagation velocities. Then, the concept of *spreading area* will be analysed again but from a mathematical point of view. In Section 4.4 all possible situations about the propagation phenomena related to the simplified structure will be analysed separately; the reflection and transmission phenomena will be explained for six different situations; then, Section 4.5 introduces different models combining the notions introduced and analysed in Section 4.4. Section 4.6 introduces the concept of potential associated to each type of wave, and it also discusses type and geometry of the waves traveling in the layered structure. Finally, Section 4.7 explains the physics of the particles motion related to the impact area.

4.2 Waves inside the Material

As discussed in the previous chapter, both *strain waves* in the structure and *pressure waves* in the fluid play an important role in the case of a wave impact because they reduce the discontinuity between liquid and structure at the moment of the impact. Both liquid and structure around the contact point need to adapt rapidly to the new situation represented by the wave impact; specifically, the pressure waves, propagating in the liquid, reduce the flow velocity around the contact point, whereas the strain waves, propagating in the structure, increase the velocity of the structure around this point. The presence of waves inside the material justifies and explains why the disturbance is also felt in all layers of the impact area, and in the regions around the loading area after a certain amount of time. The other areas, located far from the contact point, need some time before feeling the effects of the impact force (transverse force).

In the rigid dynamics, it is assumed that when a force is applied in a point on a body, then all the other parts of the body feel *instantaneously* the effects caused by this load, and forces can be considered as linear acceleration of the whole body. In this case, due to the immediate feeling of the external force in all the other regions, no wave propagation concept can be applied. Thus, this assumption is against the wave propagation concept in which it is essential consider a limited amount of time before that no surrounding area feels the effects of the external load. The waves

considered in this thesis will propagate through the thickness of the structure.

Before presenting the two types of waves that will travel in the layered structure, it needs to understand where these waves come from. In order to reach the purpose, let consider a small cube of material and the stresses acting on it:

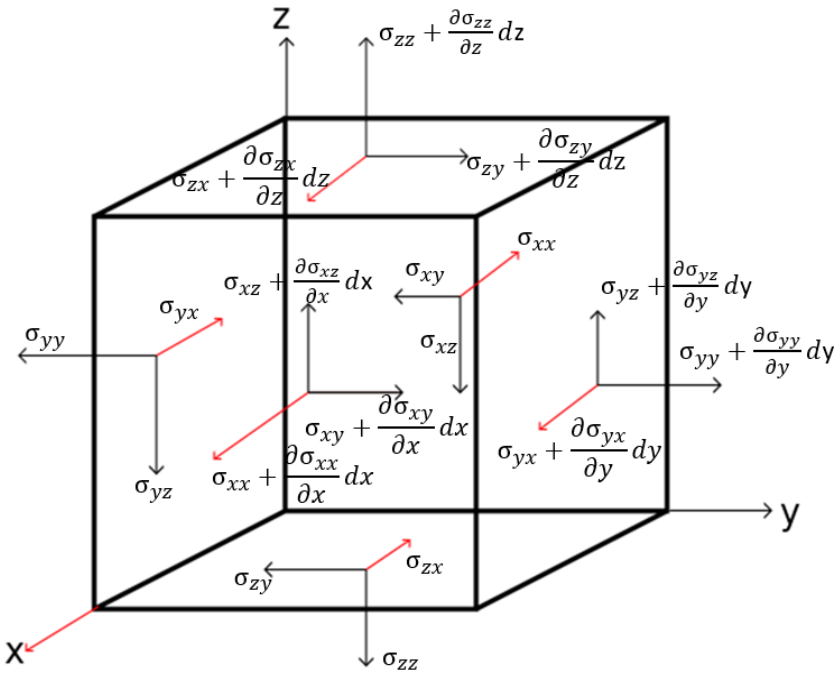

Figure 4.1: Stresses acting on a material cube.

Applying the *Newton's Second Law* in *x-direction*, it results:

$$\left(\sigma_{xx} + \frac{\partial \sigma_{xx}}{\partial x} dx\right) dydz - \sigma_{xx} dydz + \left(\sigma_{yx} + \frac{\sigma_{yx}}{\partial y} dy\right) dxdz - \sigma_{yx} dxdz +$$

$$+ \left(\sigma_{zx} + \frac{\partial \sigma_{zx}}{\partial z} dz\right) dxdy - \sigma_{zx} dxdy = (\rho V)\ddot{u}_x$$

which becomes

$$\sigma_{xx} dydz + \frac{\partial \sigma_{xx}}{\partial x} dxdydz - \sigma_{xx} dydz + \sigma_{yx} dxdz + \frac{\partial \sigma_{yx}}{\partial y} dydxdz +$$

$$-\sigma_{yx} dxdz + \sigma_{zx} dxdy + \frac{\partial \sigma_{zx}}{\partial z} dzdxdy - \sigma_{zx} dxdy = \rho(dxdydz)\dot{u}_x$$

which simplifies to

$$\frac{\partial \sigma_{xx}}{\partial x} + \frac{\partial \sigma_{yx}}{\partial y} + \frac{\partial \sigma_{zx}}{\partial z} = \rho \ddot{u}_x$$

Using the generalized form of *Hooke's Law*, the equation of motion can be expressed in terms of the displacement components:

$$\sigma_{xx} = \lambda\Delta + 2\mu\epsilon_{xx}, \qquad \sigma_{yx} = \mu\epsilon_{yx}, \qquad \sigma_{zx} = \mu\epsilon_{zx}$$

$$\Delta = \epsilon_{xx} + \epsilon_{yy} + \epsilon_{zz} \qquad \epsilon_{xx} = \frac{\partial u_x}{\partial x} \qquad \epsilon_{yy} = \frac{\partial u_y}{\partial y}$$

$$\epsilon_{zz} = \frac{\partial u_z}{\partial z} \qquad \epsilon_{yx} = \frac{\partial u_y}{\partial x} + \frac{\partial u_x}{\partial y} \qquad \epsilon_{zx} = \frac{\partial u_z}{\partial x} + \frac{\partial u_x}{\partial z}$$

Thus, substituting, it results:

$$\frac{\partial}{\partial x}(\lambda(\frac{\partial u_x}{\partial x} + \frac{\partial u_y}{\partial y} + \frac{\partial u_z}{\partial z}) + 2\mu\frac{\partial u_x}{\partial x}) + \frac{\partial}{\partial y}(\mu(\frac{\partial u_y}{\partial x} + \frac{\partial u_x}{\partial y})) + \frac{\partial}{\partial z}(\mu(\frac{\partial u_z}{\partial x} + \frac{\partial u_x}{\partial z})) = \rho\ddot{u}_x$$

$$\lambda\frac{\partial}{\partial x}(\frac{\partial u_x}{\partial x} + \frac{\partial u_y}{\partial y} + \frac{\partial u_z}{\partial z}) + 2\mu\frac{\partial^2 u_x}{\partial x^2} + \mu\frac{\partial^2 u_y}{\partial y \partial x} + \mu\frac{\partial^2 u_x}{\partial y^2} + \mu\frac{\partial^2 u_z}{\partial z \partial x} + \mu\frac{\partial^2 u_x}{\partial z^2} = \rho\ddot{u}_x$$

$$\lambda\frac{\partial}{\partial x}(\frac{\partial u_x}{\partial x} + \frac{\partial u_y}{\partial y} + \frac{\partial u_z}{\partial z}) + \mu\frac{\partial}{\partial x}(\frac{\partial u_x}{\partial x} + \frac{\partial u_y}{\partial y} + \frac{\partial u_z}{\partial z}) + \mu(\frac{\partial^2 u_x}{\partial x^2} + \frac{\partial^2 u_x}{\partial y^2} + \frac{\partial^2 u_x}{\partial z^2}) = \rho\ddot{u}_x$$

$$(\lambda + \mu)\frac{\partial\Delta}{\partial x} + \mu(\nabla^2 u_x) = \rho\ddot{u}_x \tag{4.1}$$

because $\Delta = \frac{\partial u_x}{\partial x} + \frac{\partial u_y}{\partial y} + \frac{\partial u_z}{\partial z}$, and $\nabla^2 = \frac{\partial^2}{\partial x^2} + \frac{\partial^2}{\partial y^2} + \frac{\partial^2}{\partial z^2}$.
The same procedure can be applied in the *y-direction* and *z-direction* giving:

$$(\lambda + \mu)\frac{\partial\Delta}{\partial y} + \mu(\nabla^2 u_y) = \rho\ddot{u}_y \tag{4.2}$$

$$(\lambda + \mu)\frac{\partial\Delta}{\partial z} + \mu(\nabla^2 u_z) = \rho\ddot{u}_z \tag{4.3}$$

The three equations 4.1, 4.2 and 4.3 can be also expressed in the following form:

$$(\lambda + \mu)\nabla\nabla.u + \mu\nabla^2 u = \rho\ddot{u} \tag{4.4}$$

where $\nabla.u = \Delta$. Notice that the body forces are neglected in the previous equations.

The three equations 4.1, 4.2 and 4.3, or equation 4.4 are called *Navier's equations for the media.* [8]

By applying the *Helmholtz Theorem* it is possible to express equation 4.4 in a simpler way. The *Helmholtz Theorem* states that any sufficiently continuous vector field can be represented as the sum of the gradient of a scalar potential and the *curl* of a vector potential:

$$u = \nabla\Phi + \nabla \times \Psi, \qquad \nabla.\Psi = 0$$

where Φ is the scalar potential and Ψ is the vector potential.

Substituting, it results:

$$(\lambda+\mu)\nabla\nabla.(\nabla\Phi + \nabla\times\Psi) + \mu\nabla^2(\nabla\Phi + \nabla\times\Psi) = \rho(\nabla\ddot{\Phi} + \nabla\times\ddot{\Psi})$$

$$(\lambda+\mu)(\nabla\nabla.\nabla\Phi + \nabla\nabla.\nabla\times\Psi) + \mu\nabla^2\nabla\Phi + \mu\nabla^2\nabla\times\Psi = \rho\nabla\ddot{\Phi} + \rho\nabla\times\ddot{\Psi}$$

$$(\lambda+\mu)\nabla\nabla^2\Phi + (\lambda+\mu)\nabla\nabla.\nabla\times\Psi + \mu\nabla^2\nabla\Phi + \mu\nabla^2\nabla\times\Psi - \rho\nabla\ddot{\Phi} - \rho\nabla\times\ddot{\Psi} = 0$$

$$\nabla[(\lambda+\mu)\nabla^2\Phi + \mu\nabla^2\Phi - \rho\ddot{\Phi}] + \nabla\times[(\lambda+\mu)\nabla\nabla.\Psi + \mu\nabla^2\Psi - \rho\ddot{\Psi}] = 0$$

$$\nabla[(\lambda+2\mu)\nabla^2\Phi - \rho\ddot{\Phi}] + \nabla\times[\mu\nabla^2\Psi - \rho\ddot{\Psi}] = 0$$

This equation is satisfied if each bracketed term is equal to zero:

$$[(\lambda+2\mu)\nabla^2\Phi - \rho\ddot{\Phi}] = 0$$

$$[\mu\nabla^2\Psi - \rho\ddot{\Psi}] = 0$$

Then, it results:

$$\nabla^2\Phi = \frac{1}{\left(\frac{\lambda+2\mu}{\rho}\right)}\ddot{\Phi} \qquad \rightarrow \qquad \nabla^2\Phi = \frac{1}{\alpha^2}\frac{\partial^2\Phi}{\partial t^2} \tag{4.5}$$

which is the wave equation for compression/dilatation waves, propagating at velocity $\alpha = \sqrt{\frac{\lambda+2\mu}{\rho}}$,

$$\nabla^2\Psi = \frac{1}{\left(\frac{\mu}{\rho}\right)}\ddot{\Psi} \qquad \rightarrow \qquad \nabla^2\Psi = \frac{1}{\beta^2}\frac{\partial^2\Psi}{\partial t^2} \tag{4.6}$$

which is the wave equation for distortion/shear waves, propagating at velocity $\beta = \sqrt{\frac{\mu}{\rho}}$.

Therefore, compression (or dilatation) waves characterized by a velocity α and distortion (or shear) waves characterized by a velocity β can propagate inside a medium and are considered body waves.

4.3 Compression and Distortion Waves

The structure introduced in Chapter 2 is composed by several layers that have different dimensions and material characteristics which will affect the propagation velocities of the waves.

It is assumed that two types of waves are generated and propagate inside the simplified model: *compression waves* and *distortion waves*. Compression waves can also be called *dilatation waves* and distortion waves can also be called *shear waves*. The main difference between these two types of waves lies on the propagation velocities; compression waves propagate inside the material with a velocity that will be identified with α and it depends on density, bulk modulus and shear modulus, instead distortion waves propagate with a velocity identified with β which depends on density and shear modulus, as shown in the following formulas:

$$\alpha = \sqrt{\frac{1}{\rho}(k + \frac{4G}{3})} \tag{4.7}$$

$$\beta = \sqrt{\frac{G}{\rho}} \tag{4.8}$$

where ρ, k, G are density, bulk modulus, and shear modulus, respectively.

It is important to specify that the propagation of a compression wave is subjected to a combination of compression and shear. In order to better understand this concept, consider a cube of material (for instance, located inside the impact area), a coordinate system (x, y, z), and a compression wave which is travelling in the x-direction (see Figure 4.2). During the passage of the compression wave, the cross-sectional areas of the cube perpendicular to the x-axis (highlighted in yellow) are not going to modify their shape, whereas the cross-sectional areas parallel to the x-axis (highlighted in red) are going to be changed. Therefore, there is a change in the shape of the cube and as well as in the volume. Figure 4.2 shows the cube of material before and after the passage of the compression wave.

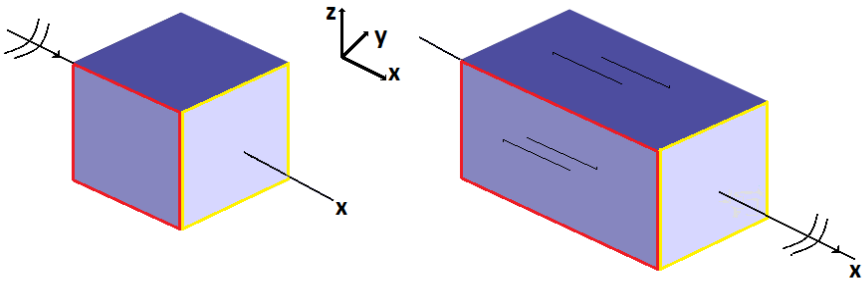

Figure 4.2: Material cube before (on the left) and after (on the right) the passage of a compression wave propagating in x-direction.

Equations 4.7 and 4.8 can also be expressed in terms of the first and the second Lame' constants (λ, μ). If density, Poisson ratio, and elastic modulus (ρ, ν, E) are known, then it results:

$$\alpha = \sqrt{\frac{\lambda + 2\mu}{\rho}} \tag{4.9}$$

$$\beta = \sqrt{\frac{\mu}{\rho}} \tag{4.10}$$

Notice that k is expressed as $k = \lambda + \frac{2\mu}{3}$ and it is defined as the ratio between the applied force and the dilatation Δ. The detailed procedure that demonstrates the equivalence between equations 4.7 and 4.9, and between equations 4.8 and 4.10 can be found in Appendix A.1.

Based on the equations 4.9 and 4.10, and assuming that the values of density, Poisson ratio and elastic modulus (ρ, ν, E) are known for each layer, as shown in Table 2.1, at first it is possible to find the Lame' constants (λ, μ), and then to calculate the wave propagation velocities (α, β). Table 4.1 shows the numerical results for the four layers:

Layers	λ	μ	α	β	α/β
	MPa	MPa	m/s)	m/s	-
Top plywood	1959.337	3803.419	3670.625	2314.504	1.586
Primary RPUF	20.021	35.593	871.816	544.619	1.601
Secondary RPUF	20.021	35.593	871.816	544.619	1.601
Back plywood	1959.337	3803.419	3670.625	2314.504	1.586

Table 4.1: Lame' constants and propagation velocities for each layer

Notice that for calculating the Lame' constants, the following formulas have been used:

$$\lambda = \frac{E\nu}{(1+\nu)(1-2\nu)} \tag{4.11}$$

$$\mu = \frac{3}{2}(k - \lambda) \tag{4.12}$$

where

$$k = \frac{E}{3(1-2\nu)} \tag{4.13}$$

From Table 4.1 it is possible to notice that $\frac{\alpha}{\beta} = \sqrt{\frac{\lambda+\mu}{\mu}} > \sqrt{2}$. Thus, any compression wave will propagate faster than any distortion wave. It results $\frac{\alpha}{\beta} \approx 1.60$ in each layer.

As mentioned in Section 2.4.1, the rate of change of the spreading area, namely the increase of the dimensions $(r(t), h(t))$, depends on the propagation velocities of the waves. From Table 4.1 it can be noticed how only the velocity of the compression waves affects the rate of change of the spreading area because $\alpha_j > \beta_j$ for $j = 1, 2, 3, 4$ in each layer. The following graph relates time and space (thickness of each layer) in the impact area:

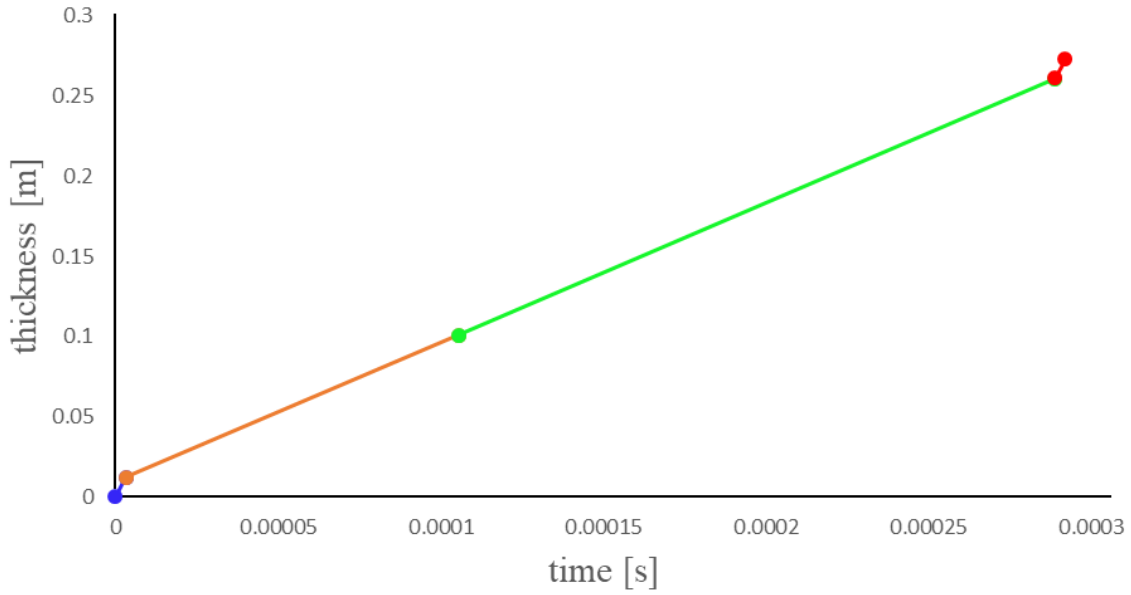

Figure 4.3: Spreading Area: Time-Space relationship for each layer: — top plywood, — primary RPUF, — secondary RPUF and — back plywood.

The graph in Figure 4.3 shows the relationship between space and time in each layer. Only the compression propagation velocities α_j have been considered. Blue and red lines represent the time-space relationship for top plywood and back plywood, respectively, whereas the orange and the green lines those for the primary RPUF and secondary RPUF, respectively. The slope in the graph in Figure 4.3 is the velocity α_j in each layer. The larger the thickness of each layer, the more time the compression wave takes to reach the interface.

4.4 Wave Propagation Phenomena

In this section, the wave propagation phenomena will be analysed separately for all possible situations related to the simplified model. The expression *wave propagation phenomena* means the reflection and the transmission of an incident wave that impinges on an interface which separates two media.

As mentioned before, there will be two kinds of waves, compression and distortion waves; in this thesis, six types of waves will be taken into account: incident compression wave (ICW), reflected compression wave (RCW), transmitted compression wave (TCW), incident distortion wave (IDW), reflected distortion wave (RDW), transmitted distortion wave (TDW). Looking at the configuration of the simplified model in Figure 2.7, it is possible to identify three types of interfaces: a free interface which separates the first layer (L1) from the external environment, the interface at the wall which separates the last layer from the wall, and the interface which separates two layers (for instance, layer 1 from layer 2). In this section, the reflection and transmission phenomena will be only shown at these three types of interface to better understand the generation of new waves as a consequence of an incident

(compression or distortion) wave. The six situations that are going to be discussed will be considered as isolated cases; later, in the chapter, they will be combined together and the global wave propagation phenomena of reflection and transmission will be shown. Considering the simplified model introduced in Chapter 2, it is possible to identify six situations:

Situation 1. elastic layer - external environment, with incident compression wave;

Situation 2. elastic layer - external environment, with incident distortion wave;

Situation 3. elastic layer - elastic layer, with incident compression wave;

Situation 4. elastic layer - elastic layer, with incident distortion wave;

Situation 5. elastic layer - wall, with incident compression wave;

Situation 6. elastic layer - wall, with incident distortion wave;

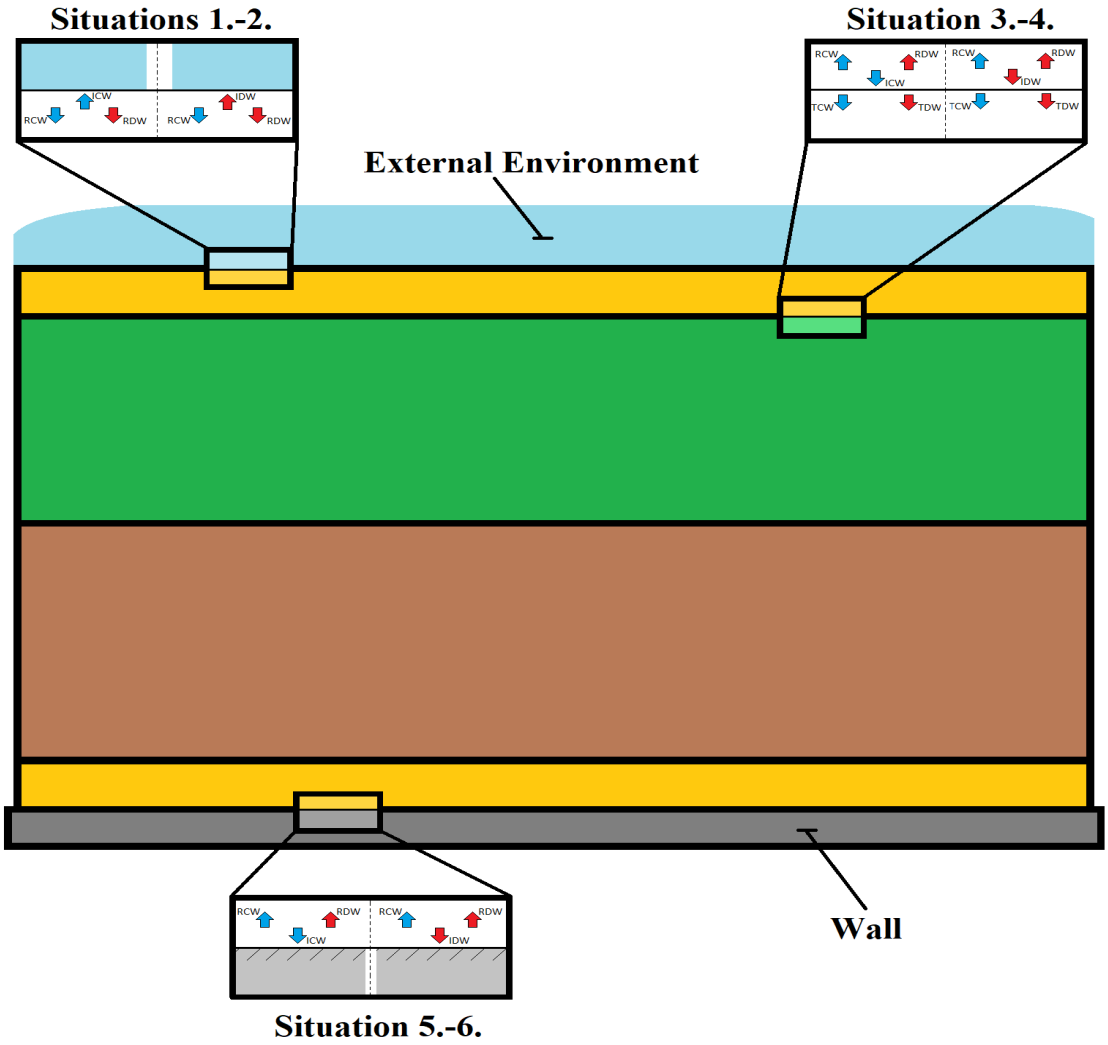

Figure 4.4: Situations 1.-6. located in the simplified model.

Notice that in the first two situations, the expression *external environment* has been chosen in order to identify the place where there are air and water. It is the portion of space where the wave impact and the phenomena described in the previous chapter take place. The expression *elastic layer* identifies each material that composes the simplified structure. The wall is rigid and fixed; it means no wave propagates inside. Furthermore, the source that generates the waves inside the material is located on the free interface that separates layer 1 from the external environment in Situations 1. and 2 (Figures 4.5 and 4.6).

Situation 1. Figure 4.5 shows a free boundary which corresponds to the *interface 0* of the simplified structure. It divides layer 1 (which is the top plywood) from the external environment. Notice that the external environment is identified with light blue colour in the Figure 4.5. If an incident compression wave hits the free boundary, then there will be the generation of two new waves that will be reflected back. One of them will be a compression wave and the other one will be a distortion wave. No wave will develop and travel beyond the free interface.

Situation 2. Figure 4.6 shows the same case of Situation 1. except for the type of incident wave which hits the free interface. Also in this case the incident distortion wave will generate both a reflected compression wave and a reflected distortion wave; they will travel back in layer 1.

It will be seen that the incident compression wave (ICW) in Figure 4.5 and the incident distortion wave (IDW) in Figure 4.6 which generate two couples (RCW and RDW) of waves are the reflected waves that, in turn, have been generated by an incident compression wave at interface I1. As it will be seen later in Section 4.5, the processes shown in Figures 4.5-4.6 are two examples of II order wave propagation phenomena.

Situation 3. Figure 4.7 shows two solid elastic media, with different material properties, that are connected together through an interface. In this situation the interface is hit by an incident compression wave (ICW). As can be seen, it generates four new waves: a reflected compression wave (RCW) and a reflected distortion wave (RDW) that will propagate back in the first layer, and a transmitted compression wave (TCW) and a transmitted distortion wave (TDW) that will propagate in the second layer.

Situation 4. Figure 4.8 shows the same case of Situation 3 with the only difference that an incident distortion wave (IDW) hits the interface. It will also generate four new waves: two will be reflected back, (RCW), and (RDW), and the other two will be transmitted in the next medium, (TCW) and (TDW).

The incident compression wave (ICW) in Figure 4.7 and the incident distortion wave (IDW) in Figure 4.8 can be considered the reflected waves which appear in Figure 4.5 or in Figure 4.6.

Situation 5. Figure 4.9 shows a solid elastic medium in contact with a wall hit by an incident compression wave. It is supposed no wave is generated inside the wall, and, therefore, there will only be reflected waves (RCW) and (RDW).

Situation 6. Figure 4.10 is the same as Situation 5. but an incident distortion wave is taken into account. Also in this case, there will be only two reflected waves (compression and distortion) that will propagate back in the medium.

The incident compression wave (ICW) in Figure 4.9 and the incident distortion wave (IDW) in Figure 4.10 are the transmitted waves which have been generated by another incident wave in the previous layer (that is layer 3).

It is important to specify that in all Figures 4.5-4.10 the blue arrows represent compression waves and the red arrows represent distortion waves, as can be noticed by the acronyms. These pictures do not provide any additional information about the 'nature' of the waves (their geometry, amplitudes, etc.), but they are only schematic representations to show the propagation directions.

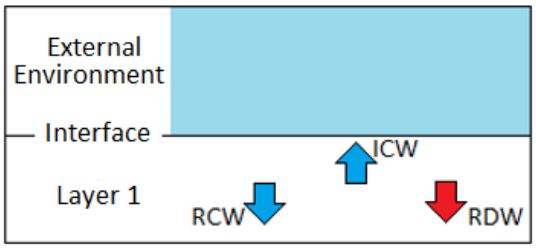

Figure 4.5: Situation 1. Generation of reflected waves due to an incident compression wave ICW at free interface.

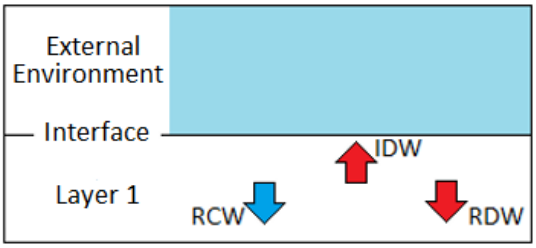

Figure 4.6: Situation 2. Generation of reflected waves due to an incident distortion wave IDW at free interface.

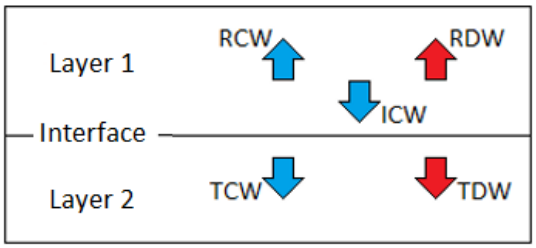

Figure 4.7: Situation 3. Generation of reflected and transmitted waves due to an incident compression wave ICW.

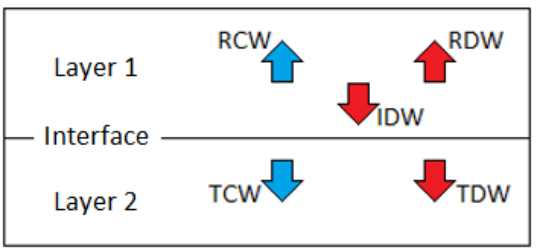

Figure 4.8: Situation 4. Generation of reflected and transmitted waves due to an incident distortion wave IDW.

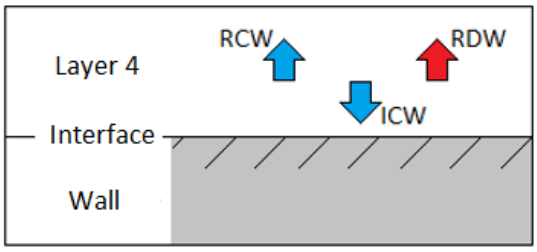

Figure 4.9: Situation 5. Generation of reflected waves due to an incident compression wave ICW at the last interface.

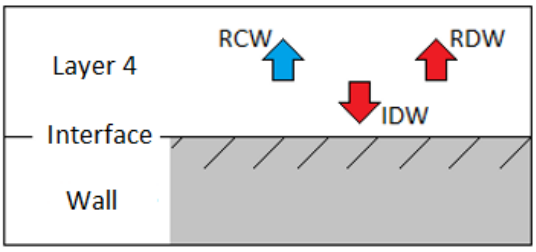

Figure 4.10: Situation 6. Generation of reflected waves due to an incident distortion wave IDW at the last interface.

In summery, a incident (compression or distortion) wave generates four waves every time it hits a boundary between two solid elastic media. Even though no wave propagates in the air or in the wall (Situations 1,2 and 5,6), two reflected waves are generated back. If only a wave is supposed to reflect back in the medium, then the boundary conditions at the interface are nor satisfied anymore at the same time.

In the next section it will be proved mathematically that the boundary conditions at the interface which divides two media are not satisfied at the same time if a reflected distortion wave is not taken into account.

4.4.1 Mathematical Demonstration of Situation 1.

The purpose of this section is to demonstrate that the boundary conditions are not satisfied if only a reflected compression wave is taken into account.

The demonstration will be done only for Situation 1 shown in Figure 4.5 in the previous section. The interface will be a free boundary and both normal stress and shear stress need to be zero at $y = 0$. It will be considered an incident compression wave with an angle γ_1 with the x-axis. At first, only a reflected compression wave will be taken into account.

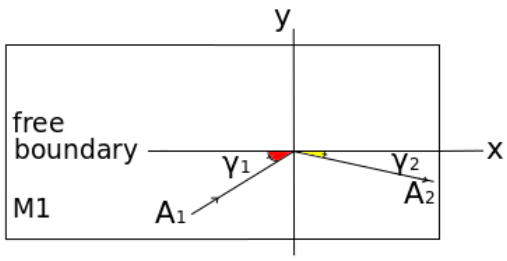

Figure 4.11: Incident compression (plane) wave at free interface and reflected compression wave, assuming no reflected distortion wave.

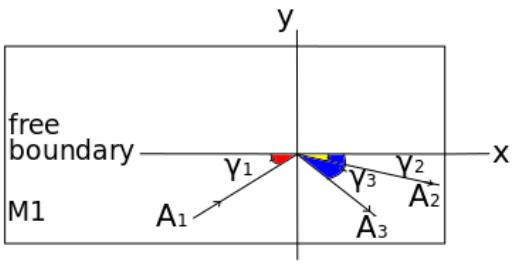

Figure 4.12: Incident compression (plane) wave at free interface and reflected compression and distortion waves.

In Figure 4.11 it is shown the incident (harmonic) compression wave with amplitude A_1 and angle γ_1 with x-axis; its displacement perpendicular to the wave front will be:

$$\Phi_1 = A_1 sin(pt + f_1 x + g_1 y) \tag{4.14}$$

where $f_1 = \frac{p}{\alpha_1} \cos\gamma_1$, $g_1 = \frac{p}{\alpha_1} \sin\gamma_1$. Notice that α_1 is the propagation velocity of the compression wave.

The displacement of the reflected compression plane wave will be:

$$\Phi_2 = A_2 sin(pt + f_2 x - g_2 y + c_1) \tag{4.15}$$

where $f_2 = \frac{p}{\alpha_1}\cos\gamma_2$, $g_2 = \frac{p}{\alpha_1}\sin\gamma_2$. Also this wave will travel with a velocity α_1. Notice that c_1 is a constant that allows any change in phase of the wave on reflection.

In addition, the displacements parallel to the x-axis and y-axis will be defined with $q_{1/2}$ and $w_{1/2}$, respectively, where:

$$q_1 = \Phi_1\cos(\gamma_1) \qquad w_1 = \Phi_1\sin(\gamma_1)$$

$$q_2 = \Phi_2\cos(\gamma_1) \qquad w_2 = \Phi_2\sin(\gamma_1)$$

As can be seen in Figure 4.11, the free boundary is represented by the xz plane. The normal stress and shear stress will be expressed by the following equations:

$$\sigma_{yy} = \lambda\Delta + 2\mu\frac{\partial w}{\partial y} = \lambda(\frac{\partial q_1}{\partial x} + \frac{\partial q_2}{\partial x} + \frac{\partial w_1}{\partial y} + \frac{\partial w_2}{\partial y}) + 2\mu(\frac{\partial w_1}{\partial y} + \frac{\partial w_2}{\partial y}) \tag{4.16}$$

$$\sigma_{yx} = \mu\left(\frac{\partial w}{\partial x} + \frac{\partial q}{\partial y}\right) = \mu(\frac{\partial q_1}{\partial y} + \frac{\partial q_2}{\partial y} + \frac{\partial w_1}{\partial x} + \frac{\partial w_2}{\partial x}) \tag{4.17}$$

Substituting all the partial derivatives calculated in Appendix A.3, it results:

$$\begin{aligned}\sigma_{yy} = \tfrac{p}{\alpha_1}\left[\lambda + 2\mu\sin^2\gamma_1\right]A_1\cos(pt + f_1x + g_1y) + \\ [+\lambda + 2\mu\sin^2\gamma_2]\tfrac{p}{\alpha_1}A_2\cos(pt + f_2x - g_2y + c_1)\end{aligned}$$

$$\begin{aligned}\sigma_{xy} = \mu(\tfrac{p}{\alpha_1}A_1\cos(pt + f_1x + g_1y)\sin(2\gamma_1) \\ -\tfrac{p}{\alpha_1}A_2\cos(pt + f_2x - g_2y + c_1)\sin(2\gamma_2))\end{aligned}$$

At the interface, $y = 0$, $\sigma_{yy} = 0$ and $\sigma_{xy} = 0$. Then, the previous equations become:

$$0 = \left[\lambda + 2\mu\sin^2\gamma_1\right]\frac{p}{\alpha_1}A_1\cos(pt+f_1x) + [\lambda+2\mu\sin^2\gamma_2]\frac{p}{\alpha_1}A_2\cos(pt+f_2x+c_1) \tag{4.18}$$

$$0 = \mu\frac{p}{\alpha_1}(A_1\cos(pt + f_1x + g_1y)\sin(2\gamma_1) - \cos(pt + f_2x - g_2y + c_1)\sin(2\gamma_2)) \tag{4.19}$$

Equation 4.18 is satisfied for all values of t and x if:

$f_1 = f_2$ (i.e. $\gamma_1 = \gamma_2$), and either $c_1 = 0$ and $A_1 = -A_2$
$f_1 = f_2$ (i.e. $\gamma_1 = \gamma_2$), and either $c_1 = \pi$ and $A_1 = +A_2$

Equation 4.19 is satisfied for all values of t and x if:

$f_1 = f_2$ (i.e. $\gamma_1 = \gamma_2$), and either $c_1 = 0$ and $A_1 = +A_2$
$f_1 = f_2$ (i.e. $\gamma_1 = \gamma_2$), and either $c_1 = \pi$ and $A_1 = -A_2$

Since the boundary conditions are not satisfied at the same time, it needs to take into account a second reflected wave: a reflected distortion plane wave (see Figure 4.12)

$$\Phi_3 = A_3 sin(pt + f_3 x - g_3 y + c_1) \tag{4.20}$$

where $f_3 = \frac{p}{\beta_2}\cos\gamma_3$, $g_3 = \frac{p}{\beta_2}\sin\gamma_3$. The deformations will be:

$$q_3 = \Phi_3 \sin(\gamma_3) \qquad w_3 = \Phi_3 \cos(\gamma_3)$$

Adding $[\lambda(\frac{\partial q_3}{\partial x}) + 2\mu(\frac{\partial w_1}{\partial y})]_{y=0}$ to equation 4.18, it results:

$$\begin{aligned}\sigma_{yy} = 0 = \tfrac{A_1}{\alpha_1}\left[\lambda + 2\mu\sin^2\gamma_1\right]\cos(pt + f_1 x) + \\ [\lambda + 2\mu\sin^2\gamma_2]\tfrac{A_2}{\alpha_1}\cos(pt + f_2 x + c_1) \\ -2\mu\tfrac{A_3}{\beta_2}\cos(pt + f_3 x + c_2)\cos\gamma_3\sin\gamma_3\end{aligned}$$

This equation can be satisfied for all values of t and x when: $f_1 = f_2 = f_3$ and $c_1 = c_2 = 0$, then $\frac{sin\gamma_1}{\alpha_1} = \frac{sin\gamma_2}{\alpha_1} = \frac{sin\gamma_3}{\beta_2}$

with $\gamma_1 = \gamma_2$, (hence $\frac{sin\gamma_1}{sin\gamma_3} = \frac{\alpha_1}{\beta_2}$), then, it results:

$$\begin{aligned}0 = \tfrac{A_1}{\alpha_1}\left[\lambda + 2\mu\sin^2\gamma_1\right]\cos(pt + f_1 x) + \\ [\lambda + 2\mu\sin^2\gamma_2]\tfrac{A_2}{\alpha_1}\cos(pt + f_1 x) \\ -2\mu\tfrac{A_3}{\beta_2}\cos(pt + f_1 x)\cos\gamma_3\sin\gamma_3\end{aligned}$$

$$0 = \tfrac{(A_1+A_2)}{\alpha_1}\left[\lambda + 2\mu\sin^2\gamma_1\right] - \mu\tfrac{A_3}{\beta_2}\sin(2\gamma_3)$$

Adding $[\mu(\frac{\partial w_3}{\partial x} + \frac{\partial q_3}{\partial y})]_{y=0}$ to equation 4.19, it results:

$$\begin{aligned}\sigma_{xy} = 0 = \tfrac{A_1}{\alpha_1}\cos(pt + f_1 x)\sin(2\gamma_1) - \tfrac{A_2}{\alpha_1}\cos(pt + f_2 x + c_1)\sin(2\gamma_2) \\ +\tfrac{A_3}{\beta_2}\cos(pt + f_3 x + c_2)(-\cos(2\gamma_3))\end{aligned}$$

This equation can be satisfied for all values of t and x when: $f_1 = f_2 = f_3$ and $c_1 = c_2 = 0$, then it results:

$$\begin{aligned}0 = \tfrac{A_1}{\alpha_1}\cos(pt + f_1 x)\sin(2\gamma_1) - \tfrac{A_2}{\alpha_1}\cos(pt + f_1 x)\sin(2\gamma_2) \\ +\tfrac{A_3}{\beta_2}\cos(pt + f_1 x)(-\cos(2\gamma_3))\end{aligned}$$

$$0 = \tfrac{(A_1-A_2)}{\alpha_1}\sin(2\gamma_1) - \tfrac{A_3}{\beta_2}\cos(2\gamma_3)$$

In addition, substituting $\mu = \rho\beta_2^2$, $\lambda = \rho\alpha_1^2 - 2\rho\beta_2^2$, and $\frac{sin\gamma_1}{sin\gamma_3} = \frac{\alpha_1}{\beta_2}$ the previous equations becomes:

$$(A_1 + A_2)\left(1 - 2\frac{\sin^2\gamma_3\cos^2\gamma_1}{\sin^2\gamma_1}\right) - 2A_3\cos\gamma_3\frac{\sin^2\gamma_3}{\sin\gamma_1} = 0 \tag{4.21}$$

$$2\cos\gamma_1 \sin\gamma_3 (A_1 - A_2) - A_3 \cos(2\gamma_3) = 0 \tag{4.22}$$

From equations 4.21 and 4.22 it is possible to obtain the amplitudes of the two reflected waves. If the incident wave is perpendicular to the free interface ($\gamma_1 = \frac{\pi}{2}$), then $A_3 = 0$ from the second equation and it results $A_1 = -A_2$.

The complete calculations for obtaining the equations above can be found in the Appendix A.3

4.5 Global Wave Propagation Phenomena

After analysing all situations of reflection and transmission phenomena separately at different types of interface in the simplified structure, the next step is to focus on the Global Wave Propagation Phenomena (G.W.P.P.). In this thesis, the expression *Global Wave Propagation Phenomena* will identify the reflection and transmission phenomena that continuously take place at the interfaces in the entire simplified structure (see Figure 2.7), as time goes on. It was decided to approach the problem starting from the easiest case. In the next sections, different types of wave propagation models will be presented by considering different assumptions. Each model will satisfy two of the following conditions:

C1. $\alpha_j = \beta_j$, with $j = 1, 2, 3, 4$

C2. $\alpha_j \neq \beta_j$, with $j = 1, 2, 3, 4$

C3. $A_j(t_i) = A_j(t_{i+1}) = A_{j+1}(t_{i+1})$, with $j = 1, 2, 3$ and $i \in N$

C4. $A_j(t_i) \neq A_j(t_{i+1}) \neq A_{j+1}(t_{i+1})$, with $j = 1, 2, 3$ and $i \in N$

Condition **C1** assumes that compression and distortion waves propagate at the same velocity in each layer j; thus, no distinction between compression and distortion waves will be done for the models which will satisfy condition **C1**. Condition **C2** distinguishes between α and β in each layer. Condition **C3** assumes there is no change in the amplitudes of the waves, whereas condition **C4** assumes a change (decrease) in the amplitudes of the waves when reflection and transmission phenomena take place at the interfaces. Notice that A represents a general term to identify a general wave amplitude. To be more precised, conditions **C3** and **C4** can be expressed for both compression and distortion waves: if Π_j represents the amplitude of compression waves in layer j, and P_j represents the amplitude of distortion waves in layer j, then it results:

C3a. $\Pi_i^{(j)} = \Pi_r^{(j)} = \Pi_{tr}^{(j+1)}$, with $j = 1, 2, 3$
C3b. $P_i^{(j)} = P_r^{(j)} = P_{tr}^{(j+1)}$, with $j = 1, 2, 3$

C4a. $\Pi_i^{(j)} \neq \Pi_r^{(j)} \neq \Pi_{tr}^{(j+1)}$, with $j = 1, 2, 3$
C4b. $P_i^{(j)} \neq P_r^{(j)} \neq P_{tr}^{(j+1)}$, with $j = 1, 2, 3$

If condition **C3a** is applied to the layers L1 and L2, then it results: $\Pi_i^{(1)} = \Pi_r^{(1)} = \Pi_{tr}^{(2)}$ that means the amplitudes of incident compression wave $\Pi_i^{(1)}$, of reflected compression wave $\Pi_r^{(1)}$, and of transmitted compression wave $\Pi_{tr}^{(2)}$ are the same. Notice that the incident compression wave will exist at an instant of time t_n whereas both reflected and transmitted waves will exist at another instant of time, for instance, t_{n+1}, with $n \in N$. The purpose of each of the following sections is to show a wave propagation model for partial/entire structure, based on conditions **C1-C4**, with respect to time. After evaluating all scenarios, the most suitable final global wave propagation phenomena model will be chosen.

In order to express the wave propagation phenomena with respect to time, the *compression propagation-time* (t_{α_j}) and the *distortion propagation-time* (t_{β_j}) need to be considered. For each model all propagation-times for compression and distortion waves in each layer will be expressed in terms of t_{α_1}. t_{α_j} and t_{β_j} represent the time needed by compression and distortion waves respectively, in layer j, to reach the next interface. The numerical approximations of the propagation times, and compression and distortion velocities can be found in Appendix A.2.

Furthermore, Figure 4.13 shows the concepts of *I order wave propagation phenomena* (in green) and *II order wave propagation phenomena* (in orange). To understand the difference between I and II order wave propagation phenomena, consider the following examples related to Figure 4.13: when the incident compression wave (ICW1) impinges on interface 1 (I1), then a reflected compression wave (RCW1) in L1 and a transmitted compression wave (TCW2) in L2 are generated; this is an example of I order wave propagation phenomena. When the incident compression wave ($TCW2 = ICW2$) in L2 impinges on the interface 2 (I2), then a reflected compression wave (RCW2) and a transmitted compression wave (TCW3) are generated; this is another example of I order wave propagation phenomena. When the RCW2 travels back in L2 and impinges on the interface 1 (I1), a new reflected compression wave (RCW1') and a new transmitted compression wave (TCW2') are generated; this is an example of II order wave propagation phenomena. Notice that in order to simplify the explanation, the generation of reflected and transmitted distortion waves has been omitted, but the same considerations are also valid for distortion waves.

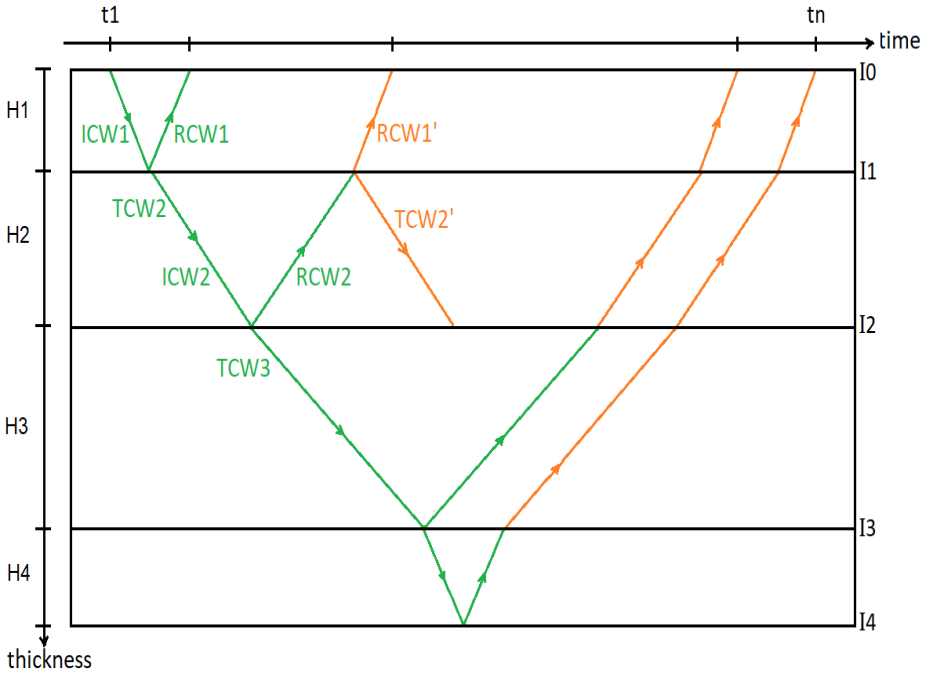

Figure 4.13: I order wave propagation phenomena (in green) and II order wave propagation phenomena (in orange).

The following sections will introduce different models by considering conditions **C1**-**C4**. Notice that the wave propagation velocities will be expressed in function of the compression velocity α_1, and the same will be done for the wave propagation-times that will be expressed in function of t_{α_1}.

Based on the conditions **C1**-**C4**, each section will provide different types of graphs, where time t in seconds will be on the horizontal axis, whereas the thickness of each layer will be on the vertical axis; for better showing the wave-paths and the waves amplitudes, the thicknesses H_j, with $j = 1, 2, 3, 4$, will not be to scale. The consequence is a rather large thickness for top and back plywood (L1 and L4). However, in all graphs it will be respected the following condition:

$$H_3 > H_2 > H_1,\ H_4$$

4.5.1 G.W.P.P. for L1 and L2, with C1 and C3

The case analysed in this section will be identified as **GWPP1**.

The analysis of the global wave propagation phenomena begins by considering the easiest case: two layers (top plywood and primary RPUF) with three interfaces (I0, I1, I2), assuming the same wave propagation velocities ($\alpha_j = \beta_j$, for $j = 1, 2$). Thus, the G.W.P.P. model for L1 and L2, with conditions **C1** and **C3** will be discussed.

For this case, only compression velocities (α_1, α_2) will be considered. In order to build the wave propagation model in function of the same parameters, α_2 and t_{α_2} will be expressed in function of α_1 and t_{α_1}, respectively. Thus, it results:

- $\alpha_1 = \beta_1, \qquad \alpha_2 = \beta_2$
- $\Pi_i^{(1)} = \Pi_r^{(1)} = \Pi_{tr}^{(2)} = P_i^{(1)} = P_r^{(1)} = P_{tr}^{(2)}$
- $\alpha_2 \simeq 0.25 \cdot \alpha_1, \qquad t_{\alpha_2} \simeq 30 \cdot t_{\alpha_1}$

The following two graphs describe the relationship between the propagation phenomena in L1 and L2 with respect to time. Notice that both Figures 4.14 and 4.15 do not provide any information about the shape of the waves; the straight lines represent the wave path with respect to time, namely, how many times the wave generated by the source (in red) is subjected to reflection and transmission phenomena at the interfaces.

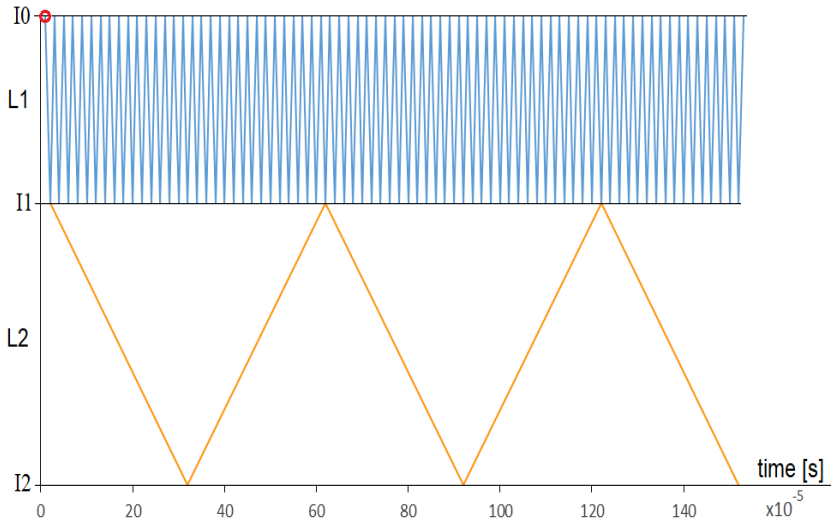

Figure 4.14: Waves-path for L1 and L2 without II order wave propagation phenomena.

Figure 4.14 does not take into account the II order wave propagation phenomena; the incident compression wave is reflected (represented by the wave-path in blue) in L1, and transmitted (represented by the wave-path in orange) in L2. Notice that only the wave-path due to the first transmitted wave has been represented in L2. Due to the large thickness that distinguishes the top plywood and the primary RPUF, the number of reflections in L1 will be higher that those in L2 in terms of time. The incident compression wave in L2 (ICW2) will need $30 \cdot t_{\alpha_1}$ to reach the interface 2. This means that if ICW1 is reflected and transmitted at $t = t_2$, then the transmitted (incident) compression wave in L2 (ICW2) will be reflected (and transmitted) at $t = t_{32}$. Figure 4.15 includes the II order wave propagation phenomena. Notice that the wave represented by the wave-path in yellow in L1, due to the impinging of the reflected back compression wave (RCW2) on interface 1 overlaps with the wave represented by the wave-path in blue. It happens again at $t = t_{122}$ (in green).

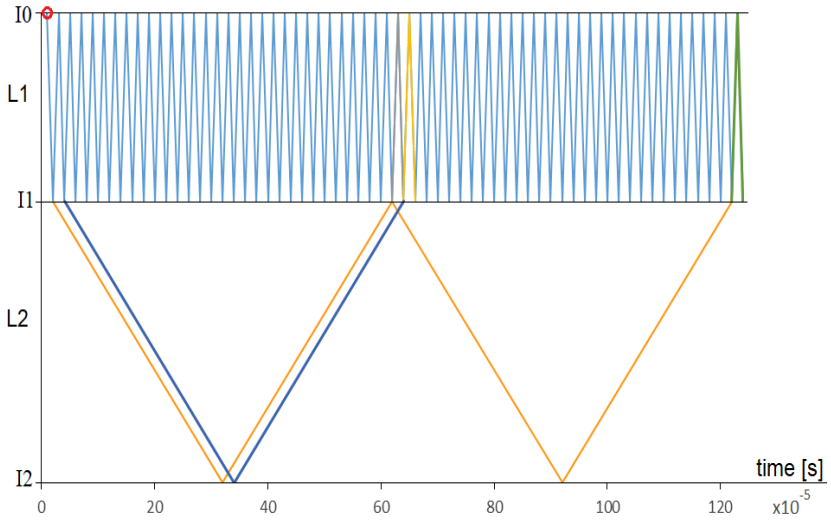

Figure 4.15: Wave-path for L1 and L2 with II order wave propagation phenomena.

If only the I order wave propagation phenomena are considered, then it is possible to express mathematically the number of each type of wave, as time goes on, as follows:

$$N_{ICW1} = 2^{2n+1}|_{t=2n+3} \qquad N_{IDW1} = 2^{2n+1}|_{t=2n+3} \qquad n \in N$$
$$N_{RCW1} = 2^{2n}|_{t=2n+2} \qquad N_{RDW1} = 2^{2n}|_{t=2n+2} \qquad n \in N$$
$$N_{ICW2} = 2^{2n}|_{t=2n+2} \qquad N_{IDW2} = 2^{2n}|_{t=2n+2} \qquad n \in N$$
$$N_{RCW2} = 2^{2n+1}|_{t=2n+32} \qquad N_{RDW2} = 2^{2n+1}|_{t=2n+32} \qquad n \in N$$

At each instant of time, it is possible to calculate the exact number of waves in both layers. It has been calculated the exact number of waves in L1 and L2 as a consequence of the continuous reflection and transmission phenomena that occur at the interfaces. The next graphs show the relationship between the number of each type of wave with time. It has been chosen to show the waves of the same type in the same graph. Notice that the number of each type of wave increases exponentially in both layers. Specifically, in Figures 4.16 and Figure 4.18 the number of waves starts increasing largely around t_{40}; indeed, around this instant of time, the II order wave propagation phenomena take place and there is an overlapping of the same waves. Looking at graphs on the left (Figures 4.16, 4.18 and 4.20), it might seem that in the interval $t_{40} - t_1$ the number of waves is zero; actually, the number of waves after t_{40} is much larger than that before t_{40} and it can seem that there is no wave before instant t_{40}. To clarify this possible misunderstanding, the same situations are shown in the graphs on the right but for smaller intervals of time. From $t = t_1$ in ahead, there are waves in L1. The same considerations are valid for the other graphs.

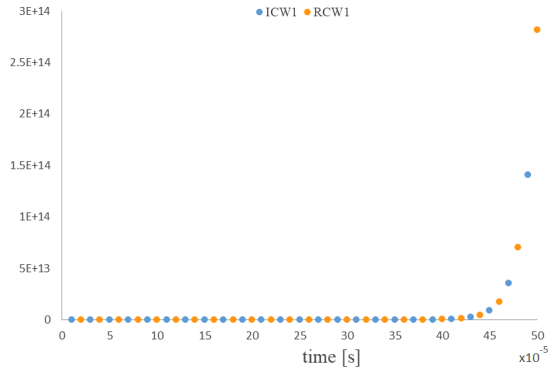

Figure 4.16: Number of incident and reflected compression waves in L1 for $\Delta t = 50$ s.

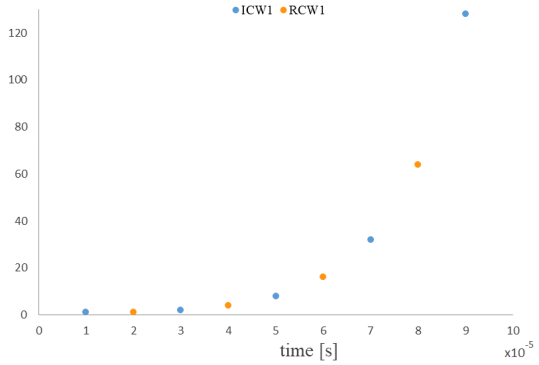

Figure 4.17: Number of incident and reflected compression waves in L1 for $\Delta t = 10$ s.

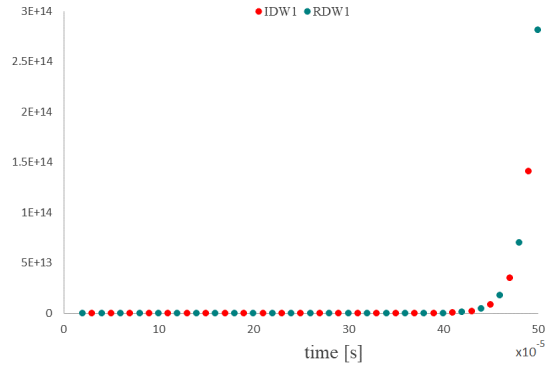

Figure 4.18: Number of incident and reflected distortion waves in L1 for $\Delta t = 50$ s.

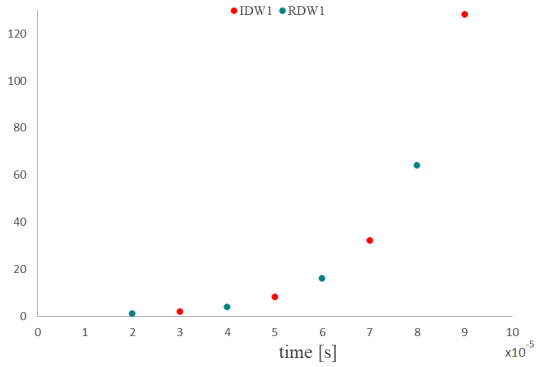

Figure 4.19: Number of incident and reflected distortion waves in L1 for $\Delta t = 10$ s.

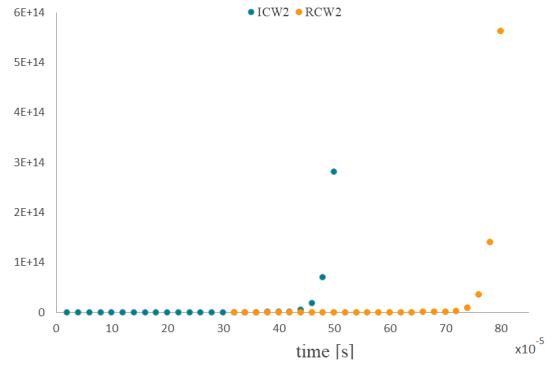

Figure 4.20: Number of incident and reflected compression waves in L2 for $\Delta t = 80$ s.

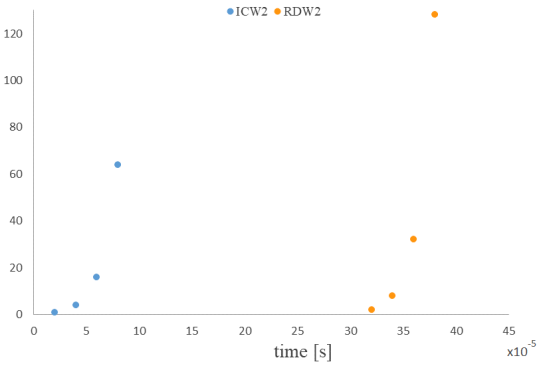

Figure 4.21: Number of incident and reflected compression waves in L2 for $\Delta t = 45$ s.

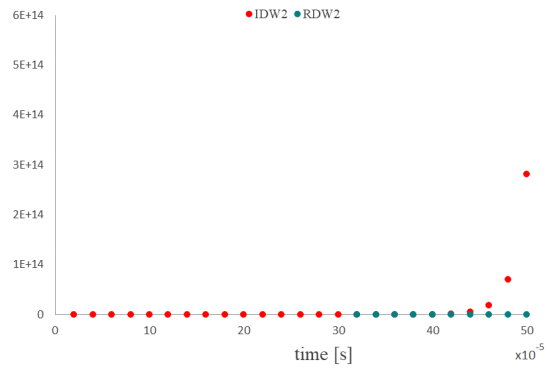

Figure 4.22: Number of incident and reflected distortion waves for $\Delta t = 50$ s.

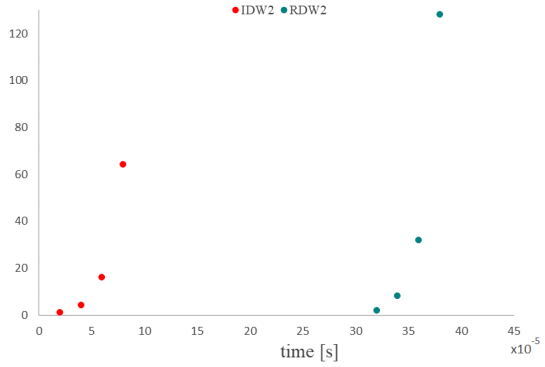

Figure 4.23: Number of incident and reflected distortion waves for $\Delta t = 45$ s.

It is possible to conclude that the number of each type of wave will increase exponentially as time goes on and it will reach the highest value in the last instant of time in the interval considered.

4.5.2 G.W.P.P. for L1 and L2, with C1 and C4

The case analysed in this section will be identified as **GWPP2**.

The model introduced in Section 4.5.1 was based on condition **C1**, namely it was considered no distinction between compression and distortion propagation velocities, and it was also assumed no change in the amplitudes of the waves. The main difference in this case will concern condition **C4**. It will be supposed a decrease in the amplitudes after an incident wave is reflected and transmitted at the interface. First, of all, the conditions valid for **GWPP2** are:

- $\alpha_1 = \beta_1, \qquad \alpha_2 = \beta_2$
- $\Pi_i^{(1)} \neq \Pi_r^{(1)} \neq \Pi_{tr}^{(2)} \neq P_i^{(1)} \neq P_r^{(1)} \neq P_{tr}^{(2)}$
- $\alpha_2 \simeq 0.25 \cdot \alpha_1, \qquad t_{\alpha_2} \simeq 30 \cdot t_{\alpha_1}$

For this case, attention will be only focused on the change in the amplitudes, and neither wave-paths without/with II order wave propagation phenomena nor graphs with the total number of each type of wave will be provided.

Since condition **C1** is still valid for this case, only compression waves will be taken into account. In order to show the change in the amplitude of both incident and reflected compression waves, the amplitude will be assumed composed by a constant value $A_{type}^{(j)}$ ($A_i^{(1)}$ for incident wave in L1, $A_r^{(1)}$ for reflected waves in L1, $A_i^{(2)}$ for incident wave in L2, and $A_r^{(2)}$ for reflected waves in L2), and an exponential term $e^{-\frac{t}{\tau_j}}$, where $\frac{1}{\tau_j}$ is the damping factor. Thus, $A_{type,tot}^{(j)} = A_{type}^{(j)} e^{-\frac{t}{\tau_j}}$.

The following graphs show the decrease in the amplitude of each type of wave.

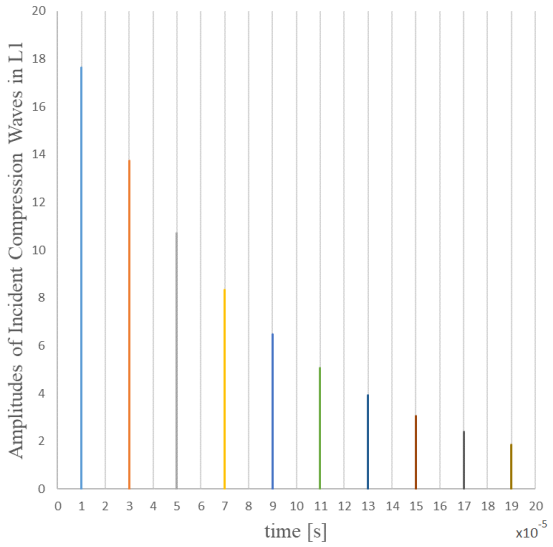

Figure 4.24: Change in amplitude for incident compression waves in L1, for $\Delta t = 20$ s.

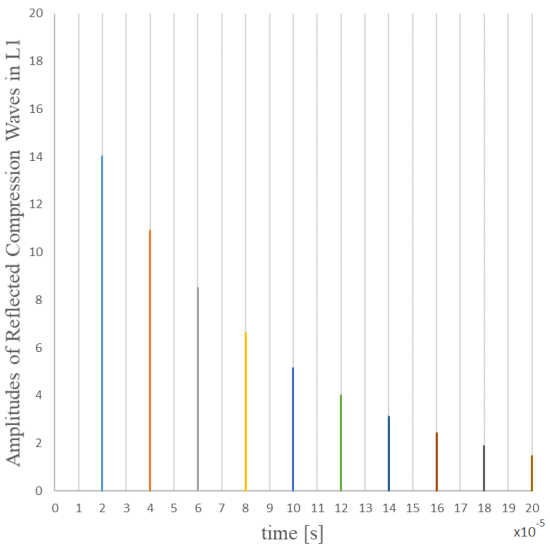

Figure 4.25: Change in amplitude for reflected compression waves in L1, for $\Delta t = 20$ s.

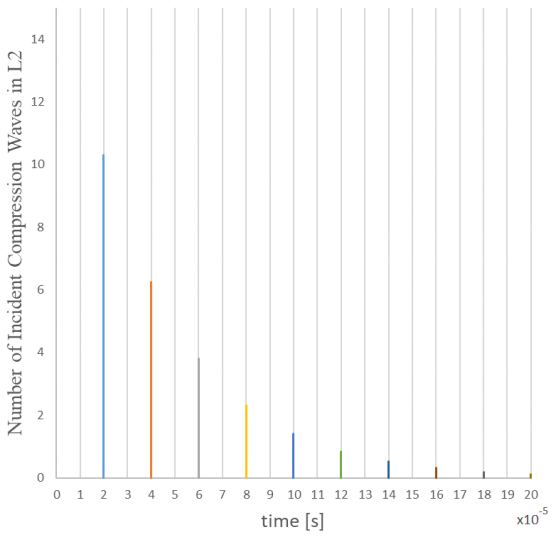

Figure 4.26: Change in amplitude for incident compression waves in L2, for $\Delta t = 20$ s.

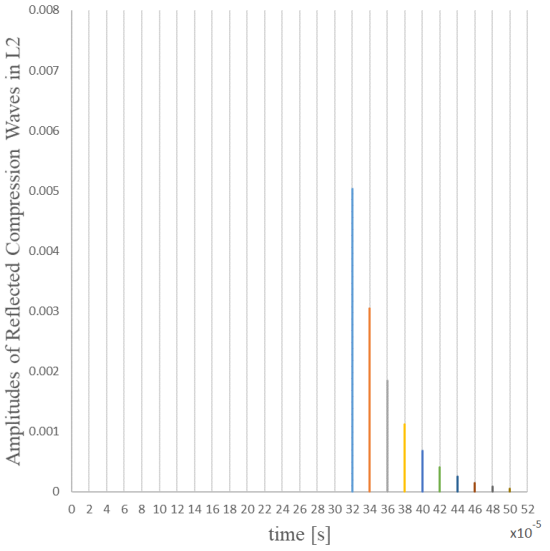

Figure 4.27: Change in amplitude for reflected compression waves in L1, for $\Delta t = 52$ s.

For this case, arbitrary values have been chosen but taking into account that the amplitude of the incident wave is bigger than the amplitudes of reflected and transmitted waves:

$$A^{(1)}_{i,tot} > A^{(1)}_{r,tot}, \quad A^{(2)}_{tr,tot}$$

$$A^{(2)}_{i,tot} = A^{(2)}_{tr,tot} > A^{(2)}_{r,tot}$$

It was chosen the same value of damping for L1 and L4, and the same value of damping for L2 and L3, supposing that the decrease in the amplitudes is the same in the layers of the same material. Notice that an interval of time of $\Delta t = 20s$ has been considered for the first three graphs, but in the last case a larger interval of time was taken into account because reflected compression waves start traveling back in L2 only from t_{32}. On the vertical axis of graphs in Figures 4.24-4.27 the numerical values of $A^{(j)}_{type,tot}$, with $j = 1, 2$ are displayed.

Figure 4.28 shows the decrease of the amplitudes for incident and reflected compression waves in L1 and L2. It was chosen an interval of $\Delta t = 20s$ for incident, reflected and transmitted compression waves in L1 and an interval $\Delta t = 50s$ for reflected compression waves in L1. This picture has the purpose to show the decrease of the wave amplitudes after each reflection and transmission at the interfaces. Notice that the amplitudes of RCW2 in L2 are much smaller than the amplitudes of the incident waves ICW2.

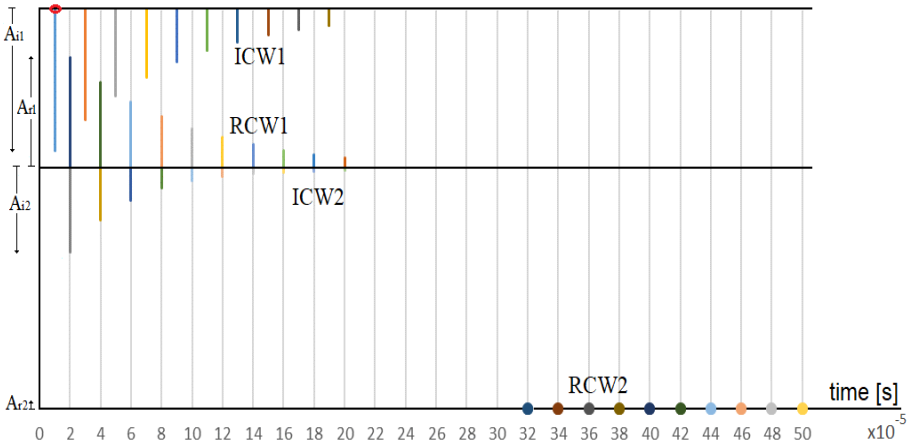

Figure 4.28: Decrease in the amplitude of incident, reflected and transmitted compression waves in L1 and L2.

4.5.3 G.W.P.P. for L1 and L2 with C2 and C3

The case analysed in this section will be identified as **GWPP3**.

The main difference between the model that is going to be introduced in this section and the model of Section 4.5.1 is the distinction between compression and distortion velocities. In order to provide a global wave wave propagation phenomena model according to conditions **C2** and **C3**, some additional simplifications need to be done. First of all, the conditions valid for this case are:

- $\alpha_1 \neq \beta_1, \qquad \alpha_2 \neq \beta_2$
- $\Pi_i^{(1)} = \Pi_r^{(1)} = \Pi_{tr}^{(2)} = P_i^{(1)} = P_r^{(1)} = P_{tr}^{(2)}$
- $\alpha_2 \simeq 0.25 \cdot \alpha_1, \qquad \beta_1 \simeq 0.6 \cdot \alpha_1, \qquad \beta_2 \simeq 0.15 \cdot \alpha_1$
- $t_{\alpha_2} \simeq 30 \cdot t_{\alpha_1}, \qquad t_{\beta_1} \simeq 2.0 \cdot t_{\alpha_1} \qquad t_{\beta_2} \simeq 50 \cdot t_{\alpha_1}$

If only the first layer (L1) is considered, then the wave propagation phenomena (incidence and reflection between interface 0 and interface 1) can be seen in Figure 4.29. The concentration of waves increases with time because every single wave that impinges on an interface generates two additional waves (compression and distortion); in turn, each of them will generate new couples of waves at different instants of time. Furthermore, it is important to notice that from $t = t_5$ the waves of the same type but generated by different waves (namely a reflected compression wave generated by an incident compression wave and a reflected compression wave generated by an incident distortion wave) start overlapping. This kind of superposition will occur often as time goes on. Different colours have been used to show the superposition of the waves, but basically there are only two types of waves in L1, compression and distortion waves.

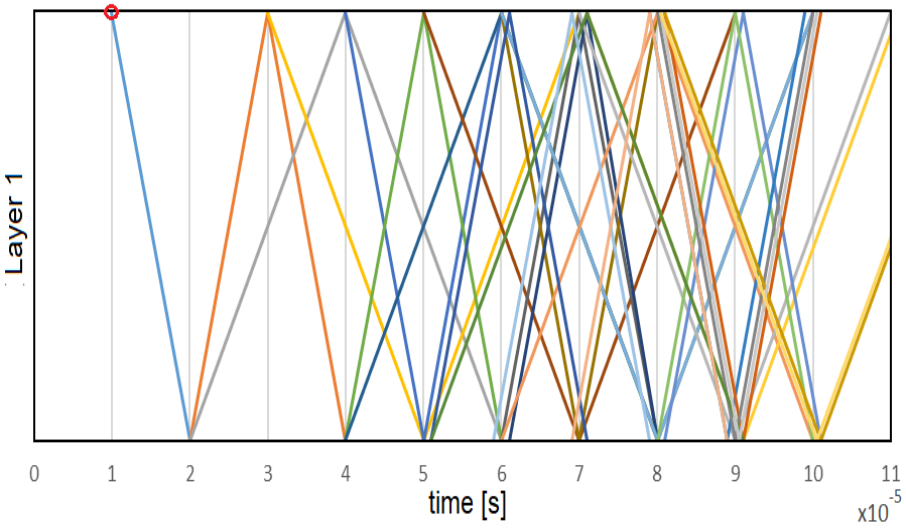

Figure 4.29: Compression and distortion waves in layer 1 for $\Delta t = 10$ s.

Figure 4.30 shows both compression and distortion waves in L1 and L2 without including II order wave propagation phenomena, and without considering the continuous generation of compression and distortion waves at the interfaces. This means it is shown only the path of the waves generated at the beginning. Figure 4.31 includes the II order wave propagation phenomena. Notice that in the first layer there is an overlapping of both compression and distortion waves at the instants of time when the reflected waves in the second layer reach interface 1 and are transmitted.

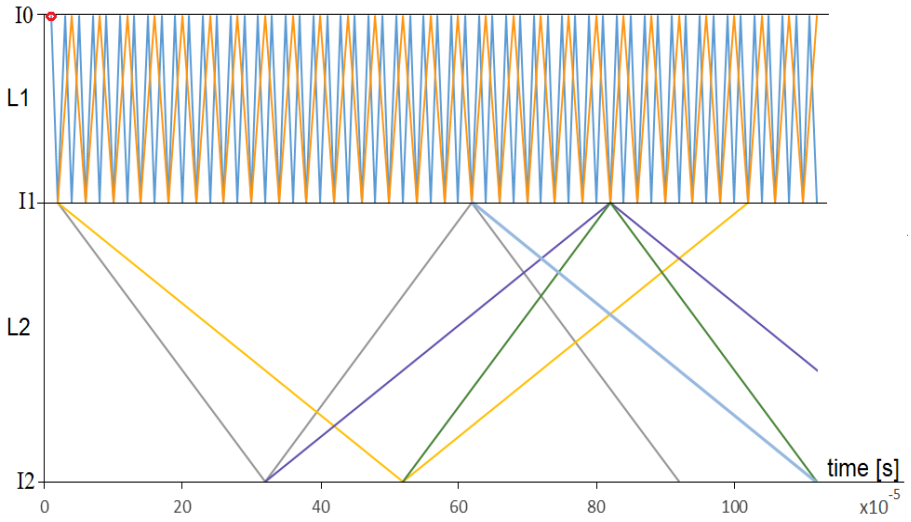

Figure 4.30: Wave-path for L1 and L2 without II order Wave propagation phenomena

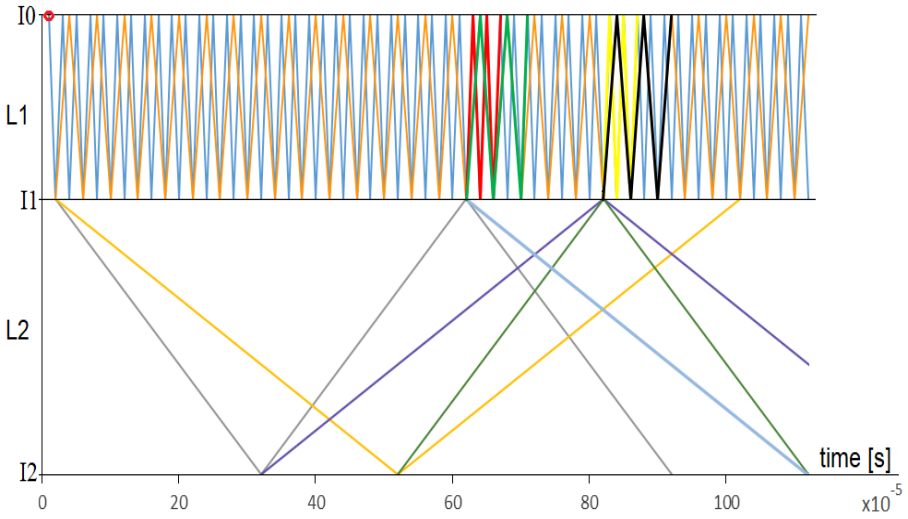

Figure 4.31: Wave-path for L1 and L2 with II order Wave propagation phenomena

Due to the complexity of the propagation phenomena, it has been decided to calculate the exact number of waves in L1 only for the first seventeenth instants of time, and then evaluating the propagation phenomena in the next layer as a consequence

of waves developed in the interval of time $\Delta t = t_{17} - t_1$. The following graphs show the exact number of incident compression/distortion waves and reflected compression/distortion waves, respectively, in L1 and L2. From the graphs below, it is possible to notice an exponential increase in the number of each type of wave as time goes on. In Figure 4.34 there are some intervals of time such as $(t_{64} - t_{16})$ where no wave travels in L2; basically, waves develop and travel through L2 also in these instants of time but in this case they are missing because the propagation phenomena have been considered only in $\Delta t = t_{17} - t_1$. In summary, Figures 4.32 and 4.33 show the exact number of a group of waves developed in the first seventeenth seconds in L1, and therefore, Figures 4.34 and 4.35 show the exact number of waves developed as a consequence of the waves generated in $\Delta t = t_{17} - t_1$.

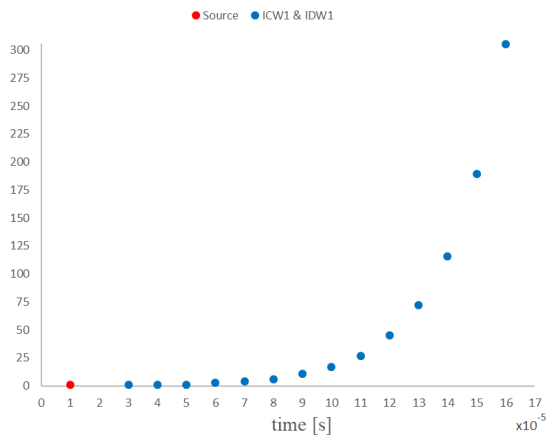

Figure 4.32: Number of incident compression and distortion waves in L1 for $\Delta t = 17$ s.

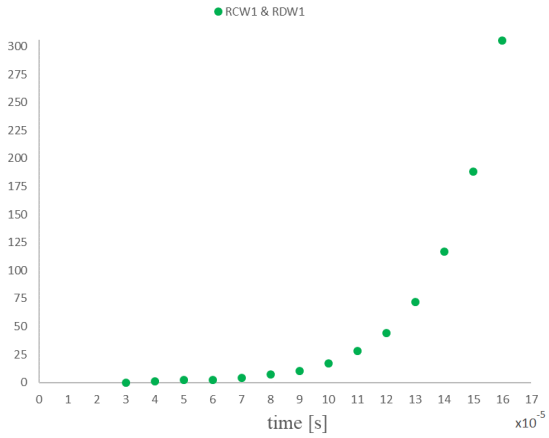

Figure 4.33: Number of reflected compression and distortion waves in L1 for $\Delta t = 17$ s.

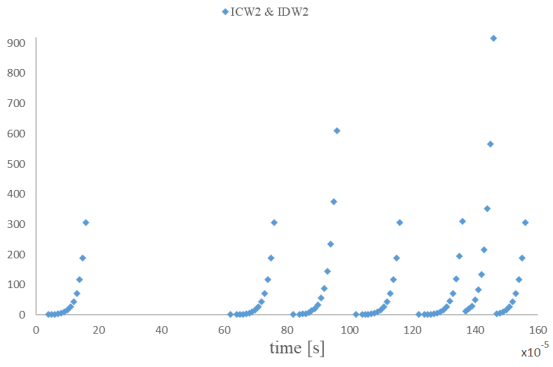

Figure 4.34: Number of incident compression and distortion waves in L2 for $\Delta t = 160$ s.

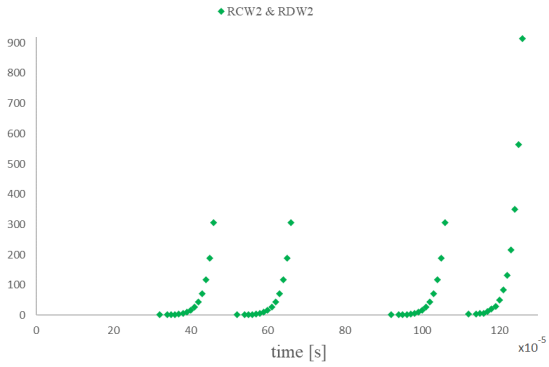

Figure 4.35: Number of reflected compression and distortion waves in L2 for $\Delta t = 130$ s.

4.5.4 G.W.P.P. for L1 and L2 with C2 and C4

The case analysed in this section will be identified as **GWPP4**.

In this section, the last case related to L1 and L2 will be considered. Since conditions **C2** and **C4** are valid, compression and distortion waves will be distinguished as in Section 4.5.3, and it will be assumed a decrease in the amplitudes of both compression and distortion incident/reflected waves in L1 and L2. The conditions valid for **GWPP4** are:

- $\alpha_1 \neq \beta_1, \qquad \alpha_2 \neq \beta_2$
- $\Pi_i^{(1)} \neq \Pi_r^{(1)} \neq \Pi_{tr}^{(2)} \neq P_i^{(1)} \neq P_r^{(1)} \neq P_{tr}^{(2)}$
- $\alpha_2 \simeq 0.25 \cdot \alpha_1, \qquad \beta_1 \simeq 0.6 \cdot \alpha_1, \qquad \beta_2 \simeq 0.15 \cdot \alpha_1$
- $t_{\alpha_2} \simeq 30 \cdot t_{\alpha_1}, \qquad t_{\beta_1} \simeq 2.0 \cdot t_{\alpha_1} \qquad t_{\beta_2} \simeq 50 \cdot t_{\alpha_1}$

Also for this case, attention will be only focused on the change in the amplitudes, and neither wave-paths without/with II order wave propagation phenomena nor graphs with the total number of each type of wave will be provided.

Only graphs of the amplitudes related to the distortion waves will be shown because the graphs for compression waves are the same as those in Section 4.5.2 (**GWPP2**). Each amplitude will be assumed composed by a constant value $A_{type}^{(j)}$ ($A_i^{(1)}$ for incident wave in L1, $A_r^{(1)}$ for reflected waves in L1, $A_i^{(2)}$ for incident wave in L2, and $A_r^{(2)}$ for reflected waves in L2), and an exponential term $e^{-\frac{t}{\tau_j}}$, where $\frac{1}{\tau_j}$ is the damping factor. The following graphs show the decrease in the distortion wave amplitude for L1 and L2.

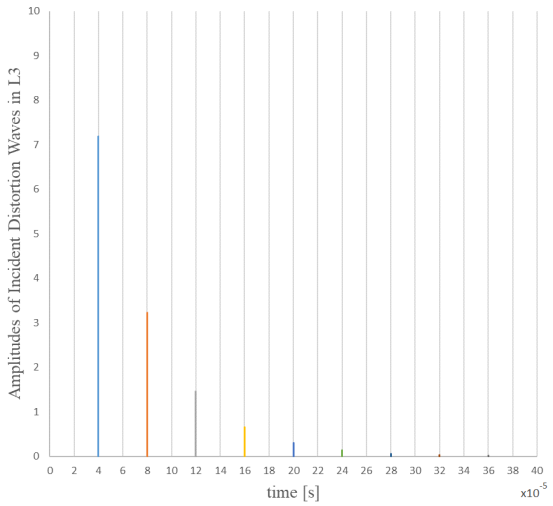

Figure 4.36: Change in amplitude for incident distortion waves in L3, for $\Delta t =$ 40 s.

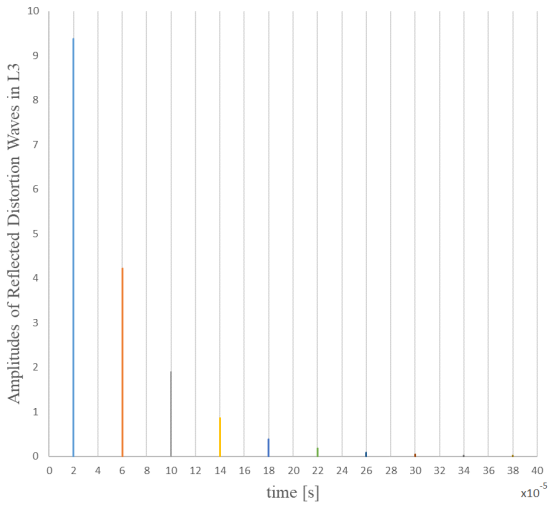

Figure 4.37: Change in amplitude for reflected distortion waves in L3, for $\Delta t =$ 40 s.

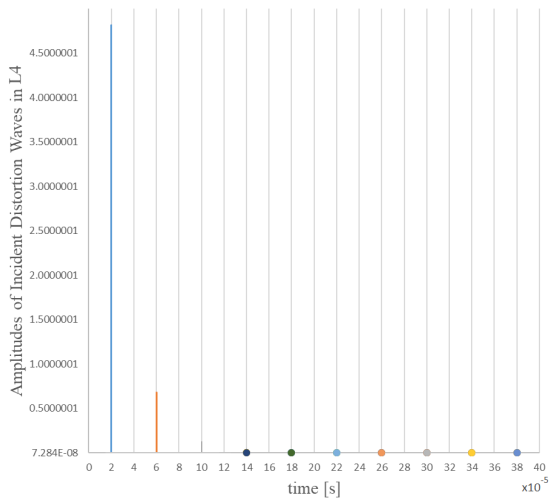

Figure 4.38: Change in amplitude for incident distortion waves in L4, for $\Delta t = 40$ s.

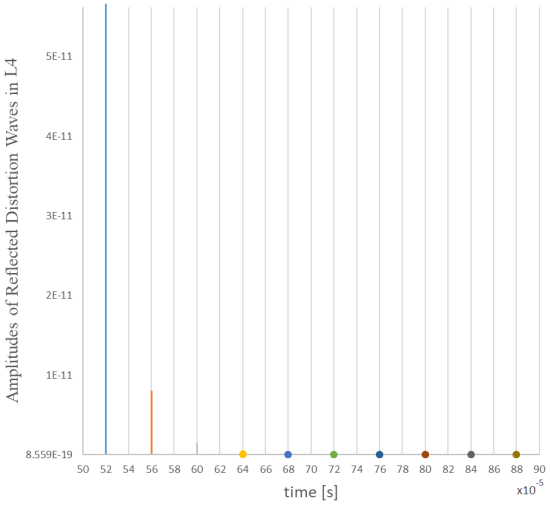

Figure 4.39: Change in amplitude for reflected distortion waves in L4, for $\Delta t = (90 - 50)$ s.

As done for **GWPP2**, arbitrary values have been chosen but taking into account that the amplitude of the generated waves are smaller than the amplitude of the impinging wave. Looking at the graphs in Figures 4.36-4.37, the first amplitude of the incident distortion wave is smaller than the first amplitude of the reflected distortion wave; the reason is that the first incident distortion wave (IDW1) is generated at interface I0 from the first reflected distortion wave (RDW1). Indeed, the RDW1 starts propagating at t_2 whereas the IDW1 is generated and propagates at t_4 (see Figure 4.40 where compression waves, in blue, and distortion waves, in red, are shown in L1).

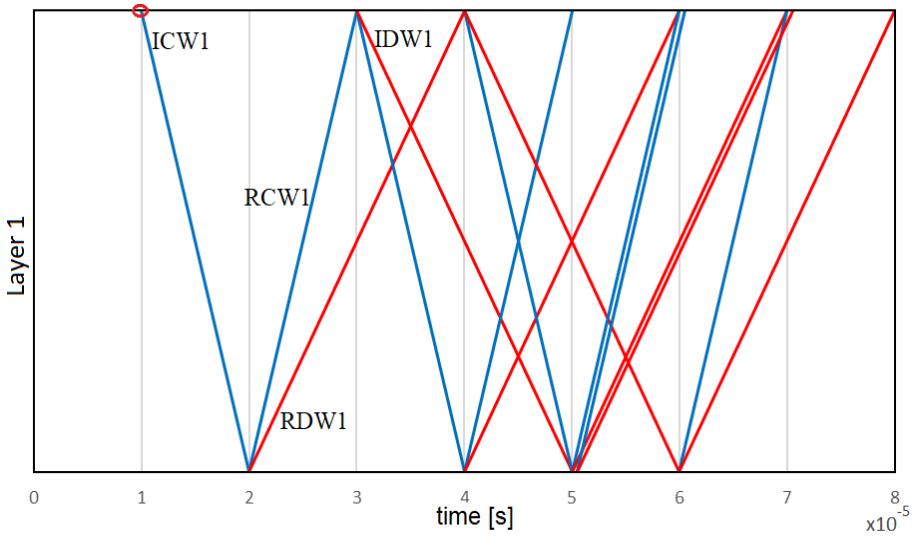

Figure 4.40: Waves-Path in L1 for $\Delta t = t_6 - t_1$

Thus, in this case, for the interval considered, it results:

$$A^{(1)}_{r,tot} > A^{(1)}_{i,tot}$$
$$A^{(2)}_{i,tot} = A^{(2)}_{i,tot} > A^{(2)}_{r,tot}$$

Notice that the amplitudes of the distortion waves are very small compared to the first one in Figures 4.38-4.39.

In addition, it was chosen the same value of damping for L1 and L4, and the same value of damping for L2 and L3, supposing that the decrease in the amplitudes is the same in the layers of the same material. Notice that an interval of time of $\Delta t = 40s$ has been considered for the first three graphs, and for the last graph an interval of $\Delta = 90 - 50$ has been taken into account because reflected distortion waves start traveling back later in L2. On the vertical axis of graphs in Figures 4.36-4.39 the numerical values of $A^{(j)}_{type,tot}$, with $j = 1, 2$ are displayed.

Figure 4.41 shows the decrease of the amplitudes for incident and reflected distortion waves in L1 and L2. The decrease for compression waves was already discussed in Section 4.5.2. It was chosen an interval of $\Delta t = 40s$ for incident, reflected (in L1) and transmitted (in L2) distortion wave and an interval $\Delta t = (88-50)s$ for reflected distortion waves in L1. Also this picture has the purpose to show the decrease of the wave amplitudes after each reflection and transmission at the interfaces. Notice that the amplitudes decrease faster because it was chosen a damping factor for distortion waves larger than that chosen for compression waves.

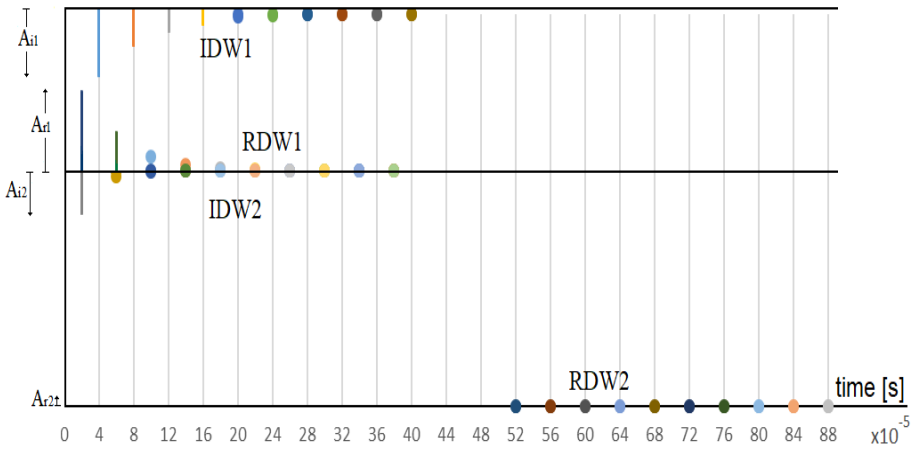

Figure 4.41: Decrease in the amplitude of incident, reflected and transmitted distortion waves in L1 and L2.

4.5.5 G.W.P.P. for Lj with C1 and C3

The case analysed in this section will be identified as **GWPP5**.

The model that will be presented in this section can be considered as the complete case of model introduced in Section 4.5.1. Thus, the same conditions used in the **GWPP1** will be valid for this case. It results:

- $\alpha_1 = \beta_1 \qquad \alpha_2 = \beta_2 \qquad \alpha_3 = \beta_3 \qquad \alpha_4 = \beta_4$
- $\Pi_i^{(j)} = \Pi_r^{(j)} = \Pi_{tr}^{(j+1)} = P_i^{(j)} = P_r^{(j)} = P_{tr}^{(j+1)}, \quad \text{with } j = 1, 2, 3$
- $\alpha_2 \simeq 0.25 \cdot \alpha_1 \qquad \alpha_3 \simeq 0.25 \cdot \alpha_1 \qquad \alpha_4 \simeq 1.00 \cdot \alpha_1$
- $t_{\alpha_2} \simeq 30 \cdot t_{\alpha_1} \qquad t_{\alpha_3} \simeq 56 \cdot t_{\alpha_1} \qquad t_{\alpha_4} \simeq 1.00 \cdot t_{\alpha_1}$

The following figures show the relationship between the propagation phenomena and time for the entire structure. Notice that L1 and L4 have the same characteristic properties and the same thickness, therefore the behaviour and wave-path is the same. The same consideration is also valid for L2 and L3 which have the same material characteristics. Due to the large thickness of L2 and L3, few waves will be reflected and transmitted because the propagation times of both compression and distortion waves (that coincide) are large: the propagation time t_{α_3} in L3 is the around 56 times bigger than t_{α_1}. Figure 4.42 considers only I order wave propagation phenomena, whereas Figure 4.43 shows both I and II order wave propagation phenomena; the reflected waves at the bottom will be transmitted back in the other layers until impinging on the free boundary in L1. The II order wave propagation phenomena increase the number of waves in each layer.

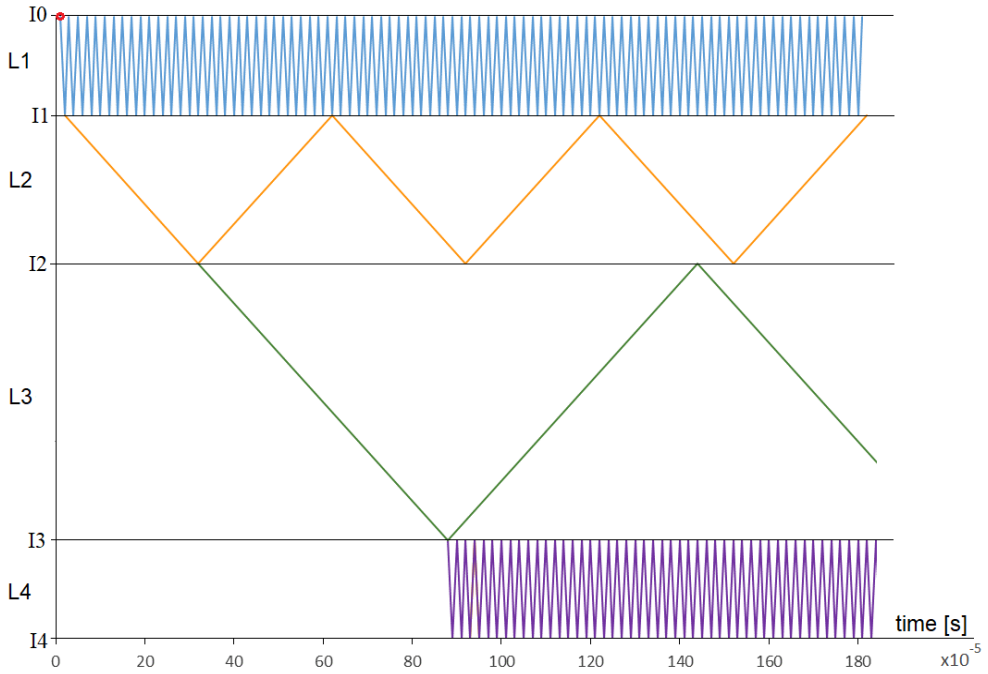

Figure 4.42: Wave-Path for L_j without II order wave propagation phenomena.

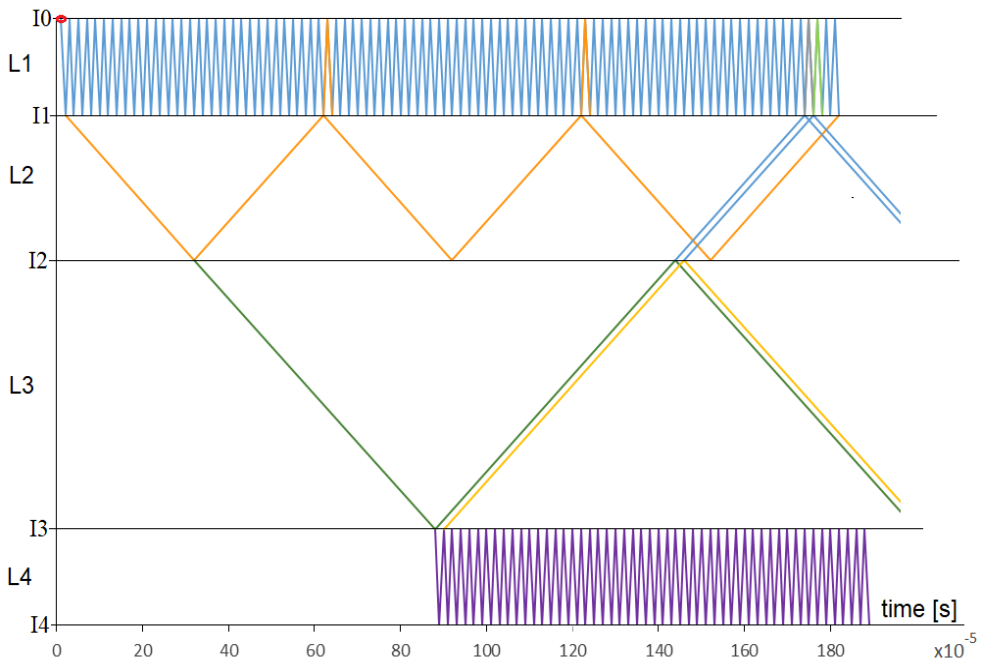

Figure 4.43: Wave-Path for L_j with II order wave propagation phenomena.

Figures 4.42 and 4.43 are the complete case of Figure 4.14 and 4.15, respectively. As mentioned before, the waves in L3 need $t_{\alpha_3} = 56 \cdot t_{\alpha_1}$, whereas the waves in L4 travel at the same velocity of α_1 and therefore $t_{\alpha_4} = t_{\alpha_1}$. If only the I order wave propagation phenomena are considered, it is possible to express mathematically the number of each type of wave as time goes on:

$$N_{ICW1} = N_{IDW1} = 2^{2n+1}|_{t=2n+3} \quad n \in N$$
$$N_{RCW1} = N_{RDW1} = 2^{2n}|_{t=2n+2} \quad n \in N$$
$$N_{ICW2} = N_{IDW2} = 2^{2n}|_{t=2n+2} \quad n \in N$$
$$N_{RCW2} = N_{RDW2} = 2^{2n+1}|_{t=2n+32} \quad n \in N$$
$$N_{ICW3} = N_{IDW3} = 2^{2n+1}|_{t=2n+32} \quad n \in N$$
$$N_{RCW3} = N_{RDW3} = 2^{2n+2}|_{t=2n+88} \quad \text{n} \in N$$
$$N_{ICW4} = N_{IDW4} = 2^{2n+2}|_{t=2n+88} \quad \text{n} \in N$$
$$N_{RCW4} = N_{RDW4} = 2^{2n+3}|_{t=2n+89} \quad \text{n} \in N$$

The following graphs show the exact number of waves in all layers. There is still an exponential increase in the number of each type of waves in all layers. The development of waves in the last two layers occurs later compared to the development of waves in L1 and L2 because waves in L3 and L4 are only a consequence of those in L2 and L1.

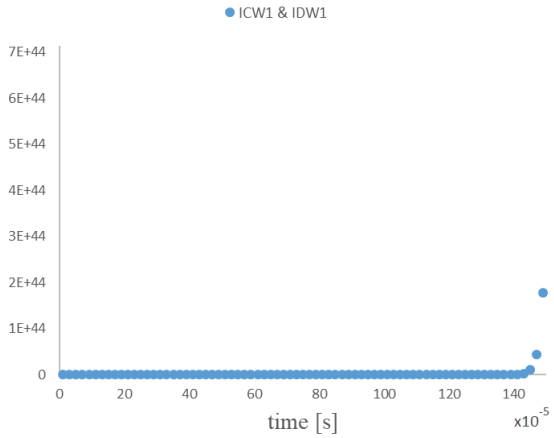

Figure 4.44: Number of incident compression and distortion waves in L1 for $\Delta t = 150$ s.

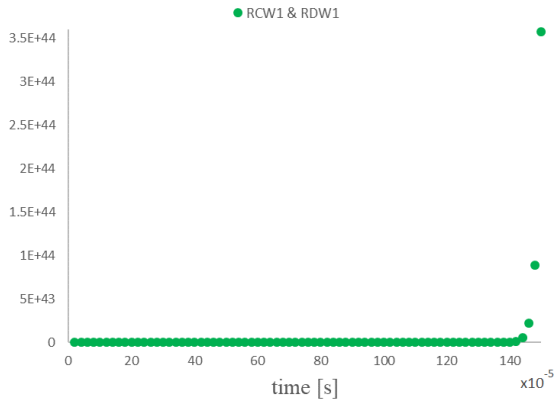

Figure 4.45: Number of reflected compression and distortion waves in L1 for $\Delta t = 150$ s.

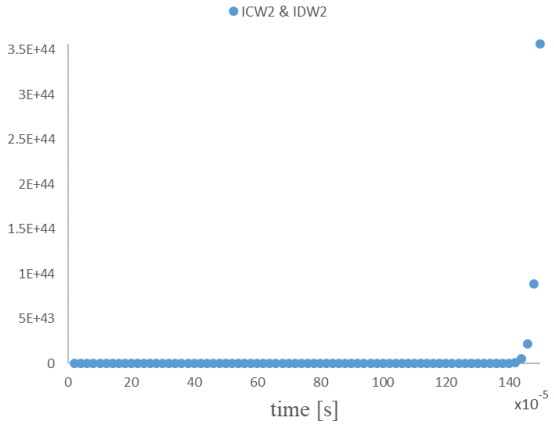

Figure 4.46: Number of incident compression and distortion waves in L2 for $\Delta t = 150$ s.

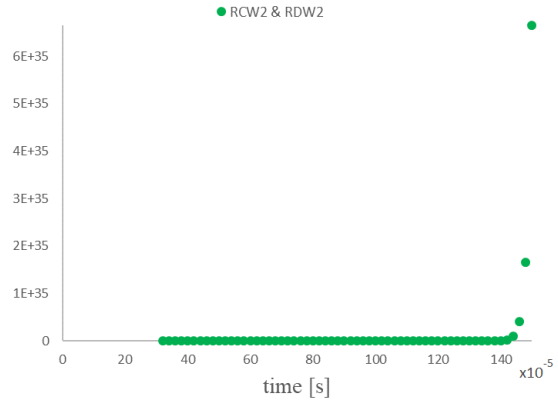

Figure 4.47: Number of reflected compression and distortion waves in L2 for $\Delta t = 150$ s.

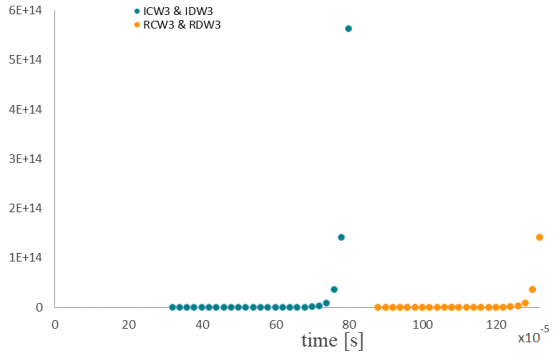

Figure 4.48: Number of incident /reflected compression/distortion waves in L3 for for $\Delta t = 130$ s.

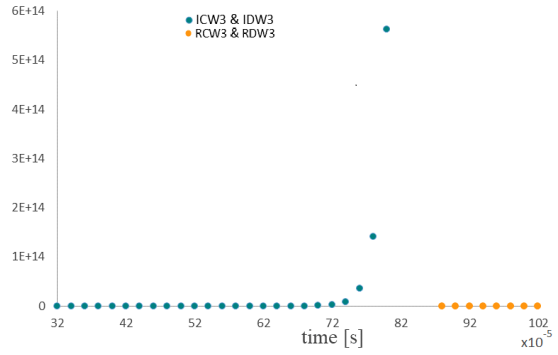

Figure 4.49: Number of incident /reflected compression/distortion waves in L3 for for $\Delta t = (32 - 102)$ s.

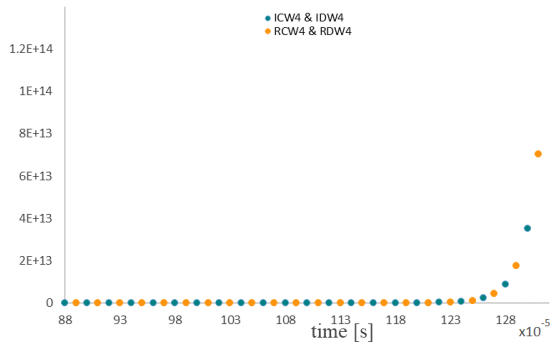

Figure 4.50: Number of incident/reflected compression/distortion waves in L4 for for $\Delta t = 130$ s.

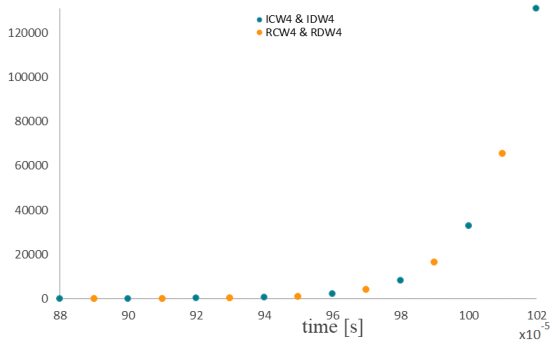

Figure 4.51: Number incident/reflected compression/distortion waves in L4 for $\Delta t = (102 - 88)$ s.

Notice that in all graphs shown above, there is a large difference, in terms of numerical values on the y-axis, between the number of waves developed at the first instants of time and those generated at the last instants of time; for this reasons it might seem the number of waves is zero for most of the interval of time considered. For this reasons, the same situations are shown of the right for a smaller interval of time.

4.5.6 G.W.P.P. for L_j with C1 and C4

The case analysed in this section will be identified as **GWPP6**.

This section can be considered as the complete case of Section 4.5.2. Therefore, same conditions and same mathematical relationships will be taken into account, but for the entire model; thus, also L3 and L4 will be considered. Notice that L4 has the same material characteristics and dimensions as L1, whereas L3 has the same material characteristics as L2. For **GWPP6**, it results:

- $\alpha_1 = \beta_1 \qquad \alpha_2 = \beta_2 \qquad \alpha_3 = \beta_3 \qquad \alpha_4 = \beta_4$
- $\Pi_i^{(1)} \neq \Pi_r^{(1)} \neq \Pi_{tr}^{(2)} \neq P_i^{(1)} \neq P_1^{(1)}{}_r \neq P_{tr}^{(2)}$
- $\alpha_2 \simeq 0.25 \cdot \alpha_1 \qquad \alpha_3 \simeq 0.25 \cdot \alpha_1 \qquad \alpha_4 \simeq 1.00 \cdot \alpha_1$
- $t_{\alpha_2} \simeq 30 \cdot t_{\alpha_1} \qquad t_{\alpha_3} \simeq 56 \cdot t_{\alpha_1} \qquad t_{\alpha_4} \simeq 1.00 \cdot t_{\alpha_1}$

As for Section 4.5.2, attention will be only focused on the change in the amplitudes, and neither wave-paths without/with II order wave propagation phenomena nor graphs with the total number of each type of wave will be provided.

Since condition **C1** is still valid for this case, only compression waves will be taken into account. As done for **GWPP2**, it will be shown the change in the wave amplitudes for L3 and L4; the graphs related to L1 and L2 will not be included because they are the same as those shown in Figures 4.24-4.27. Also in this case,

it is assumed that the amplitude is composed by a constant value $A_{type}^{(j)}$ ($A_i^{(3)}$ for incident wave in L3, $A_r^{(3)}$ for reflected waves in L3, $A_i^{(4)}$ for incident wave in L4, and $A_r^{(4)}$ for reflected waves in L4), and an exponential term $e^{-\frac{t}{\tau_j}}$, where $\frac{1}{\tau_j}$ is the damping factor. The following graphs show the decrease in the amplitude of each type of wave for L3 and L4.

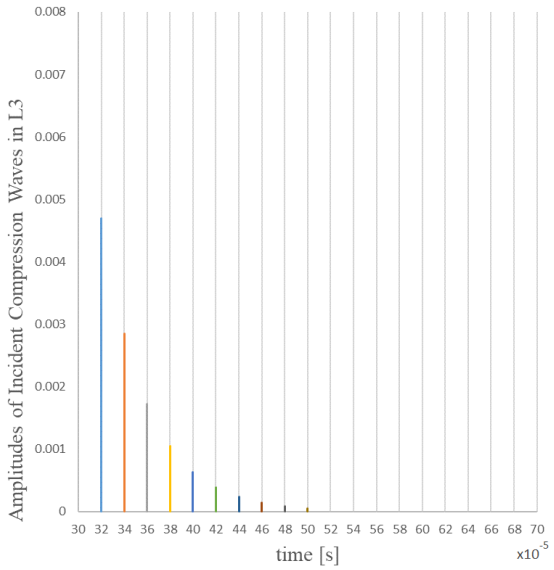

Figure 4.52: Change in amplitude for incident compression waves in L3, for $\Delta t = (70 - 30)$ s.

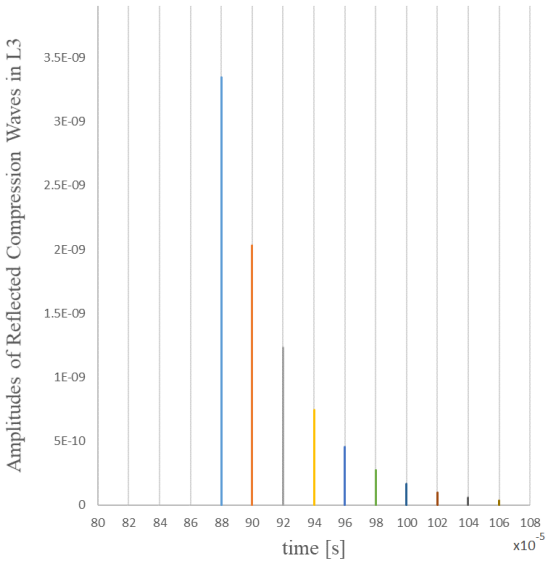

Figure 4.53: Change in amplitude for reflected compression waves in L3, for $\Delta t = (108 - 80)$ s.

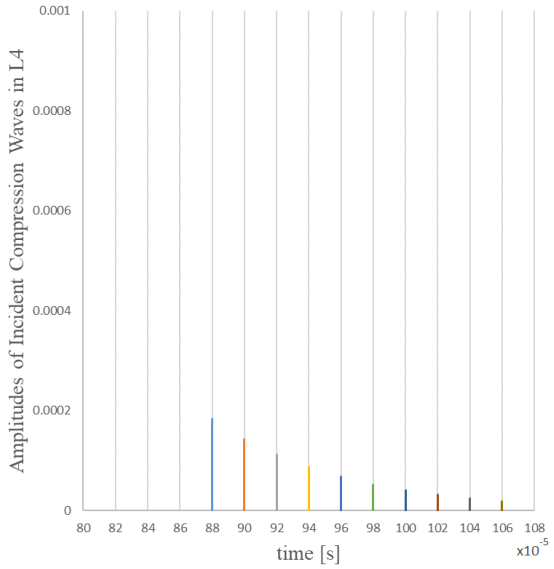

Figure 4.54: Change in amplitude for incident compression waves in L4, for $\Delta t = (108 - 80)$ s.

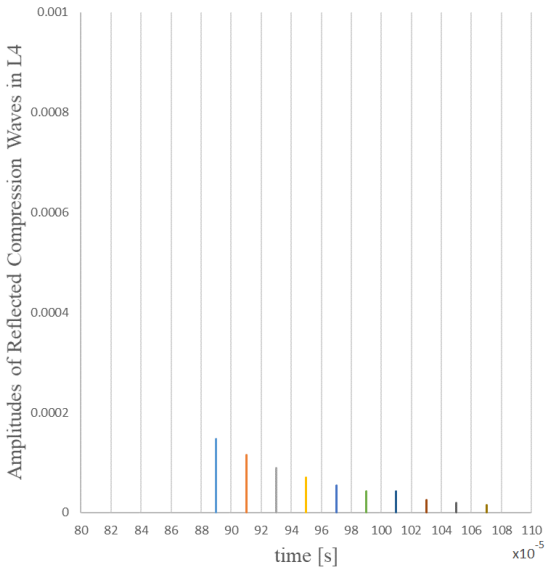

Figure 4.55: Change in amplitude for reflected compression waves in L4, for $\Delta t = (110 - 80)$ s.

Also for this case, arbitrary values have been chosen but always taking into account that the amplitude of the incident wave is bigger than the amplitudes of reflected and transmitted waves:

$$A^{(3)}_{i,tot} > A^{(3)}_{r,tot}, \;\; A^{(4)}_{tr,tot}$$

$$A^{(4)}_{i,tot} = A^{(4)}_{tr,tot} > A^{(4)}_{r,tot}$$

For L3 it was chosen the same value of damping as L2, and for L4 the same value of damping as L1, supposing that the decrease in the amplitudes is the same in the layers of the same material. For **GWPP6** it was chosen an interval starting from $t = t_{32}$ because from this instant of time waves start propagating from interface I2 in L3. On the vertical axis of graphs in Figures 4.52-4.55 the numerical values of $A^{(j)}_{type,tot}$, with $j = 1, 2$ are displayed.

4.5.7 G.W.P.P. for L_j, with C2 and C3

The case analysed in this section will be identified as **GWPP7**.

The wave propagation model that will be presented in this section can be considered the complete case of model **GWPP3**, thus the same conditions **C2** and **C3** will be taken into account. The mathematical conditions applied to Section 4.5.3 will be valid also in this section for all layers L_j; it results:

- $\alpha_1 \neq \beta_1, \qquad \alpha_2 \neq \beta_2 \qquad \alpha_3 \neq \beta_3 \qquad \alpha_4 \neq \beta_4$
- $\Pi_j(t_i) = \Pi_j(t_{i+1}) = \Pi_{j+1}(t_{i+1}) = P_j(t_i) = P_j(t_{i+1}) = P_{j+1}(t_{i+1}),\ j = 1, 2, 3$
- $\alpha_2 \simeq 0.25 \cdot \alpha_1, \qquad \alpha_3 \simeq 0.25 \cdot \alpha_1 \qquad \alpha_4 \simeq 1.00 \cdot \alpha_1$
- $\beta_1 \simeq 0.6 \cdot \alpha_1, \qquad \beta_2 \simeq 0.15 \cdot \alpha_1 \qquad \beta_3 \simeq 0.15 \cdot \alpha_1 \qquad \beta_4 \simeq 0.61 \cdot \alpha_1$
- $t_{\alpha_2} \simeq 30 \cdot t_{\alpha_1}, \qquad t_{\alpha_3} \simeq 56 \cdot t_{\alpha_1} \qquad t_{\alpha_4} \simeq 1.00 \cdot t_{\alpha_1}$
- $t_{\beta_1} \simeq 2.0 \cdot t_{\alpha_1} \qquad t_{\beta_2} \simeq 50 \cdot t_{\alpha_1} \qquad t_{\beta_3} \simeq 90 \cdot t_{\alpha_1} \qquad t_{\beta_4} \simeq 1.00 \cdot t_{\alpha_1}$

Figure 4.56 shows the wave propagation phenomena only including I order wave propagation phenomena, whereas Figure 4.57 considers both I order and II order wave propagation phenomena. From the latter figure, it is possible to notice that as time goes on the overlapping of waves, specially in L1 and L4 (yellow and green lines) increases; even if the number of both compression and distortion waves increases exponentially in L2 and L3, the number of waves will result the largest in the L1 and L4 because the reflection and transmission phenomena will occur with higher velocities than in the other two layers.

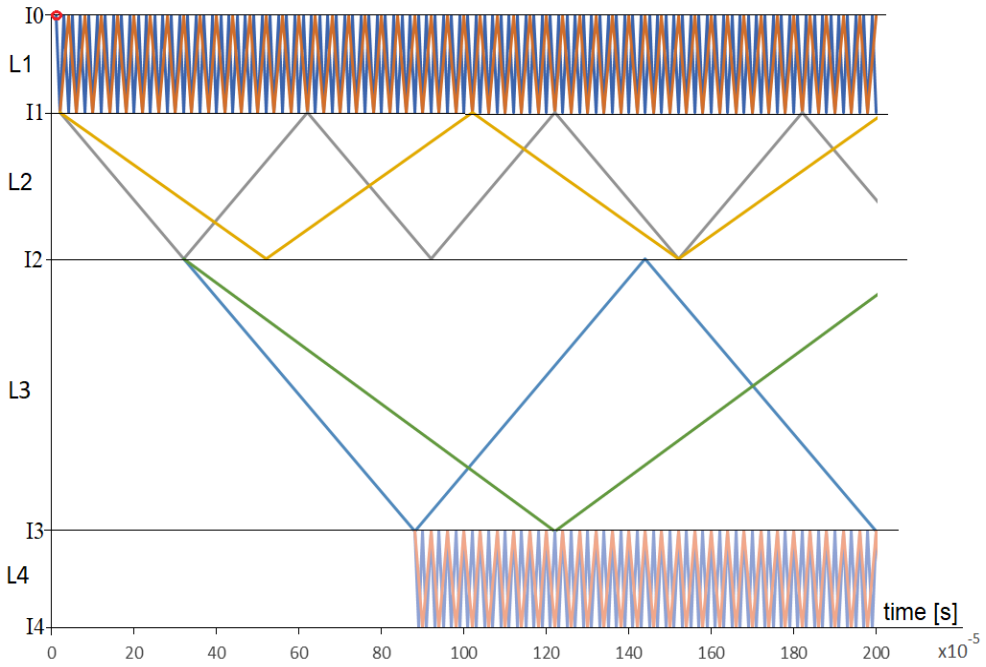

Figure 4.56: Wave-path for L_j without II order wave propagation phenomena.

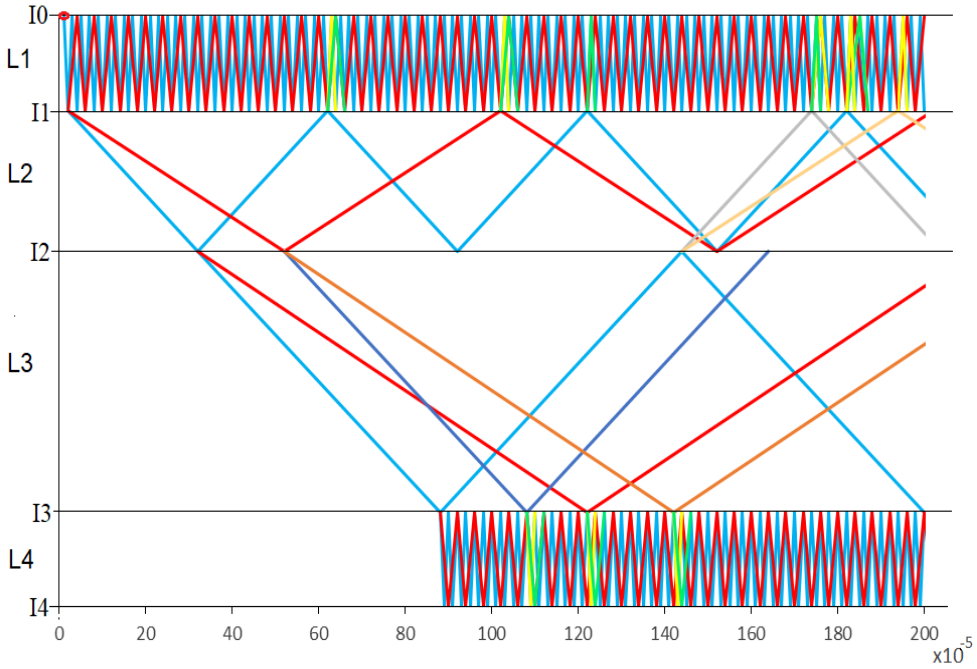

Figure 4.57: Wave-path for L_j with II order wave propagation phenomena.

The following graphs show the number of incident/reflected compression/distortion waves calculated for L3 and L4. Notice that waves start traveling in L4 at instant of time t_{88}, and then the increase of the number of both compression and distortion waves is exponential. In addition, the graphs related to L3 show some gaps; as

mentioned in Section 4.5.3, only a group of waves (those developed in the interval of time $\Delta t = t_{17} - t_1$) has been considered. In the reality there are waves in L3 from t_{32} in ahead. However, in all cases, there is an exponential increase of both compression and distortion waves.

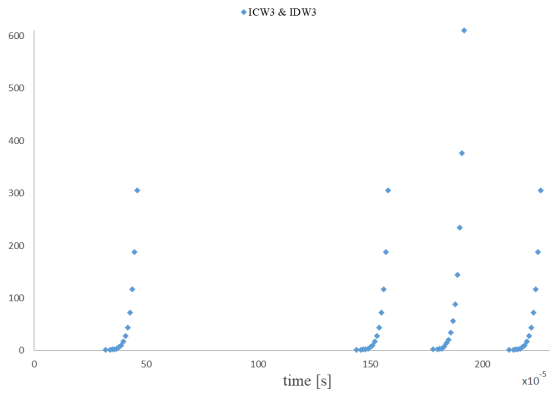

Figure 4.58: Number of incident compression and distortion waves in L3 for $\Delta t = 230$ s.

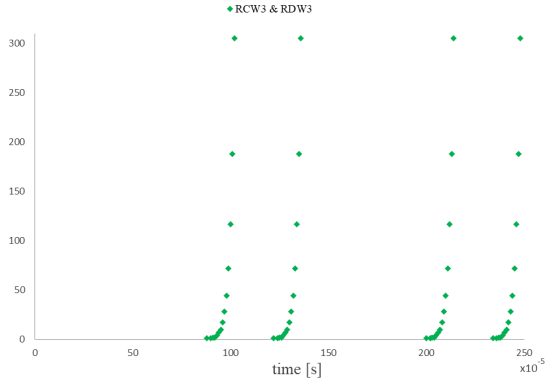

Figure 4.59: Number of reflected compression and distortion waves in L3 for $\Delta t = 250$ s.

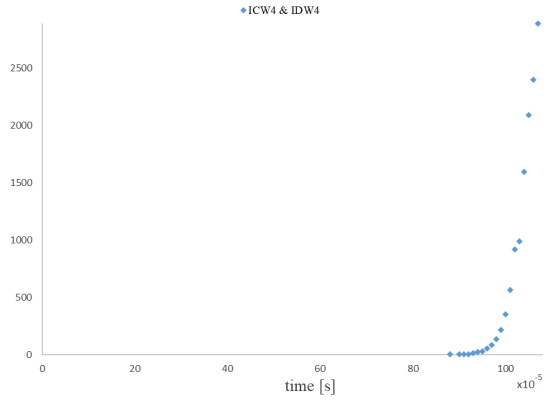

Figure 4.60: Number of incident compression and distortion waves in L4 for $\Delta t = 110$ s.

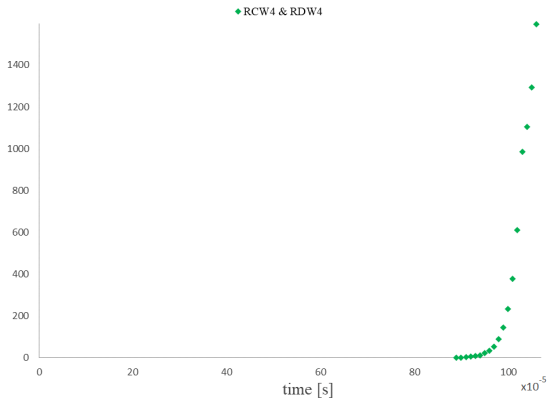

Figure 4.61: Number of reflected compression and distortion waves in L4 for $\Delta t = 110$ s.

4.5.8 G.W.P.P. for L_j with C2 and C4

The case analysed in this section will be identified as **GWPP8**.

This section can be considered as the complete case of Section 4.5.4. Therefore, same conditions and same mathematical relationships will be taken into account, but for the entire model; thus, also L3 and L4 will be considered. Notice that L4 has the same material characteristics and dimensions as L1, whereas L3 has the same material characteristics as L2. For **GWPP8**, it results:

- $\alpha_1 \neq \beta_1 \qquad \alpha_2 \neq \beta_2 \qquad \alpha_3 \neq \beta_3 \qquad \alpha_4 \neq \beta_4$
- $\Pi_i^{(1)} \neq \Pi_r^{(1)} \neq \Pi_{tr}^{(2)} \neq P_i^{(1)} \neq P_1^{(1)}{}_r \neq P_{tr}^{(2)}$
- $\alpha_2 \simeq 0.25 \cdot \alpha_1 \qquad \alpha_3 \simeq 0.25 \cdot \alpha_1 \qquad \alpha_4 \simeq 1.00 \cdot \alpha_1$
- $t_{\alpha_2} \simeq 30 \cdot t_{\alpha_1} \qquad t_{\alpha_3} \simeq 56 \cdot t_{\alpha_1} \qquad t_{\alpha_4} \simeq 1.00 \cdot t_{\alpha_1}$

As for Section 4.5.4, attention will be only focused on the change in the amplitudes, and neither wave-paths without/with II order wave propagation phenomena nor graphs with the total number of each type of wave will be provided.

Since condition **C2** is valid for this case, both compression and distortion waves will be taken into account. As done for **GWPP4**, it will be shown the change in the wave amplitudes for L3 and L4. In order to show the change in the amplitudes of both incident and reflected compression/distortion waves, each amplitude will be assumed composed by a constant value $A_{type}^{(j=2,3)}$ ($A_i^{(3)}$ for incident wave in L3, $A_r^{(3)}$ for reflected waves in L3, $A_i^{(4)}$ for incident wave in L4, and $A_r^{(4)}$ for reflected waves in L4), and an exponential term $e^{-\frac{t}{\tau_j}}$, where $\frac{1}{\tau_j}$ is the damping factor.

The following graphs show the decrease in the amplitude of each type of wave.

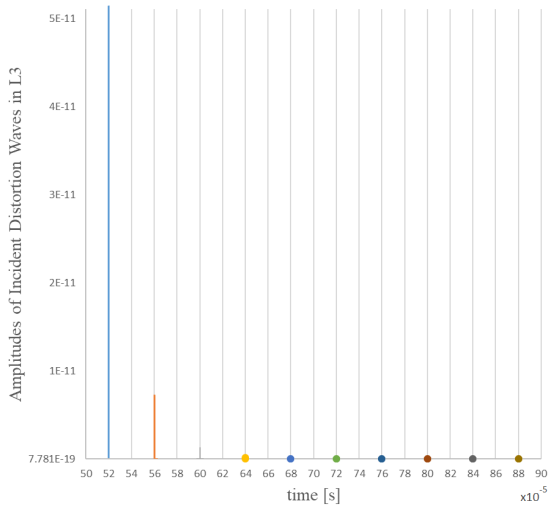

Figure 4.62: Change in amplitude for incident distortion waves in L3, for $\Delta t = (90 - 50)$ s.

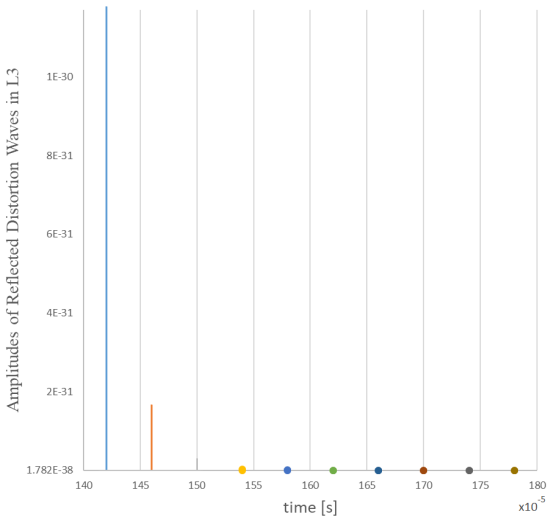

Figure 4.63: Change in amplitude for reflected distortion waves in L1, for $\Delta t = (180 - 140)$ s.

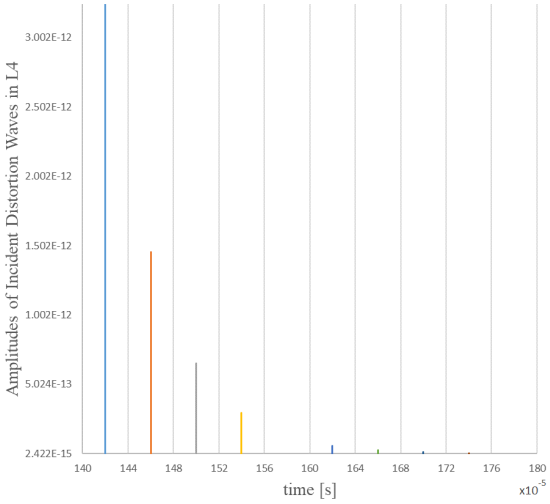

Figure 4.64: Change in amplitude for incident distortion waves in L4, for $\Delta t = (180 - 140)$ s.

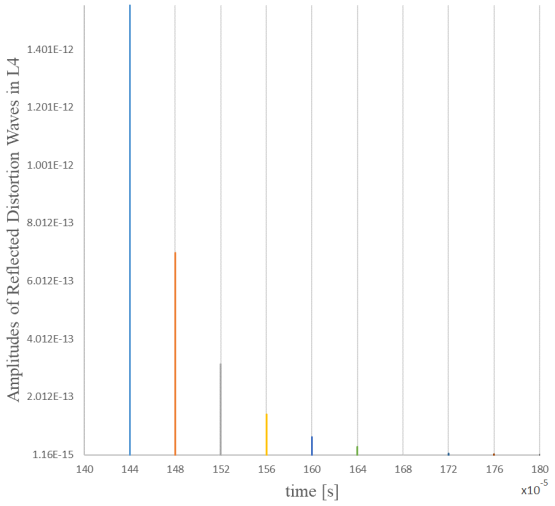

Figure 4.65: Change in amplitude for reflected distortion waves in L4, for $\Delta t = (180 - 140)$ s.

Also for this case, arbitrary values have been chosen but always taking into account that the amplitude of the incident wave is bigger than the amplitudes of reflected and transmitted waves:

$$A_{i,tot}^{(3)} > A_{r,tot}^{(3)}, \quad A_{tr,tot}^{(4)}$$

$$A_{i,tot}^{(4)} = A_{tr,tot}^{(4)} > A_{r,tot}^{(4)}$$

For L3 it was chosen the same value of damping as L2, and for L4 the same value of damping as L1, supposing that the decrease in the amplitudes is the same in the layers of the same material.

4.5.9 Final G.W.P.P. Model

In the previous sections, different types of models related to the wave propagation phenomena have been introduced by considering at first only a portion of the model (L1 and L2), and consequently the entire model (L_j). The purpose of the previous discussion was to understand how the reflection and transmission phenomena occurred with respect to time; all models proposed in Sections 4.5.1-4.5.8 were built taking into account the propagation times t_{α_j} and t_{β_j} and the other parameters mentioned in each **GWPP**-model.

The two main differences between the models **GWPPs** concern the propagation velocities ($\alpha_j = \beta_j$ or $\alpha_j \neq \beta_j$), and the amplitudes ($A_i^{(j)} = A_r^{(j)} = A_{tr}^{(j+1)}$ or $A_i^{(j)} \neq A_r^{(j)} \neq A_{tr}^{(j+1)}$).

The distinction between α_j and β_j, and the decrease in the wave amplitudes are the two important conditions that need to be respected in order to have a model close as much as possible to the reality.

The distinction between compression and distortion velocities, namely between compression and distortion waves, is relevant because, as mentioned in Section 4.3, the passage of a compression wave is associated to a combination of compression and shear; there is also a numerical difference between the two types of velocities: $\beta_j \approx 0.63\,\alpha_j$. The decrease in the wave amplitudes is considered close to the reality and explains the reason why after a certain amount of time, the process of wave propagation inside the model comes to and end; therefore, assuming that the *generated waves* (which can be reflected and transmitted waves coming from an incident wave) have a smaller amplitude than that of the *impinging wave* (which can be an incident wave or also a reflected back wave or a transmitted wave) suggests that there will not be any wave in the material at the last instant of time. In other words, if it is not assumed any decrease in amplitude (damping factor), then the process will last indefinitely. Therefore, conditions **C2** and **C4** can be considered as the closest to the reality and the most suitable ones.

It is important to specify that when distortion waves are taken into account, a 3D model needs to be involved. As can be seen in the next chapter, the mathematical analysis of the problem begins by considering a 3D model, and then moving on to a 1D model. When a 1D model is chosen, then distortion waves need to be neglected.

From the previous sections, it can be noticed that the number of waves increases as time goes on because more reflection and transmission phenomena occur at the interfaces generating more waves; For **GWPP1/5** and **GWPP3/7** it results a maximum number of waves at the last instant of the interval chosen. If it is assumed a damping term, as done for **GWPP2/6** and **GWPP4/8**, then there will be no wave at the last instant of time.

In summary, the partial models **GWPP2** and **GWPP4** or the entire models **GWPP6** and **GWPP8** can be defined the closest to the reality.

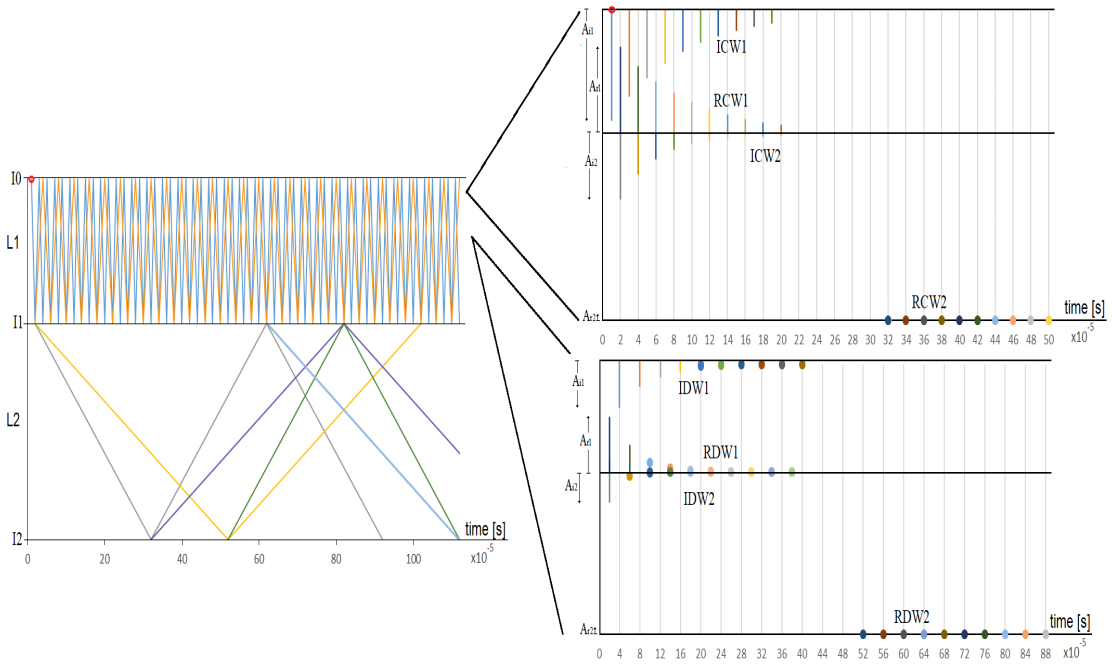

Figure 4.66: Final GWPP-model (L1 and L2) based on conditions C2 and C4.

Furthermore, analysing the problem from a mathematical point of view, conditions **C1** and **C3** can be considered more suitable and therefore, the partial models **GWPP1** and **GWPP3** or the entire models **GWPP5** or **GWPP7** can be used. Thus, it is assumed neither any distinction between compression and distortion waves nor any decrease in the wave amplitudes (no damping factor).

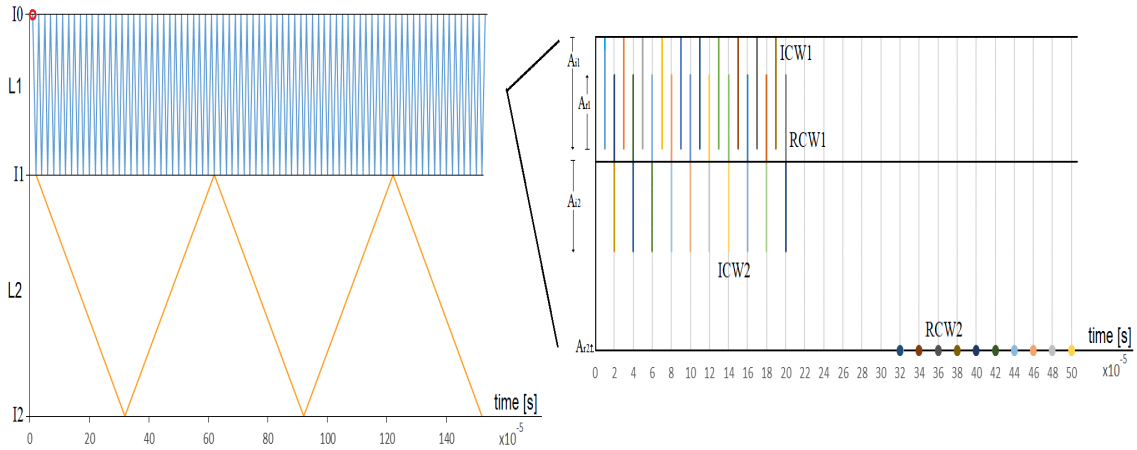

Figure 4.67: Final GWPP-model (L1 and L2) based on conditions C1 and C3.

4.6 Waves Geometry and Potentials

In the previous sections, several GWPP-models based on different conditions have been analysed; compression and distortion waves have been introduced and considered as general waves. It is important to describe the entire mechanism about the propagation phenomena that take place in the entire simplified model and also, describe the waves in terms of shape.

As mentioned in the previous sections, there are two types of waves: compression (or dilatation) waves and distortion (or shear) waves; the main difference is about the propagation velocities α and β. Both of them depend on density ρ and Lame' constants (λ, μ), as expressed from the equations 4.9 and 4.10. Both compression and distortion waves are spherical waves which propagate radially from a source (located on the free surface that is the interface 0 of the simplified structure). The external load causes the generation and propagation of an incident (compression) wave inside L1; after reaching the interface 1 (I1) which divides the top plywood and the primary RPUF, the incident wave generates four additional waves: two reflected waves (one compression and one distortion) and two transmitted (one compression and one distortion) waves. The two reflected waves will travel back in L1, whereas the two transmitted waves will propagate in L2 and will become the new incident waves for interface 2 which divides the primary and secondary RPUF (Figure 4.68). Each new incident wave will generate at I2 four new waves each, two reflected waves and two transmitted waves that will travel in L2 and L3 respectively. Therefore, at interface 2 there will be four compression waves (two reflected and two transmitted) and four distortion waves (two reflected and two transmitted) (Figure 4.69). The mechanism repeats at interface 3 that separates the secondary RPUF and the back plywood: each new incident wave will be responsible of the generation of four new waves (reflected and transmitted); the only difference is that at interface 3 there will be eight compression waves (four reflected back in L3 and other four transmitted in L4) and eight distortion waves as well (Figure 4.70). In L4 all transmitted (incident) waves generate only reflected waves at interface 4 in contact with the wall, resulting in eight reflected compression waves and eight reflected distortion waves. The same mechanism is applied to the reflected back waves: for instance, the reflected back waves generated at interface 2 will hit interface I1 generating four new waves (two reflected in L2 and two transmitted in L1) (Figure 4.71). Notice that all reflected waves which become new incident waves for interface 0 will generate only new reflected waves because no transmitted wave can propagate beyond interface 0. The number of waves increases with the number of the interfaces: the more interfaces there are in the structure, the more waves will be generated. All these waves are spherical waves which travel with a velocity α_j or β_j, with $j = 1, 2, 3, 4$. In order to completely understand the description above, consider the following pictures that represent step-by-step the mechanisms of reflection and transmission at the interfaces.

Each reflected and transmitted compression and distortion wave in the model will always have a smaller amplitude than that of the incident wave (notice that also a reflected wave generates new additional waves when it travels back in the layer).

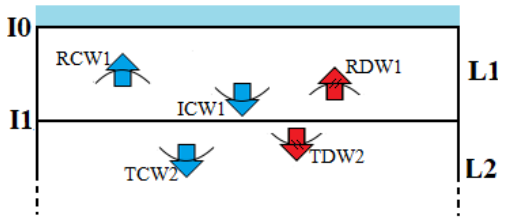

Figure 4.68: Generation of reflected waves in L1 and transmitted waves in L2 due to an incident compression wave at interface I0.

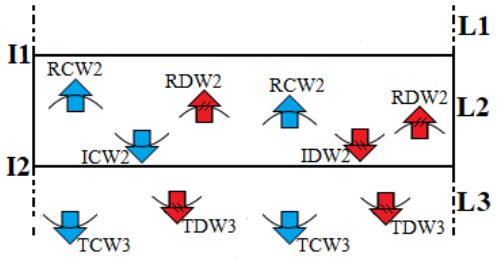

Figure 4.69: Generation of reflected waves in L2 and transmitted waves in L3 due to a compression and distortion incident waves at interface I2.

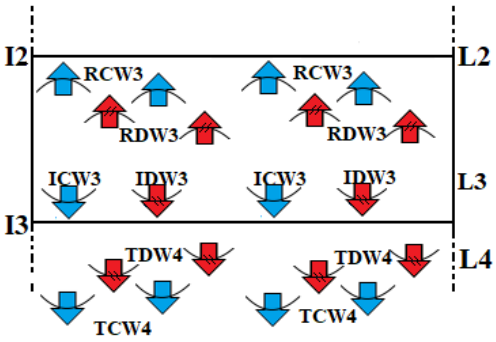

Figure 4.70: Generation of reflected waves in L3 and transmitted waves in L4 due to two compression and two distortion incident waves at interface I3.

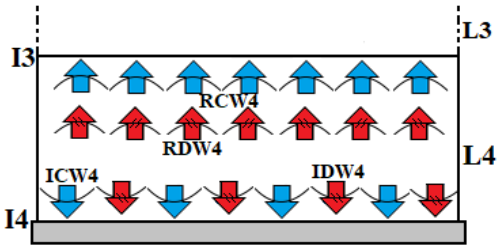

Figure 4.71: Generation of reflected waves in L4 due to four compression and four distortion incident waves at interface I4, and no transmitted waves.

Therefore, the amplitudes will decreases as time goes on (see **GWPP2/6** or also **GWPP4/8**).

Consider, for instance, all incident compression waves that propagate in L1 from interface I0 to interface I1. Looking at Figure 4.72 each arrow represents the amplitude of a compression wave, and the red one is the amplitude of the first incident wave at t_1. If an incident wave train is associated to each of these waves, it is possible to notice that as time goes on, the wave trains decrease gradually; the amplitude of the total incident wave train will be higher than that of the first incident wave. Consequently, the more the waves overlap, the more the stress related to the total wave train will be higher. The same considerations can be done for the other waves propagating in the opposite direction. Furthermore, it is important to specify that the incident and reflected waves have opposite propagation directions; it means that reflected waves will make weaker the incident waves. Notice the the other black arrows in Figure 4.72 from L0 to L1 come from II order wave propagation phenomena, namely are the consequence of the reflected back waves. Distortion waves have been neglected in this picture.

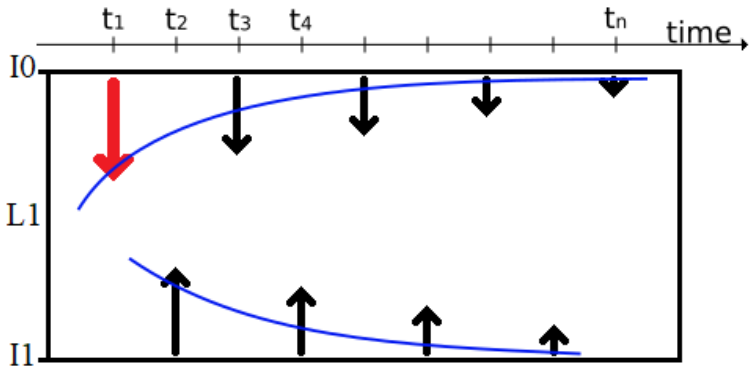

Figure 4.72: Qualitative decrease of amplitudes for incident and reflected waves in L1 with time t.

In Chapter 3 it was specified that the external load changes both in space and time; the contact area is responsible of the increase of the external force; the increase of the contact area is related to the spreading of the wave along the free surface; indeed, after ELP1 takes place, the wave spreads out along the free surface involving an increasingly wider portion of the contact area. This increase occurs over time. In Section 3.3 it was defined the velocity of the contact point and it was seen that this process comes to an end when the *critical time* t_{cr} is reached.

One of the most important concepts of this thesis is that the external force causes the wave propagation phenomena described above, but each change in the external force causes new wave propagation phenomena inside the structure. In other words, all reflected and transmitted waves are a consequence of the first incident compression wave (at $t = t_1$) which, in turn is a consequence of the external force F_1; The external force depends on time and space: each change in both time and space generates a new force that, in turn causes the generation of a new incident wave which, in turn, is responsible of new wave propagation phenomena in the material.

In order to understand how the change in the external force causes new wave propagation phenomena, consider, for instance, four theoretical values of time t: $t_1, t_2, t_3, t_4 = t_f$; then, the corresponding external force will be: $F_1 = F(t_1), F_2 = F(t_2), F_3 = F(t_3), F_f = F(t_f)$. Each external force will generate a different incident (compression) wave which, in turn, will cause the development and propagation of four different wave propagation phenomena. The following figures show separately the generation of different waves at each instant of time t_n, with $n = 1, 2, 3, 4$:

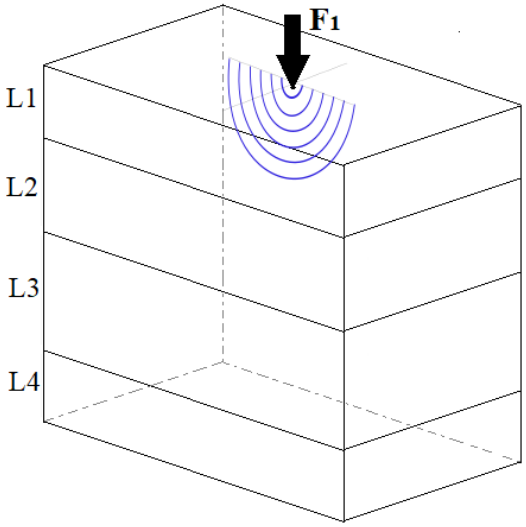

Figure 4.73: Propagation of waves inside the model due to the external force $F_1 = F(t_1)$.

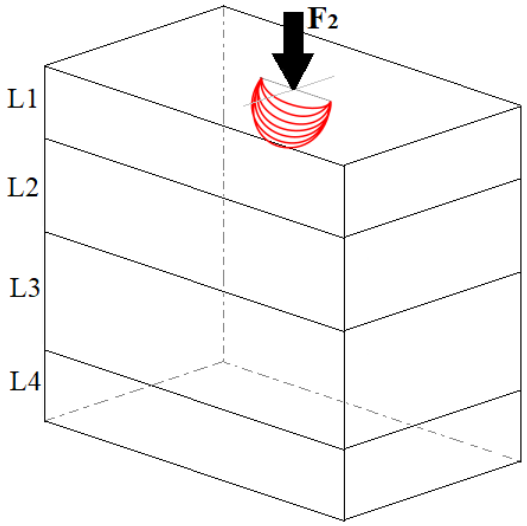

Figure 4.74: Propagation of waves inside the model due to the external force $F_2 = F(t_2)$.

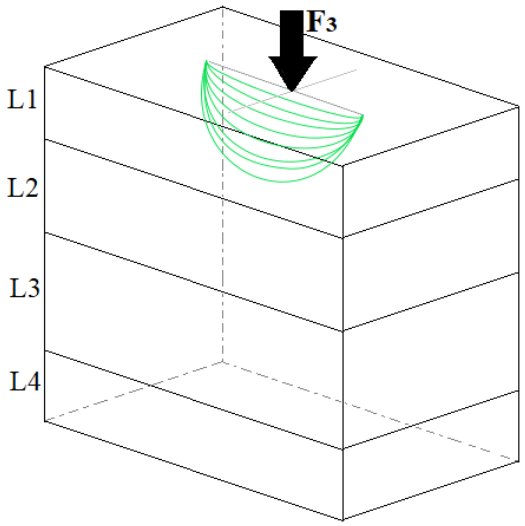

Figure 4.75: Propagation of waves inside the model due to the external force $F_3 = F(t_3)$.

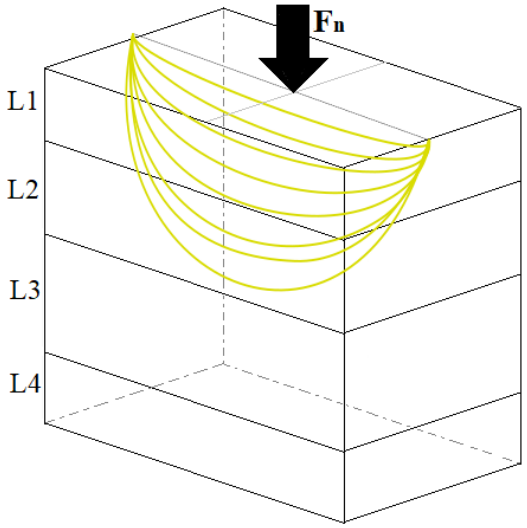

Figure 4.76: Propagation of waves inside the model due to the external force $F_n = F_f = F(t_f)$.

Notice that in the Figures 4.73-4.76 the external force is depicted as a black arrow that becomes bigger and bigger as time goes on due to the increase of the contact area. Specifically, Figures 4.73-4.76 show the propagation of the incident wave due to the external force, whereas Figures 4.77-4.80 focus on the wave fronts of the incident wave in each situation:

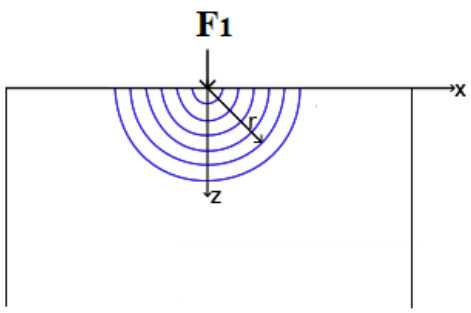

Figure 4.77: Front view of the propagating waves due to the external force F_1.

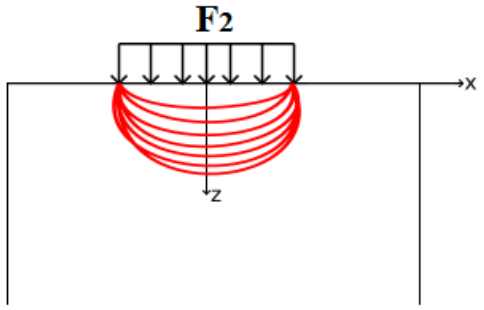

Figure 4.78: Front view of the propagating waves due to the external force F_2.

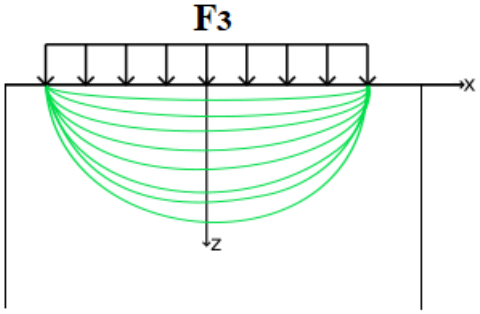

Figure 4.79: Front view of the propagating waves due to the external force F_3.

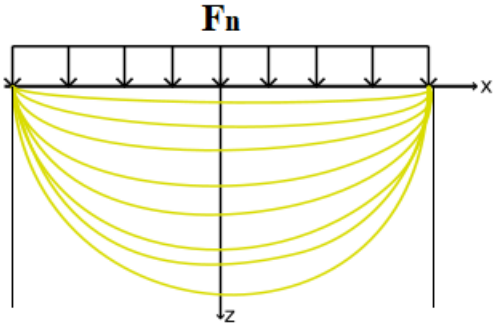

Figure 4.80: Front view of the propagating waves due to the external force F_n.

As can be seen, the shape of the wave fronts changes as the external force increases; notice that the first case (Figures 4.73 and 4.77) concerns the load point, namely the first contact between liquid and structure, whereas the last case (Figures 4.76 and 4.80) involves the entire contact area. Immediately after t_1 the wave front of the incident wave, generated by F_2, is not perfectly spherical anymore, but it changes its shape gradually. For instance, looking at Figure 4.76 (or Figure 4.80), it is possible to see that at the beginning of the process the wave assumes a plane shape and then, gradually curves until assuming a spherical shape, and then, deforming again. The shear effects, located at both ends of the impact area, are considered the cause of this curvature that occurs at the both ends of the impact area. Indeed, the principal direction of the stresses turns as the wave propagates in the structure. More precisely, the wave front keeps curving as the wave travels through the material. [9]

If the spreading area concept is applied to the situation shown, for instance, in Figure 4.76 (and Figure 4.80), then, the spreading area introduced in Chapter 2 (Section 2.4.1) becomes:

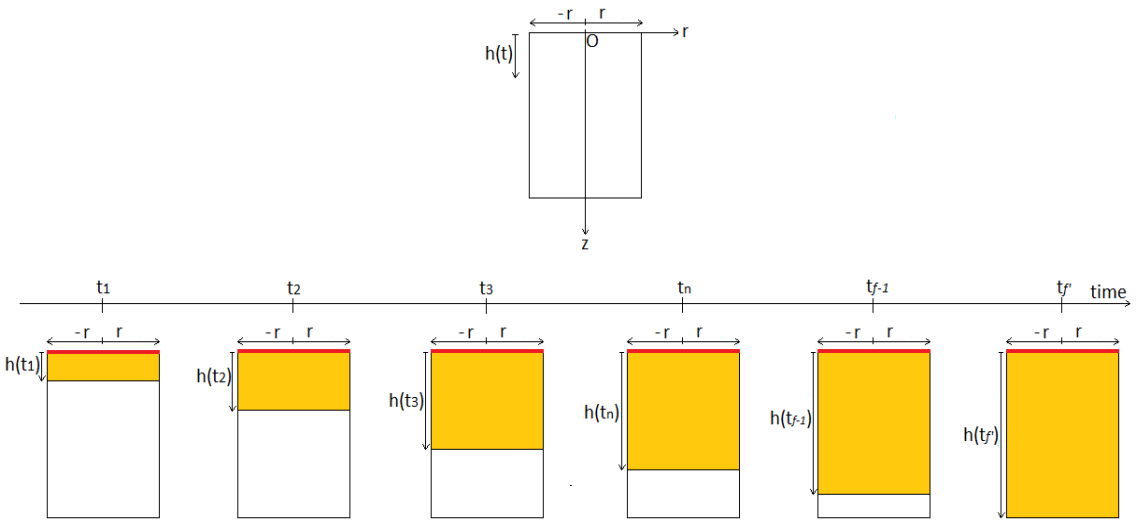

Figure 4.81: Qualitative change of the spreading area (in yellow) after an external load (in red along the entire horizontal length) impinges on the surface

As can be seen, the horizontal length of the spreading area is fixed from the first instant and does not change with time differently from the vertical dimension h that is still a function of time.

Therefore, the waves caused by the force F_n will add to the waves generated by the force F_3 which, in turn, are added to the waves caused by the force F_2 that, in turn, have been added to the waves generated by the force F_1. Combining all together these four situations analysed separately, then the amplitude of every wave needs to take into account this change at each instant of time.

In order to describe from a mathematical point of view the waves in the layers, the concept of *potential* will be used. In Section 4.2 the potentials have already been introduced by applying the *Helmholtz Theorem*. Each different type of wave will be associated with a potential. Basically, the potential should describe the waves propagating in the layers. Since there are two kinds of waves inside the material, there will be two kinds of potentials as well: compression potentials identified with Φ and distortion potentials identified with Ψ. Figure 4.82 shows the generation of waves (which are still represented by arrows) and the corresponding potentials as a consequence of the incident compression wave that in turn is a consequence of the external load acting on the free surface of L1. The number of waves increases after each wave-incidence on an interface, and consequently the number of potentials increases as well. Notice that each potential has a subscript to identify the *type* (incidence, reflection or transmission), and a superscript to identify the layer.

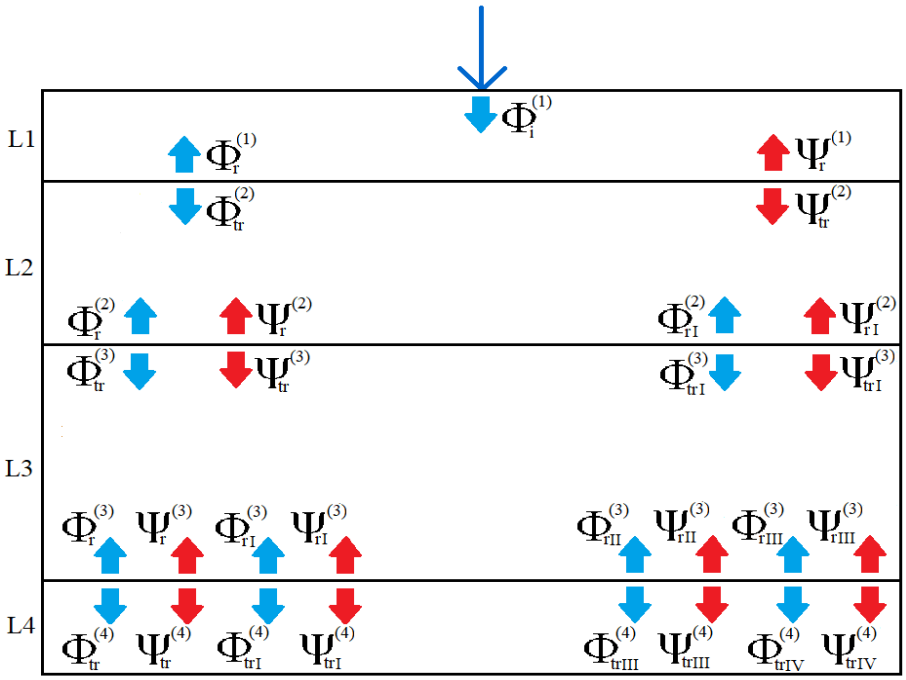

Figure 4.82: Compression and distortion potentials due to the external load acting on the external surface of L1 at $t = t_1$.

In L2 the transmitted compression and distortion potentials become the incident compression and distortion potentials for the second layer; as a consequence there are two reflected compression potentials $\Phi_r^{(2)}$ and $\Phi_{rI}^{(2)}$: the first one represents a reflected compression wave generated by an incident compression wave, whereas the second one represents a reflected compression wave generated by an incident distortion wave. Although these two potentials are generated by two different sources, it is possible to assume no distinction between $\Phi_r^{(2)}$ and $\Phi_{rI}^{(2)}$. The same consideration can be done for $\Psi_r^{(2)}$ and $\Psi_{rI}^{(2)}$, and for the other compression and distortion potentials in the other layers. Then, Figure 4.82 becomes

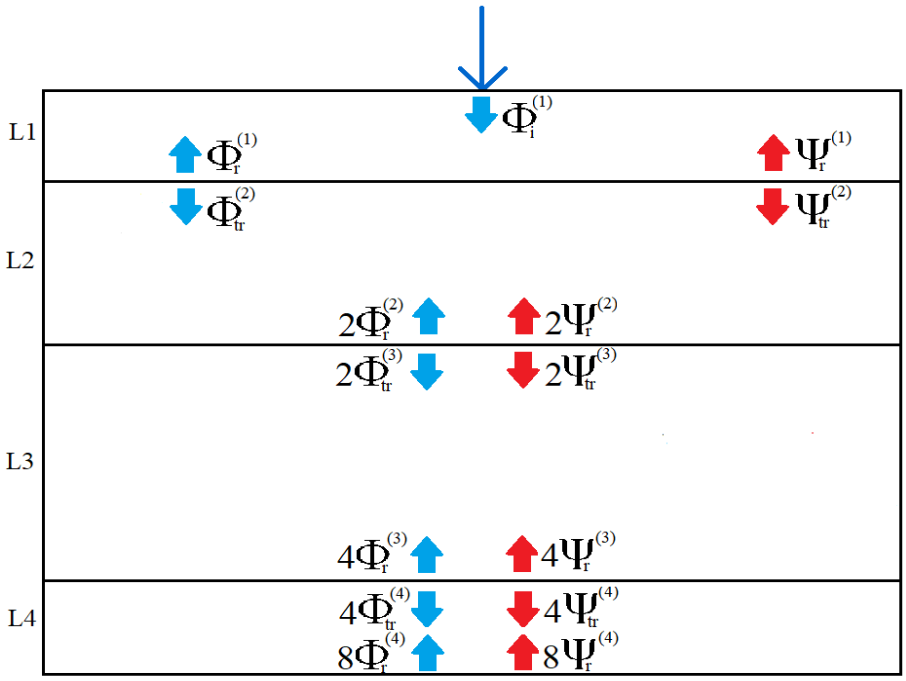

Figure 4.83: Compression and distortion potentials due to the external load with simplifications.

Figures 4.82 and 4.83 are two simplified representations for waves which propagate through the interfaces in each layer. Notice the both compression waves (in blue) and distortion waves (in red) are represented again by arrows. From these figures, it might seem that compression and distortion waves are parallel each other; in reality distortion waves are transverse, and even if no motion is assumed in the plane perpendicular to that of the compression waves, the vibrations need to be taken into account.

Potentials depend on the compression and distortion propagation velocities α_j and β_j, (and therefore, on density ρ_j, and Lame' constants λ_j, μ_j), on the propagation directions $\pm z$, angular velocity ω, and time t. In addition, damping terms (c_j, d_j) are included in order to have a decrease in the wave amplitudes. Thus, considering a cylindrical coordinate system $(O; r, \theta, z)$, where the source is located in O, the z-axis is perpendicular to the interfaces and positive downwards, and the free interface I0 is located at $z = 0$, then, the potentials can be expressed as follows: [10] [11]

$$\Phi_i^{(j)}(r,z,t,w) = \int_0^\infty A_j J_0(kr) e^{iwt} e^{-z\omega\alpha_j} e^{-\frac{t}{c_j}} dk$$

$$\Phi_r^{(j)}(r,z,t,w) = \int_0^\infty B_j J_0(kr) e^{iwt} e^{z\omega\alpha_j} e^{-\frac{t}{c_j}} dk$$

$$\Psi_r^{(j)}(r,z,t,w) = \int_0^\infty C_j k J_1(kr) e^{iwt} e^{z\omega\beta_j} e^{-\frac{t}{d_j}} dk$$

$$\Phi_{tr}^{(j+1)}(r,z,t,w) = \int_0^\infty D_{j+1} J_0(kr) e^{iwt} e^{-z\omega\alpha_{j+1}} e^{-\frac{t}{c_{j+1}}} dk = \Phi_i^{(j+1)}$$

$$\Psi_{tr}^{(j+1)}(r,z,t,w) = \int_0^\infty E_{j+1} k J_1(kr) e^{iwt} e^{-z\omega\beta_{j+1}} e^{-\frac{t}{d_{j+1}}} dk = \Psi_i^{(j+1)}$$

where $j = 1, 2, 3$, J_0 and J_1 are the Bessel functions of zero and first order, respectively, and A_j, B_j, C_j, D_{j+1} and E_{j+1}, are the amplitudes.

The formulas above explain why, for instance $\Phi_r^{(2)}$ and $\Phi_{rI}^{(2)}$ are the same: although they are generated by different types of waves, both $\Phi_r^{(2)}$ and $\Phi_{rI}^{(2)}$ depend on the same parameters α_2, and therefore on the same Lame' constants (λ_2, μ_2), the same propagation direction, the same damping factor $\frac{1}{c_2}$.

Based on the type of wave, each potential will satisfy one of the two following wave equations derived in Section 4.2:

$$\nabla^2 \Phi_{type}^{(j)} = \frac{1}{\alpha_j^2} \frac{\partial^2 \Phi_{type}^{(j)}}{\partial t^2} \qquad \nabla^2 \Psi_{type}^{(j)} = \frac{1}{\beta_j^2} \frac{\partial^2 \Psi_{type}^{(j)}}{\partial t^2}$$

where $\nabla^2 = r^{-1}\partial(r\partial/\partial r)/\partial r + \partial^2/\partial z^2$.

If u_r is the displacement in the horizontal direction, u_z is the displacement in the vertical direction, σ_{zz} is the normal stress, and τ_{rz} the shear stress, then it results:

$$u_{r_j} = \frac{\partial \Phi_{tot}^{(j)}}{\partial r} - \frac{\partial \Psi_{tot}^{(j)}}{\partial z} \qquad u_{z_j} = \frac{\partial \Phi_{tot}^{(j)}}{\partial z} + \frac{\partial \Psi_{tot}^{(j)}}{\partial r} + \frac{\Psi_{tot}^{(j)}}{r}$$

$$\sigma_{zz_j} = \lambda_j \nabla^2 \Phi_{tot}^{(j)} + 2\mu_j \left(\frac{\partial^2 \Phi_{tot}^{(j)}}{\partial z^2} + \frac{\partial^2 \Psi_{tot}^{(j)}}{\partial z \partial r} + \frac{1}{r} \frac{\partial \Psi_{tot}^{(j)}}{\partial z} \right)$$

$$\tau_{rz_j} = \mu_j \left[2 \left(\frac{\partial^2 \Phi_{tot}^{(j)}}{\partial r \partial z} - \frac{\partial^2 \Psi_{tot}^{(j)}}{\partial z^2} \right) + \frac{1}{\beta_j^2} \frac{\partial^2 \Psi_{tot}^{(j)}}{\partial t^2} \right]$$

where $\Phi_{tot}^{(j)}$ is the sum of all compression potentials in layer j and $\Psi_{tot}^{(j)}$ is the sum of all distortion potentials in layer j.

Notice that the components u_r and u_z of u ($\overrightarrow{u} = u_r \overrightarrow{e_r} + u_z \overrightarrow{e_z}$) can be found applying the *Helmholtz theorem.*

Substituting:

$$\nabla \Phi = \frac{\partial \Phi}{\partial r} \overrightarrow{e_r} + \frac{1}{r} \frac{\partial \Phi}{\partial \theta} \overrightarrow{e_\theta} + \frac{\partial \Phi}{\partial z} \overrightarrow{e_z}$$

and

$$\nabla \times \Psi = \left(\frac{1}{r} \frac{\partial \Psi_z}{\partial \theta} - \frac{\partial \Psi_\theta}{\partial z} \right) \overrightarrow{e_r} - \left(\frac{\partial \Psi_z}{\partial r} - \frac{\partial \Psi_r}{\partial z} \right) \overrightarrow{e_\theta} + \frac{1}{r} \left(\frac{\partial (r\Psi_\theta)}{\partial r} - \frac{\partial \Psi_r}{\partial \theta} \right) \overrightarrow{e_z}$$

into

$$u = \nabla \Phi + \nabla \times \Psi$$

then it is possible to find the expressions of the displacements written above. For the stresses the following formulas are applied:

$$\sigma_{zz} = \lambda \left(\frac{\partial u_r}{\partial r} + \frac{u_r}{r} + \frac{\partial u_z}{\partial z} \right) + 2\mu \left(\frac{\partial u_z}{\partial z} \right) \qquad \tau_{rz} = \mu \left(\frac{\partial u_r}{\partial z} + \frac{\partial u_z}{\partial r} \right)$$

4.7 Particle motion

The physical basis for the propagation of a disturbance lies on the interaction of the discrete atoms of the solid, even if the medium is considered as continuous in solid and fluid mechanics. If a model is believed as composed by discrete atoms, then it is possible to replace the particles and the bonds that connect each atom to the surrounding atoms with a series of interconnected mass-spring systems, where atoms (or particles) and bonds stand for masses and springs, respectively. If a mass particle is subjected to a disturbance, then it will propagate to the next mass particle through the bond-spring; thus, the disturbance is propagated and felt in the surrounding regions as well. In the case of a continuous, first of all the mass and the elastic parameters are considered continuous functions and are distributed in terms of mass density and elastic moduli. In this case, the disturbance is spread out in two- or three- dimensional directions, and a wavefront is generally associated with the outward spreading disturbance. Furthermore, after experiencing the motion due to the disturbance, the particles behind the front may oscillate for a small additional time, whereas the particles ahead the front have experienced no motion yet.

The waves described and analysed in the previous sections develop and propagate in a region that is located at the centre of the entire structure, in the loading-area. The existence of these waves concerns only the first part of the impact; in other words, after a certain amount of time the disturbance will propagate in the out-of-loading regions of the structure through longitudinal waves. It is believed that longitudinal waves propagate in the surrounding regions of the impact area. These waves in the out-of-impact areas can be considered as a consequence of strain waves in the loading area.

The disturbance will spread out from a point (the source) located on the free boundary and the particles in this region will be subjected to a displacement in both directions. The displacements in the vertical and horizontal direction are coupled.

Figure 4.84 shows the particles and the atomic bonds in both impact area (dark blue) and in out-of-impact area (light blue), whereas Figure 4.85 show the displacement of the particles in a portion of the impact area.

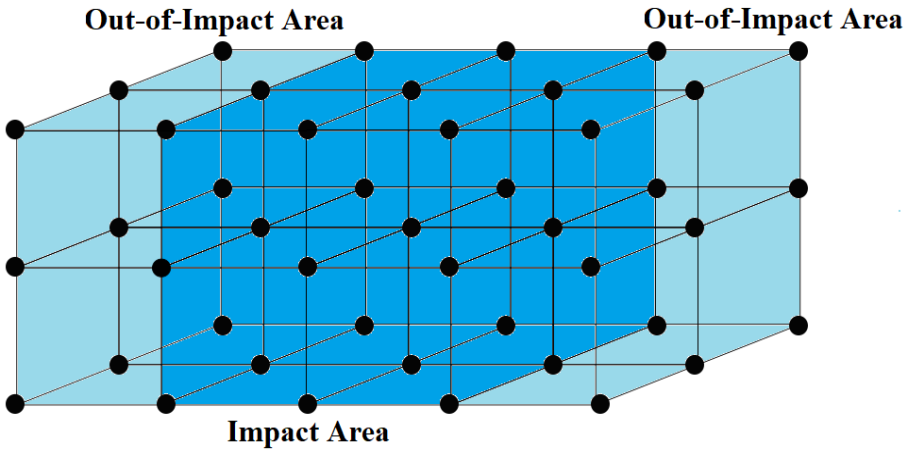

Figure 4.84: Particles and atomic bonds in the impact area (dark blue) and in the out-of-impact areas (light blue) before any external load.

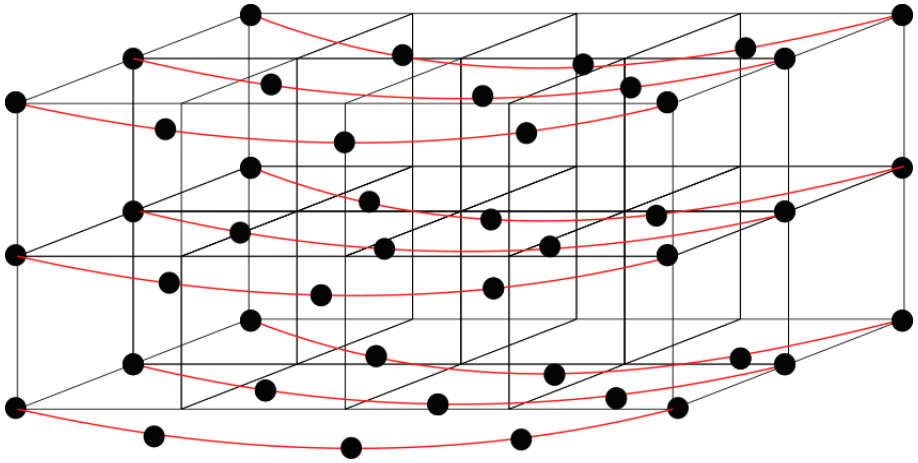

Figure 4.85: 3D view of a portion of the loading area with particles displaced from their original position.

Figure 4.86 shows the cross-section of the loading (impact) area. The atoms are represented by the points in black, connected each other by the atomic bonds, represented by the lines in black. The red points represent the displaced positions. The red atomic bonds are now deformed. In Figure 4.87 it is shown the Poisson's effect: consider the portion of space delimited by $ABCD$: a sequence of displacements that affects the atoms A, B, C and D is shown. The original space between $ABCD$ *(a.)* is compressed by the external force causing a vertical displacement AA' and BB' *(b.)*; this compression in the vertical dimension causes a dilatation in the horizontal direction inducing the displacements $A'A''$ and $B'B''$ *(c.)*; at the end, the particles A and B have been subjected to a radial displacement AA'' and BB'' *(d.)*.

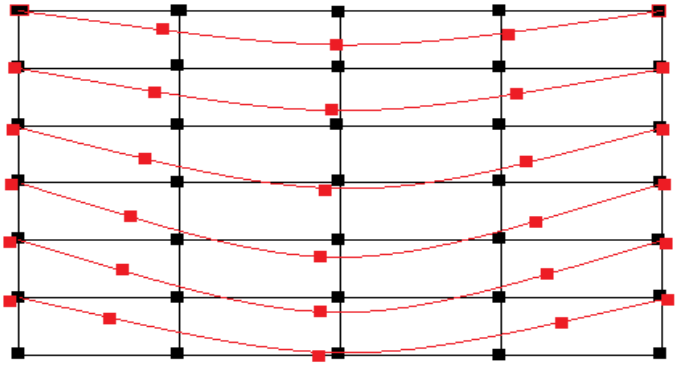

Figure 4.86: Cross-section of the loading area where particles are displaced from their original position

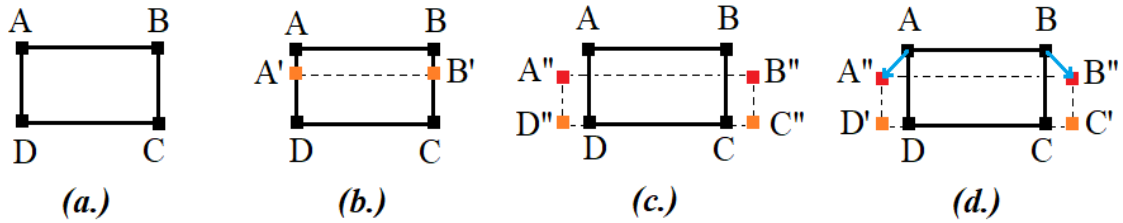

Figure 4.87: Poisson's effect, and displacements of particles A and B.

4.8 Conclusions

This chapter represented the answer to the first research question **Q1.** introduced at the beginning of the thesis. The purpose of this chapter was first of all, to understand the concept of waves which propagate inside a material, secondly analyse the propagation phenomena that take place at different interfaces, then understand the relationship between waves propagation and time, and finally to find a suitable approach to describe mathematically these waves.

It was seen that the concept of waves inside a material is fundamental to explain the reason why regions located far from the impact point (or impact area) feel, only after a certain amount of time, the effect of the external force (defined as a disturbance). The propagation of both compression and distortion waves was important from both a physical and mathematical point of view: the passage of a compression wave is a combination of shear and compression (see Section 4.3), and the generation of distortion waves together with compression waves guaranteed the validity of the boundary conditions at the interfaces. Due to the complexity of the problem, the reflection and transmission phenomena were at first analysed separately, and then combined all together in order to understand the relationship with time t. As already mentioned in Chapter 3, each change in the external process caused a change in the internal process: different external forces generated different incident compression waves in layer 1, and consequently different reflected and transmitted

waves. The potentials Φ and Ψ were considered suitable to describe the waves inside the simplified layered structure, and to define deformations and stresses.

From the analysis made in the previous sections of this chapter, it is possible to conclude that after an external force impacts a layered structure, a first incident compression wave starts propagating radially from the source (the impact point located at the free interface); due to the presence of several interfaces, the generation of reflected and transmitted compression and distortion waves takes place at each interface (as described in Section 4.6), causing a complicated system of wave propagation phenomena that comes to an end after a certain amount of time; indeed, each type of strain waves decreases its amplitude over time after impinging on an interface. Notice that the term *type* concerns the distinction between incident, reflected and transmitted compression and distortion waves.

Furthermore, the model that resulted from the study about the waves propagation is a 3D layered model (simplified model) composed by four materials in contact each other, separated by interfaces, where both compression and distortion spherical waves propagate forward and backward, for a certain amount of time, causing a displacement in all three directions of the particles which compose it.

Chapter 5

Theoretical Model

5.1 Introduction

This chapter represents the last step of this thesis that is the determination of the deformations for a simplified layered model. At first, it will be explained the approach used, then a three-layered structure will be introduced, without and with damping, then the three-layered case will be generalised for n layers, and finally, the deformation of the three-layered model will be found considering four different impact loads.

5.2 Mathematical Approach

After analysing the mathematical equations needed for defining the deformations of a general layered material, it was chosen the model MarkIII, and some simplifications were added in order to make easier the analysis of the problem. The simplifications **S0-S3** have already been discussed in Chapter 2. At beginning the model shown in Figure 2.7, with four layers, was used.

It was decided to start with a 3D case, that means it was assumed the propagation of both compression and distortion spherical waves inside the layered material; an external impact caused the generation and the propagation of an incident compression spherical wave in L1 that in turn caused the generation of reflected and transmitted waves at the other interfaces. Figures 4.82 and 4.83 summarise the process of reflection and transmission phenomena and the potentials taken into account. Due to the complexity of the equations and the high number of different types of potentials, the global problem was divided in three sub-problems:

S-P1. considering layers L1 and L2 and interface I1;

S-P2. considering layers L2 and L3 and interface I2;

S-P3. considering layers L3 and L4 and interface I3

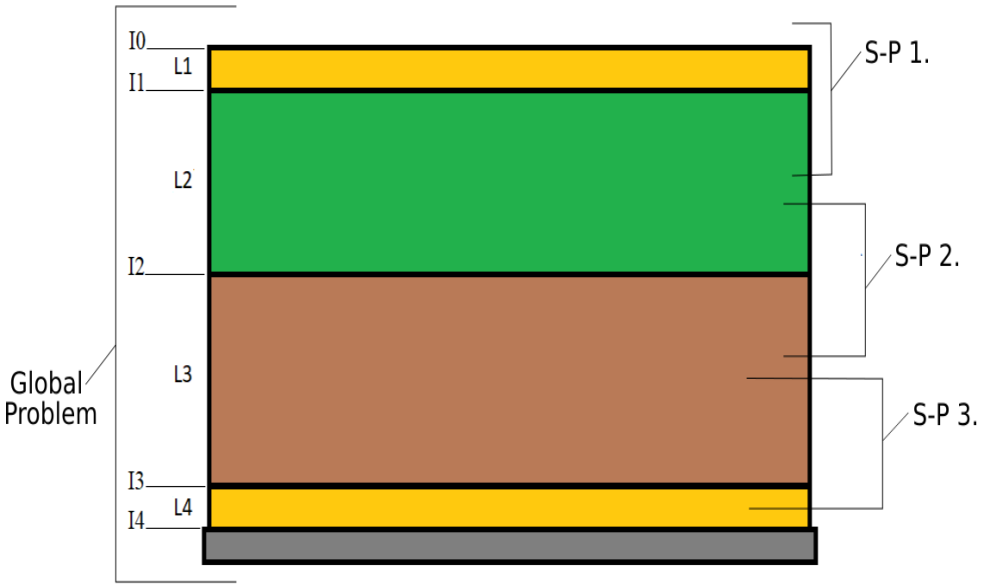

Figure 5.1: Global problem, and sub-problems (S.P.s).

In each sub-problem, there were four unknowns represented by the amplitudes of the two reflected waves and the other two transmitted waves. Applying the boundary conditions at each interface, a system of four equations in four unknowns was defined for each sub-problem; the boundary conditions guaranteed that the displacements in the horizontal (q) and vertical (w) directions for layer j were the same as the displacements in the horizontal and vertical directions in the next layer $j+1$; the conditions were also valid for normal stresses (σ_{zz}) and shear stresses (τ_{rz}):

BC1. $q_j = q_{j+1}$;

BC2. $w_j = w_{j+1}$;

BC3. $\sigma_{zz_j} = \sigma_{zz_{j+1}}$;

BC4. $\tau_{rz_j} = \tau_{rz_{j+1}}$;

The amplitude A_1 of the first incident compression wave in S-P1 was assumed known; this means all the amplitudes of the reflected and transmitted waves were found as a function of A_1. After obtaining the expressions of the amplitudes, deformations and stresses could be found by applying the respective formulas (see Section 4.6, Chapter 4). All equations considered involved compression and distortion potentials. After evaluating the results obtained for the amplitudes, it was decided to simplify the problem: starting from the 3D case, then the analysis was applied to a 1D case.

The 1D case forced to neglect distortion waves, and plane waves were considered instead of spherical waves. The consequence was to assume the propagation of an incident compression plane wave as result of an external impact force; then, the reflected and transmitted waves generated at different interfaces were compression

plane waves as well. In addition, the model shown in Figure 2.7 in Chapter 2 was further simplified: the rigid secondary barrier (RSB) was removed and L2 (primary RPUF) and L3 (secondary RPUF) were combined in one single layer.

Differently from the 3D case, it will be seen the use of density ρ_j, elastic modulus E_j and the deformations $u_{type}^{(j)}$ for the 1D case, instead of compression and distortion propagation velocities α_j and β_j, and compression and distortion potentials Φ_j and Ψ_j; this it will be due to the simplification of equation 4.4.

5.3 Model composed by 3 Layers

As mentioned in the previous paragraph, an additional simplification was made for the 1D case: the rigid secondary barrier between primary and secondary RPUF was removed and L2 and L3 were considered as one single layer (represented by L2). It was possible to make this simplification because layers 2 and 3 had the same material characteristics; the only difference was in the thickness. The model used for this case is shown in Figure 5.2:

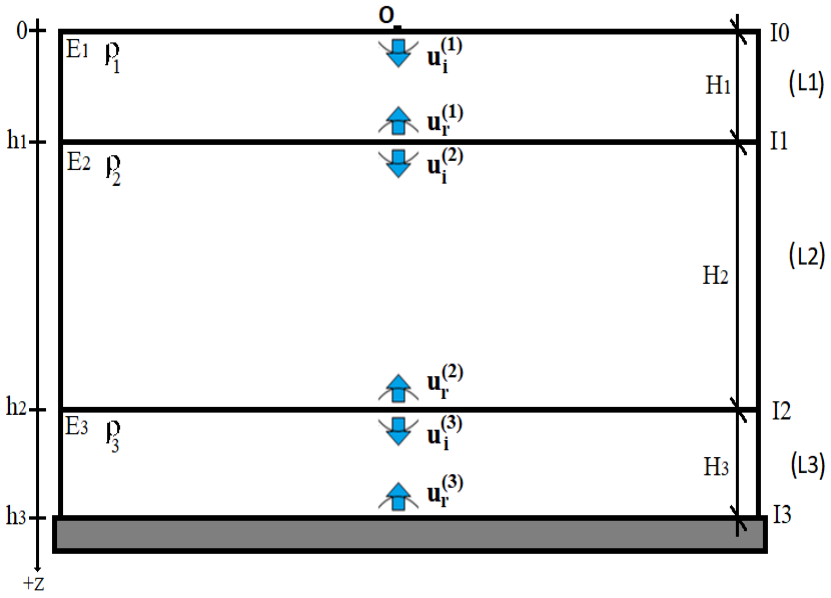

Figure 5.2: Model with three layers.

Dimensions and material characteristics are shown in the following table:

	Layers	ρ	E	H	h
		kg/m^3	MPa	m	m
1	L1	710	8900	0.012	0.012
2	L2	120	84	0.250	0.262
3	L3	710	8900	0.012	0.274

Table 5.1: Material characteristics and dimensions for the simplified three-layered model.

Notice that L1 and L3 are still made of the same material, H_j is the thickness of each layer L_j, and h_j represents the vertical distance of each interface from the origin (located in the middle on the free interface I0).

In Section 4.2 the *Navier's equations for media* were determined; the starting point was applying the *Newton's Second Law* in *x-direction*; since the problem of waves propagation is simplified to a 1D case, only the vertical direction (*z-direction*) is considered. Thus, applying the *Newton's Second Law* in *z-direction* with the same procedure and same formulas used in Section 4.2, equation 4.3 is obtained:

$$(\lambda+\mu)\frac{\partial\Delta}{\partial z}+\mu(\nabla^2 u_z)=\rho\ddot{u}_z$$

$$(\lambda+\mu)\frac{\partial}{\partial z}\left(\frac{\partial u_x}{\partial x}+\frac{\partial u_y}{\partial y}+\frac{\partial u_z}{\partial z}\right)+\mu\left(\frac{\partial^2 u_z}{\partial x^2}+\frac{\partial^2 u_z}{\partial y^2}+\frac{\partial^2 u_z}{\partial z^2}\right)=\rho\frac{\partial^2 u_z}{\partial z^2} \tag{5.1}$$

Then, neglecting the terms in *x-direction* and *y-direction*, equation 5.1 becomes

$$(\lambda+2\mu)\frac{\partial^2 u_z}{\partial z^2}=\rho\frac{\partial^2 u_z}{\partial z^2} \tag{5.2}$$

$$\frac{\partial^2 u_z}{\partial z^2}=\frac{1}{\frac{(\lambda+2\mu)}{\rho}}\frac{\partial^2 u_z}{\partial z^2} \tag{5.3}$$

Applying the formulas $\lambda=\frac{\nu E}{(1+\nu)(1-2\nu)}$ and $\mu=\frac{E}{2(1+\nu)}$ that express the Lame' constants (λ,μ) in function of E and ν (see Appendix A.1), it results:

$$(\lambda+2\mu)=\frac{E(1-\nu)}{(1+\nu)(1-2\nu)}$$

Since $\nu\to 0$, $(\lambda+2\mu)\to E$, equation 5.2 becomes

$$E\frac{\partial^2 u_z}{\partial z^2}=\rho\ddot{u}_z \tag{5.4}$$

Notice that equation 5.3 (or 5.2) is the wave equation for compression (or dilation) waves, and $\frac{(\lambda+2\mu)}{\rho}=\alpha^2$.

Governing Equation:

For notation reasons, equation 5.4 will be re-written considering u instead of u_z, but always meaning the deformation in *z-direction*.

$$E\frac{\partial^2 u}{\partial z^2} = \rho\frac{\partial^2 u}{\partial t^2} \tag{5.5}$$

where E and ρ are elastic modulus and density, respectively. In Appendix B.1 it is shown another procedure to derive the governing equation.

Mathematical Expressions of the Deformations:

Substituting $u = U(z)e^{i\omega t}$ into the governing equation, it results:

$$Ee^{i\omega t}U'' = \rho e^{i\omega t}(-\omega^2)U \rightarrow U'' + \frac{\rho\omega^2}{E}U = 0$$

where $U'' = \frac{\partial^2 U}{\partial z^2}$

Therefore,

$$U(z) = c_1 e^{-i\omega\sqrt{\frac{\rho}{E}}} + c_2 e^{i\omega\sqrt{\frac{\rho}{E}}}$$

Substituting in $u = U(z)\, e^{i\omega t}$, it results:

$$u = c_1 e^{i\omega t - i\omega\sqrt{\frac{\rho}{E}}} + c_2 e^{i\omega t + i\omega\sqrt{\frac{\rho}{E}}}$$

For the three layers, $u^{(j)}$ will be expressed by the following equations:

$$u^{(1)} = A_1\, e^{i\omega t}e^{-izk_1} + B_1\, e^{i\omega t}e^{izk_1}$$

$$u^{(2)} = A_2\, e^{i\omega t}e^{-izk_2} + B_2\, e^{i\omega t}e^{izk_2}$$

$$u^{(3)} = A_3\, e^{i\omega t}e^{-izk_3} + B_3\, e^{i\omega t}e^{izk_3}$$

where $k_j = \omega\sqrt{\frac{\rho_j}{E_j}}$ (see the **Relationship between ω and k** below). $u^{(j)}$ will satisfy the governing equation $E_j\frac{\partial^2 u^{(j)}}{\partial z^2} = \rho_j\frac{\partial^2 u^{(j)}}{\partial t^2}$. In addition, $u^{(j)}$ can also be divided in $u_i^{(j)}$ and $u_r^{(j)}$ as follows:

$$u_i^{(1)} = A_1\, e^{i\omega t}e^{-izk_1}; \quad u_r^{(1)} = B_1\, e^{i\omega t}e^{izk_1}$$

$$u_i^{(2)} = A_2\, e^{i\omega t}e^{-izk_2}; \quad u_r^{(2)} = B_2\, e^{i\omega t}e^{izk_2}$$

$$u_i^{(3)} = A_3\, e^{i\omega t}e^{-izk_3}; \quad u_r^{(3)} = B_3\, e^{i\omega t}e^{izk_3}$$

The unknowns in the expression $u_{type}^{(j)}$ are the amplitudes A_j and B_j, for $j = 1, 2, 3$.

Relationship between ω and k

If the mathematical expression of the deformation $u_i^{(1)}$ is considered and substituted in equation 5.5, then it is possible to find the relationship between ω and k, (in this case, k_1). The same relationship will be also used for the other layers.

$$\begin{cases} u_i^{(1)} = A_1 e^{(i\omega t - ik_1 z)} \\ E_1 \frac{\partial^2 u_i^{(1)}}{\partial z^2} = \rho_1 \frac{\partial^2 u_i^{(1)}}{\partial t^2} \rightarrow E_1 A_1 e^{(i\omega t - ik_1 z)}(-k_1^2) = \rho_1 A_1 e^{(i\omega t - ik_1 z)}(-\omega^2) \end{cases} \tag{5.6}$$

Thus, it results:

$$+E_1 k_1^2 = +\rho_1 \omega^2 \rightarrow k_1 = \pm\omega\sqrt{\frac{\rho_1}{E_1}} \tag{5.7}$$

For the other layers, it results:

$$k_2 = \pm\omega\sqrt{\frac{\rho_2}{E_2}} \qquad and \qquad k_3 = \pm\omega\sqrt{\frac{\rho_3}{E_3}} \tag{5.8}$$

Notice that

$$k_2 \simeq 4k_1; \qquad k_3 = k_1 \tag{5.9}$$

Expression of the external force F

The external force F will be defined by equation 5.10 and no change will be assumed.

$$F = \sigma A\, e^{i\omega t} \tag{5.10}$$

Notice that $A \approx 1$ because a *1D*-case is considered.

Boundary Conditions

The boundary conditions will be useful for finding the unknowns; there will be six boundary conditions that will allow to find A_j and B_j, for $j = 1, 2, 3$.

Boundary Condition 1.

The first boundary condition needs to be satisfied at the free boundary (I0); the external force is expressed by 5.10. Since the problem is a 1D case, then $F = \sigma e^{i\omega t}$.

$$F|_{z=0} = (\sigma e^{i\omega t})\Big|_{z=0} = E_1 \left(\frac{\partial u_i^{(1)}}{\partial z} + \frac{\partial u_r^{(1)}}{\partial z}\right)\Bigg|_{z=0}$$

Thus, at $z = 0$:

$$(-ik_1 E_1)\, A_1 + (ik_1 E_1)\, B_1 = \sigma$$

Boundary Condition 2.

The second boundary condition needs to be applied at interface I1 between L1 and L2.

$$E_1(\frac{\partial u_i^{(1)}}{\partial z} + \frac{\partial u_r^{(1)}}{\partial z})\Big|_{z=h_1} = E_2(\frac{\partial u_i^{(2)}}{\partial z} + \frac{\partial u_r^{(2)}}{\partial z})\Big|_{z=h_1}$$

Thus, at $z = h_1$:

$$(-E_1k_1e^{-ik_1h_1})A_1 + (E_1k_1e^{ik_1h_1})B_1 + (E_2k_2e^{-ik_2h_1})A_2 + (-E_2k_2e^{ik_2h_1})B_2 = 0$$

Boundary Condition 3.

The third boundary condition needs to be satisfied at interface I1 between L1 and L2.

$$(\frac{\partial u_i^{(1)}}{\partial t} + \frac{\partial u_r^{(1)}}{\partial t})\Big|_{z=h_1} = (\frac{\partial u_i^{(2)}}{\partial t} + \frac{\partial u_r^{(2)}}{\partial t})\Big|_{z=h_1}$$

Thus, at $z = h_1$:

$$(e^{-ik_1h_1})A_1 + (e^{ik_1h_1})B_1 + (-e^{-ik_2h_1})A_2 + (-e^{ik_2h_1})B_2 = 0$$

Boundary Condition 4.

The fourth boundary condition needs to be satisfied at interface I2 between L2 and L3.

$$E_2(\frac{\partial u_i^{(2)}}{\partial z} + \frac{\partial u_r^{(2)}}{\partial z})\Big|_{z=h_2} = E_3(\frac{\partial u_i^{(3)}}{\partial z} + \frac{\partial u_r^{(3)}}{\partial z})\Big|_{z=h_2}$$

Thus, at $z = h_2$:

$$(-E_2k_2e^{-ik_2h_2})A_2 + (E_2k_2e^{ik_2h_2})B_2 + (E_3k_3e^{-ik_3h_2})A_3 + (-E_3k_3e^{ik_3h_2})B_3 = 0$$

Boundary Condition 5.

The fifth boundary condition needs to be satisfied at interface I2 between L2 and L3.

$$(\frac{\partial u_i^{(2)}}{\partial t} + \frac{\partial u_r^{(2)}}{\partial t})\Big|_{z=h_2} = (\frac{\partial u_i^{(3)}}{\partial t} + \frac{\partial u_r^{(3)}}{\partial t})\Big|_{z=h_2}$$

Thus, at $z = h_2$:

$$(e^{-ik_2h_2})A_2 + (e^{ik_2h_2})B_2 + (-e^{-ik_3h_2})A_3 + (-e^{ik_3h_2})B_3 = 0$$

Boundary Condition 6.

Finally, the sixth boundary condition needs to be satisfied at interface I3 between L3 and wall.

$$(u_i^{(3)} + u_r^{(3)})\Big|_{z=h_3} = 0|_{z=h_3}$$

Thus, at $z = h_3$:

$$(e^{-ik_3h_3})A_3 + (e^{ik_3h_3})B_3 = 0$$

The complete steps to get the boundary conditions are shown in Appendix B.2. Based on the equations written above, it is possible to build the following system of equations S:

$$S := \begin{cases} (-iE_1k_1)A_1 + (iE_1k_1)B_1 = \sigma \\ (-E_1k_1e^{-ik_1h_1})A_1 + (E_1k_1e^{ik_1h_1})B_1 + (E_2k_2e^{-ik_2h_1})A_2 + (-E_2k_2e^{ik_2h_1})B_2 = 0 \\ (e^{-ik_1h_1})A_1 + (e^{ik_1h_1})B_1 + (-e^{-ik_2h_1})A_2 + (-e^{ik_2h_1})B_2 = 0 \\ (-E_2k_2e^{-ik_2h_2})A_2 + (E_2k_2e^{ik_2h_2})B_2 + (E_3k_3e^{-ik_3h_2})A_3 + (-E_3k_3e^{ik_3h_2})B_3 = 0 \\ (e^{-ik_2h_2})A_2 + (e^{ik_2h_2})B_2 + (-e^{-ik_3h_2})A_3 + (-e^{ik_3h_2})B_3 = 0 \\ (e^{-ik_3h_3})A_3 + (e^{ik_3h_3})B_3 = 0 \end{cases} \tag{5.11}$$

The system of equations S can be expressed in matrix form:

$$M\,X = C$$

where

$$M = \begin{bmatrix} -ik_1E_1 & ik_1E_1 & 0 & 0 & 0 & 0 \\ -E_1k_1e^{-ik_1h_1} & E_1k_1e^{ik_1h_1} & E_2k_2e^{-ik_2h_1} & -E_2k_2e^{ik_2h_1} & 0 & 0 \\ e^{-ik_1h_1} & e^{ik_1h_1} & -e^{-ik_2h_1} & -e^{ik_2h_1} & 0 & 0 \\ 0 & 0 & -E_2k_2e^{-ik_2h_2} & E_2k_2e^{ik_2h_2} & E_3k_3e^{-ik_3h_2} & -E_3k_3e^{ik_3h_2} \\ 0 & 0 & e^{-ik_2h_2} & e^{ik_2h_2} & -e^{-ik_3h_2} & -e^{ik_3h_2} \\ 0 & 0 & 0 & 0 & e^{-ik_3h_3} & e^{ik_3h_3} \end{bmatrix}$$

$$X := \begin{bmatrix} A_1 \\ B_1 \\ A_2 \\ B_2 \\ A_3 \\ B_3 \end{bmatrix} \qquad C = \begin{bmatrix} \sigma \\ 0 \\ 0 \\ 0 \\ 0 \\ 0 \end{bmatrix}$$

M is the matrix of coefficients, X is the column vector of the unknown terms represented by the six amplitudes A_j, B_j, with $j = 1, 2, 3$, and C is the column vector of the known terms.

Then, the amplitudes of the column vector of the unknowns X will be found:

$$X = M^{-1}\, C \tag{5.12}$$

and they will depend on ω and the load σ. Notice that the $det(M) \neq 0$.

The amplitudes can be found in Appendix B.3, and how it can be seen, they are expressed in function of σ and only in function of k_1 considering the relationships 5.9. Notice that the numerical values of density, elastic modulus, and distance of the interfaces (h_j) from the origin have been substituted in order to have a more simplified expressions of A_j and B_j. After finding the amplitudes, the expressions of the deformations are defined and it is possible to calculate the stresses:

$$\sigma_{zz}^{(j)} = E\, \frac{\partial u^{(j)}}{\partial z} \tag{5.13}$$

where $u^{(j)} = u_i^{(j)} + u_r^{(j)}$.

5.4 Improvement of the Three-Layered Model

In Section 5.3 a model composed by three layers was introduced; it was a 1D model where compression plane waves propagated inside. Equation 5.1 was simplified and the governing equation

$$E\frac{\partial^2 u}{\partial z^2} = \rho\frac{\partial^2 u}{\partial t^2}$$

that does not take into account any damping, was obtained.

An improvement to the three-layered model can be to include a damping term in the governing equation; then the previous equation becomes:

$$E\frac{\partial^2 u}{\partial z^2} = \rho\frac{\partial^2 u}{\partial t^2} + d\frac{\partial u}{\partial t} \tag{5.14}$$

where d represents the damping term.

The boundary conditions, and the corresponding system of equations S will be modified because the relationship between ω and k will include the term d.

Substituting $u = C\, e^{i\omega t - ikz}$ into equation 5.14, it results:

$$ECe^{i\omega t-ikz}(-k^2) = \rho Ce^{i\omega t-ikz}(-\omega^2) + dCe^{i\omega t-ikz}(i\omega) \;\rightarrow\; -Ek^2 = -\rho\omega^2 + id\omega$$

then, it results:

$$k = \pm\sqrt{\frac{\rho}{E}\omega^2 - i\frac{d}{E}\omega} \tag{5.15}$$

Differently from equation 5.7, the new relationship between ω and k also includes an imaginary term. It can be also possible to express ω in function of k:

$$\omega_{1/2} = \frac{id \pm \sqrt{4\rho E k^2 - d^2}}{2\rho}$$

Since there are three layers, there will be three values of k:

$$k_1 = \pm\sqrt{\frac{\rho_1}{E_1}\omega^2 - i\frac{d}{E_1}\omega}, \quad k_2 = \pm\sqrt{\frac{\rho_2}{E_2}\omega^2 - i\frac{d}{E_2}\omega}, \quad k_3 = \pm\sqrt{\frac{\rho_3}{E_3}\omega^2 - i\frac{d}{E_3}\omega}$$

In the improvement of the three-layered model, the boundary conditions and the corresponding system of equations 5.17, expressed in terms of k_j with $j = 1, 2, 3$, defined in the previous section can be still used in order to find the unknowns, but it needs to consider the new relationship between ω and k, expressed by equation 5.15.

In this current section, and in section 5.3 discussed before, two cases related to the three-layered model were analysed: the case with the presence of damping in the process and the case without damping term. As already mentioned in Chapter 4, the presence of damping makes the model much closer to the reality because its presence guarantees the end of the process considered after a certain amount of time, whereas the absence of a damping term in the equations leads the process of waves propagation to last infinitely.

Although the damping term makes more realistic the model, at the same time it complicates the relationship between ω and k as can be seen comparing the formulas 5.7 and 5.15. In the second case, the expressions of the amplitudes (A_j, B_j) become more intricate due to the presence of the term $-i\frac{d}{E_j}\omega$.

However, in both cases the external load causes the generation and propagation of an incident strain wave that, in turn, causes the generation of new waves (reflected and transmitted) at the interfaces of the three-layered model.

Although a 3D model was firstly considered for the project, then it was approximated to a 1D case; it meant that no (distortion) waves could be defined in a direction different from z, and the physical explanation about the particle motion and Poisson effect cannot be valid anymore. Furthermore, in Section 5.3 it was seen that in order to obtain the governing equation 5.4, the Poisson ratio (ν) needed to be approximated to zero; this meant no coupling between longitudinal and transverse strains.

5.5 Fourier Transform

In the previous sections, the amplitudes (A_j, B_j), with $j = 1, 2, 3$ have been derived by solving the system of equations S; as can be seen in Appendix B.3, the amplitudes for the three-layered model without damping are a function of k that in turn is a function of ω, and σ, whereas for the three-layered model with damping they also depend on the damping term d.

It is possible to generalize the specific case analysed in the previous sections as follows:

For $\sigma = \sigma_1 \rightarrow F_1(t) = \sigma_1\, e^{i\omega_1 t} \rightarrow u^{(j)} = A_j(\sigma_1)\, e^{i\omega_1 t} + B_j(\sigma_1)\, e^{i\omega_1 t}$,

For $\sigma = \sigma_2 \rightarrow F_2(t) = \sigma_2\, e^{i\omega_2 t} \rightarrow u^{(j)} = A_j(\sigma_2)\, e^{i\omega_2 t} + B_j(\sigma_2)\, e^{i\omega_2 t}$,

$\vdots$

For $\sigma = \sigma_n \rightarrow F_n(t) = \sigma_n\, e^{i\omega_n t} \rightarrow u^{(j)} = A_j(\sigma_n)\, e^{i\omega_n t} + B_j\,(\sigma_n) e^{i\omega_n t}$,

Notice that the expressions such as $A_j(\sigma_1)$ or $B_j(\sigma_1)$ mean that the amplitudes A_j and B_j depend on the value chosen for σ_1.

Thus, for $\sigma = \sigma_1 + \sigma_2 + ... + \sigma_n \rightarrow F(t) = F_1(t) + F_2(t) + ... + F_n(t)$

then,

$$F(t) = \sum_{q=1}^{n} \sigma_q\, e^{i\omega_q t} \Delta\omega \approx \int_{-\infty}^{\infty} \sigma_q\, e^{i\omega_q t} d\omega \tag{5.16}$$

From the equation 5.16 it is possible to recognize the inverse transform and the Fourier transform:

$$\mathcal{F}^{-1}[\sigma(\omega)](t) = F(t) = \int_{-\infty}^{\infty} \sigma(\omega)\, e^{i\omega t} d\omega$$

and

$$\mathcal{F}[F(t)](\omega) = \sigma(\omega) = \int_{-\infty}^{\infty} F(t)\, e^{-i\omega t} dt$$

5.6 Model composed by n-Layers

It is also possible to generalise the three-layered model taken into account in the previous sections to a n-layered material as shown in Figure 5.3:

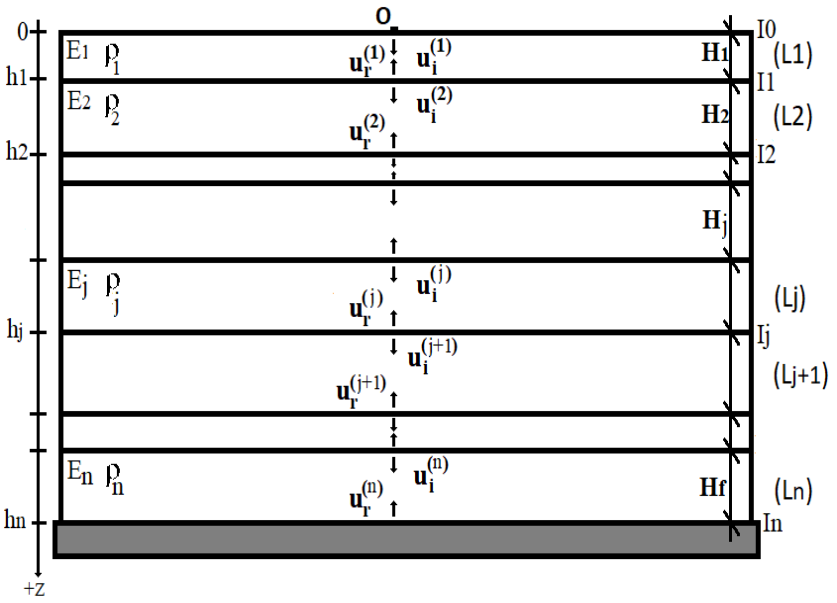

Figure 5.3: General case: model with n layers.

The general expressions of the deformations will be:

$$u_i^{(1)} = A_1\, e^{i\omega t} e^{-izk_1}; \qquad u_r^{(1)} = B_1\, e^{i\omega t} e^{izk_1}$$

$$\vdots$$

$$u_i^{(j)} = A_j\, e^{i\omega t} e^{-izk_j}; \qquad u_r^{(j)} = B_j\, e^{i\omega t} e^{izk_j}$$

$$u_i^{(j+1)} = A_{j+1}\, e^{i\omega t} e^{-izk_{j+1}}; \qquad u_r^{(j+1)} = B_{j+1}\, e^{i\omega t} e^{izk_j}$$

$$\vdots$$

$$u_i^{(n)} = A_n\, e^{i\omega t} e^{-izk_n}; \qquad u_r^{(n)} = B_n\, e^{i\omega t} e^{izk_n}$$

with

$$k_1 = \pm\omega\sqrt{\frac{\rho_1}{E_1}};\ \ ..\ k_j = \pm\omega\sqrt{\frac{\rho_j}{E_j}};\ \ k_{j+1} = \pm\omega\sqrt{\frac{\rho_{j+1}}{E_{j+1}}};\ \ ..\ k_n = \pm\omega\sqrt{\frac{\rho_n}{E_n}}$$

if there is no damping, whereas

$$k_1 = \pm\sqrt{\frac{\rho_1}{E_1}\omega^2 - i\frac{d}{E_1}\omega};\ \ ..\ k_j = \pm\sqrt{\frac{\rho_j}{E_j}\omega^2 - i\frac{d}{E_j}\omega};..\quad k_n = \pm\sqrt{\frac{\rho_n}{E_n}\omega^2 - i\frac{d}{E_n}\omega}$$

if there is a damping term d.

The boundary conditions will be satisfied at three types of interfaces:

– At I0 which is a free interface and divides the first layer from the external environment ($z = 0$):

$$F|_{z=0} = (\sigma e^{i\omega t})\Big|_{z=0} = E_1 \,(\frac{\partial u_i^{(1)}}{\partial z} + \frac{\partial u_i^{(1)}}{\partial z})\Big|_{z=0}$$

– At I_j, with $1 < j < n-1$, the interface which divides layer j from layer $j+1$ ($z = h_j$):

$$E_j(\frac{\partial u_i^{(j)}}{\partial z} + \frac{\partial u_r^{(j)}}{\partial z})\Big|_{z=h_j} = E_{j+1}(\frac{\partial u_i^{(j+1)}}{\partial z} + \frac{\partial u_r^{(j+1)}}{\partial z})\Big|_{z=h_j}$$

$$(\frac{\partial u_i^{(j)}}{\partial t} + \frac{\partial u_r^{(j)}}{\partial t})\Big|_{z=h_j} = (\frac{\partial u_i^{(j+1)}}{\partial t} + \frac{\partial u_r^{(j+1)}}{\partial t})\Big|_{z=h_j}$$

– At I_n which divides the last layer from the wall ($z = h_n$):

$$(u_i^{(n)} + u_r^{(n)})\Big|_{z=h_n} = 0|_{z=h_n}$$

The system of equations S in the general case becomes:

$$\begin{cases} (-iE_1k_1)A_1 + (iE_1k_1)B_1 = \sigma \\ (-E_1k_1e^{-ik_1h_1})A_1 + (E_1k_1e^{ik_1h_1})B_1 + (E_2k_2e^{-ik_2h_1})A_2 + (-E_2k_2e^{ik_2h_1})B_2 = 0 \\ (e^{-ik_1h_1})A_1 + (e^{ik_1h_1})B_1 + (-e^{-ik_2h_1})A_2 + (-e^{ik_2h_1})B_2 = 0 \\ \vdots \\ (-E_jk_je^{-ik_jh_j})A_j + (E_jk_je^{ik_jh_j})B_j + (E_{j+1}k_{j+1}e^{-ik_{j+1}h_j})A_{j+1} + (-E_{j+1}k_{j+1}e^{ik_{j+1}h_j})B_{j+1} = 0 \\ (e^{-ik_jh_j})A_j + (e^{ik_jh_j})B_j + (-e^{-ik_{j+1}h_j})A_{j+1} + (-e^{ik_{j+1}h_j})B_{j+1} = 0 \\ \vdots \\ (e^{-ik_nh_n})A_n + (e^{ik_nh_n})B_n = 0 \end{cases} \tag{5.17}$$

Then, the system of equations can be expressed in matrix form:

$$M_G \, X_G = C_G$$

where the general matrix M_G of coefficients is:

$$M_G = \begin{bmatrix} -ik_1E_1 & ik_1E_1 & 0 & 0 & 0 & 0 \\ -E_1k_1e^{-ik_1h_1} & E_1k_1e^{ik_1h_1} & E_2k_2e^{-ik_2h_1} & -E_2k_2e^{ik_2h_1} & 0 & 0 \\ e^{-ik_1h_1} & e^{ik_1h_1} & -e^{-ik_2h_1} & -e^{ik_2h_1} & 0 & 0 \\ \vdots & \vdots & \vdots & \vdots & \vdots & \vdots \\ -E_jk_je^{-ik_jh_j} & E_jk_je^{ik_jh_j} & E_{j+1}k_{j+1}e^{-ik_{j+1}h_j} & -E_{j+1}k_{j+1}e^{ik_{j+1}h_j} & 0 & 0 \\ e^{-ik_jh_j} & e^{ik_jh_j} & -e^{-ik_{j+1}h_j} & -e^{ik_{j+1}h_j} & 0 & 0 \\ \vdots & \vdots & \vdots & \vdots & \vdots & \vdots \\ 0 & 0 & 0 & 0 & e^{-ik_nh_n} & e^{ik_nh_n} \end{bmatrix}$$

and the general column vectors X_G and B_G of unknown and known terms, respectively, are:

$$X_G = \begin{bmatrix} A_1 \\ B_1 \\ \vdots \\ A_j \\ B_j \\ \vdots \\ A_n \\ B_n \end{bmatrix} \qquad C_G = \begin{bmatrix} \sigma \\ 0 \\ \vdots \\ 0 \\ 0 \\ \vdots \\ 0 \\ 0 \end{bmatrix}$$

Then, the unknowns represented by the column vector X will be found:

$$X_G = M_G^{-1} \, C_G$$

with $det(M_G) \neq 0$.

From Sections 5.3 and 5.6 it is possible to notice that for a three-layered model M is a (6x6) matrix, for n-layers M becomes a ($2n$x$2n$) matrix.

The generalisation of the three-layered model to a n-layered model has the advantage that it can be easily used for all models which have the same configuration *external environment-interface-layer-interface-layer-interface-wall*, and it suggests the use of the n-layered model in which, for instance, the plywood (layer 1) is composed by numerous sub-layers (see Recommendations in Chapter 6).

5.7 Deformation of the three-layered model for different impact loads

Based on the layered model shown in Section 5.3, the equations and the procedure for defining the deformation of the structure, the presence of the damping term in the governing equation for the 1D case, and the Fourier transform related to the external force, it was decided to take into account different impact loads in order to understand how the corresponding deformations of the layered model could differ each other. Each case listed below has a particular value for the pressure p and for the duration time t:

case 1: Impact load with 1 bar and 10 ms;

case 2: Impact load with 10 bar and 1 ms;

case 3: Impact load with 100 bar and 0.1 ms;

case 4: Impact load with 1000 bar and 0.01 ms.

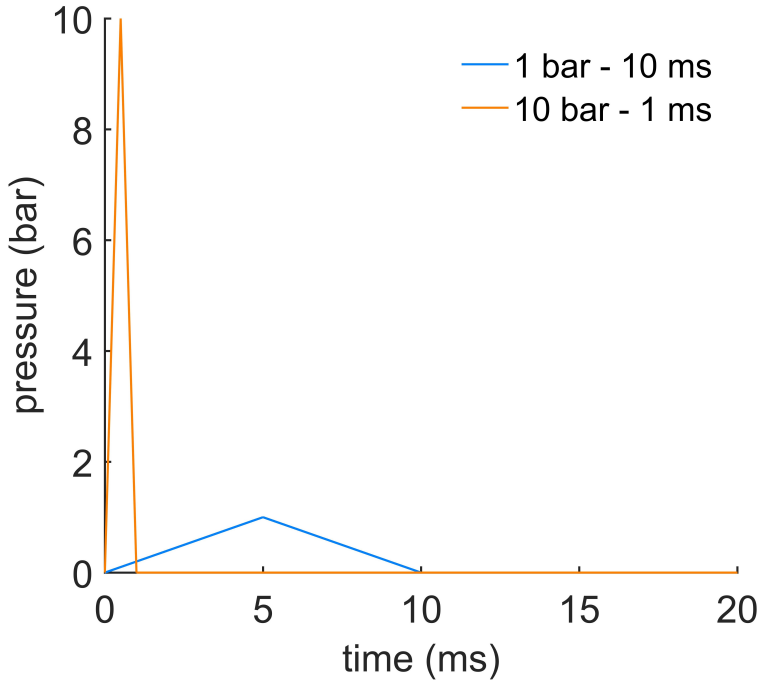

Figure 5.4: Isosceles triangle load with $p = 1\,bar$ and $t = 10\,ms$, and isosceles triangle load with $p = 10\,bar$ and $t = 1\,ms$.

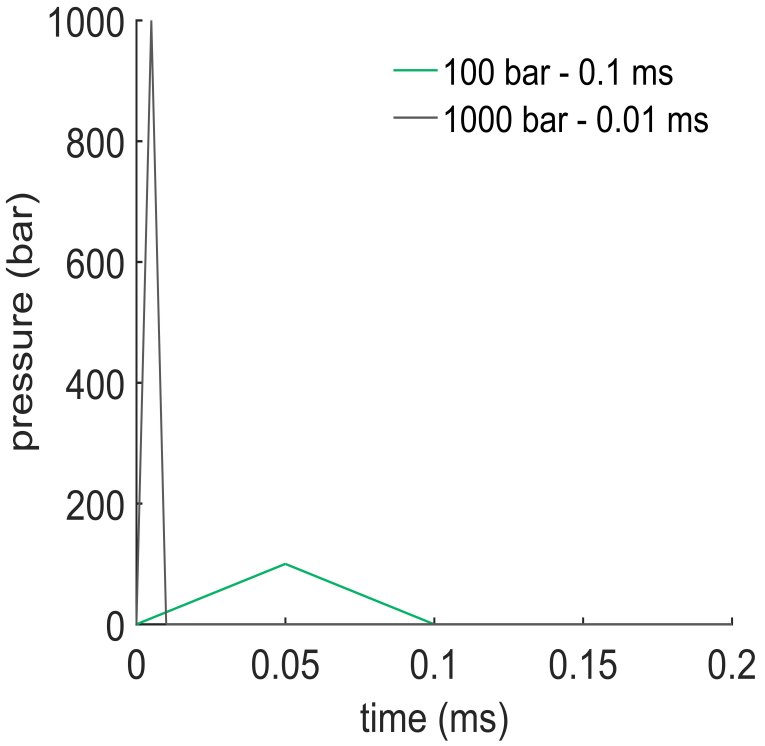

Figure 5.5: Isosceles triangle load with $p = 100\,bar$ and $t = 0.1\,ms$, and isosceles triangle load with $p = 1000\,bar$ and $t = 0.01\,ms$.

As can be noticed from the graphs shown above, the type of load is described by a triangle function, specifically, an isosceles triangle function. Graph in Figure 5.4 shows the isosceles triangle load for the first case with $p = 1\,bar$ and $t = 10\,ms$ (in blue), and the isosceles triangle load for the second case with $p = 10\,bar$ and $t = 1\,ms$ (in orange), whereas Graph in Figure 5.5 shows the isosceles triangle load for the third case with $p = 100\,bar$ and $t = 0.1\,ms$ (in green), and the isosceles triangle load for the fourth case with $p = 1000\,bar$ and $t = 0.01\,ms$ (in black).

Since the impulse can be defined by using the following formula

$$J = \int F(t)\,dt$$

namely, the integral of the load time history, then the area under the four curves (the isosceles triangle functions) in Figures 5.4 and 5.5 is the same, even if the values of p and t are different in each case.

Applying the Fourier transform to each of the isosceles triangles loads, it is possible to see the frequency distribution of the energy.

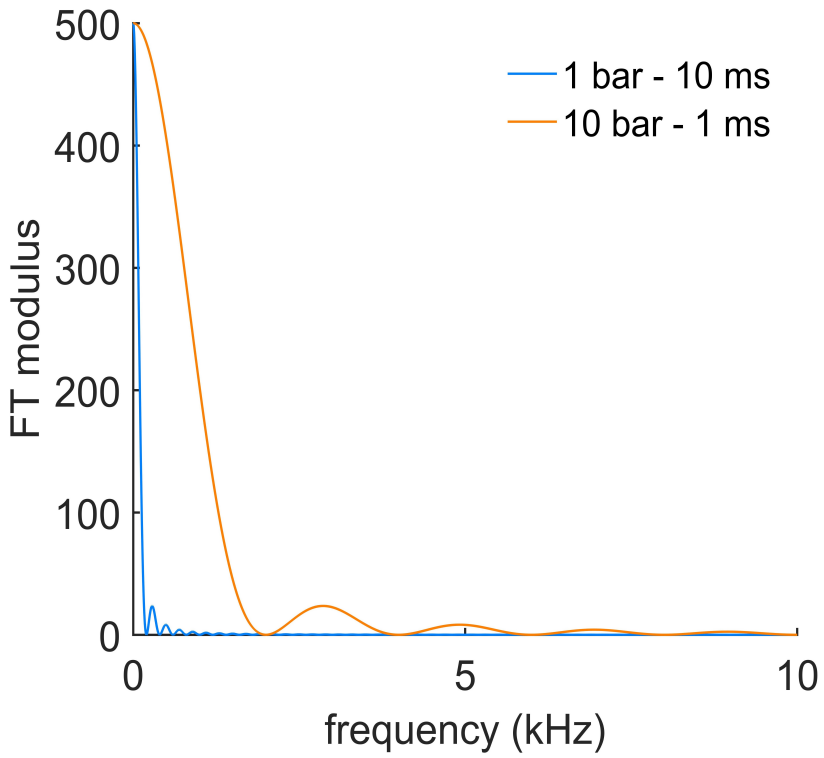

Figure 5.6: Fourier transform of the isosceles triangle for $p = 1\,bar$ and $t = 10\,ms$ and for $p = 10\,bar$ and $t = 1\,ms$.

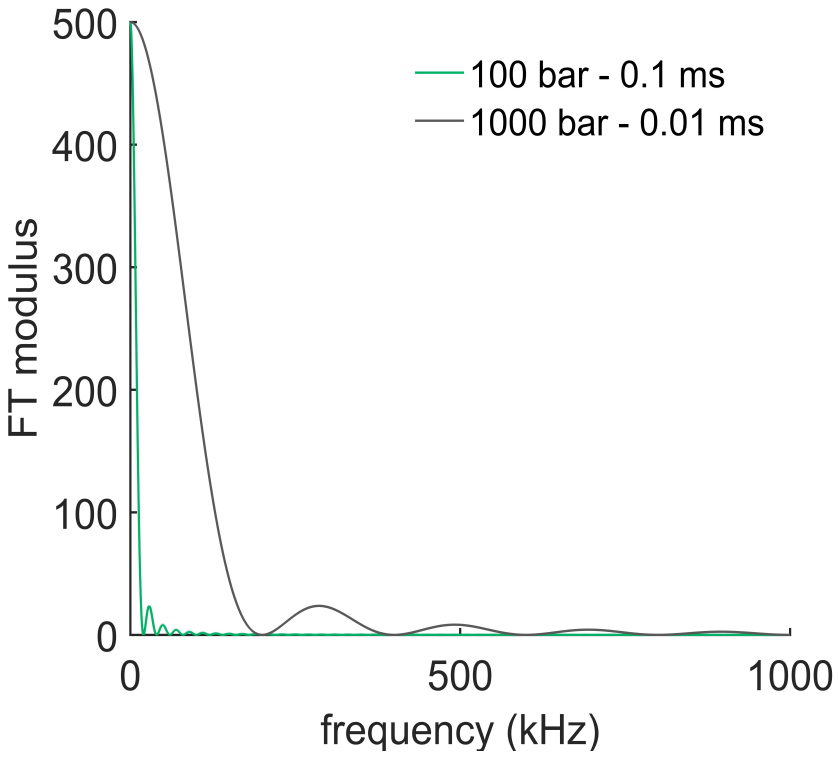

Figure 5.7: Fourier transform of the isosceles triangle for $p = 100\ bar$ and $t = 0.1\ ms$ and for $p = 1000\ bar$ and $t = 0.01\ ms$

The following graphs will show the displacement for each isosceles triangle load. Based on the equations of the previous sections, the deformation is also a function of the vertical position z; for this reason, it has been calculated for different locations (see Figure 5.8) of the layered structure. Notice that for each case, the second graph represents the same situation but it is a bit more enlarged on the time axis.

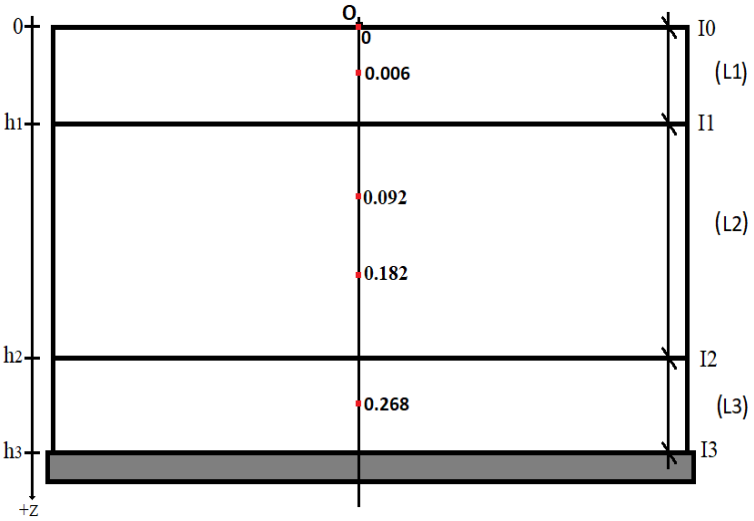

Figure 5.8: Locations where deformations have been evaluated for different impact loads.

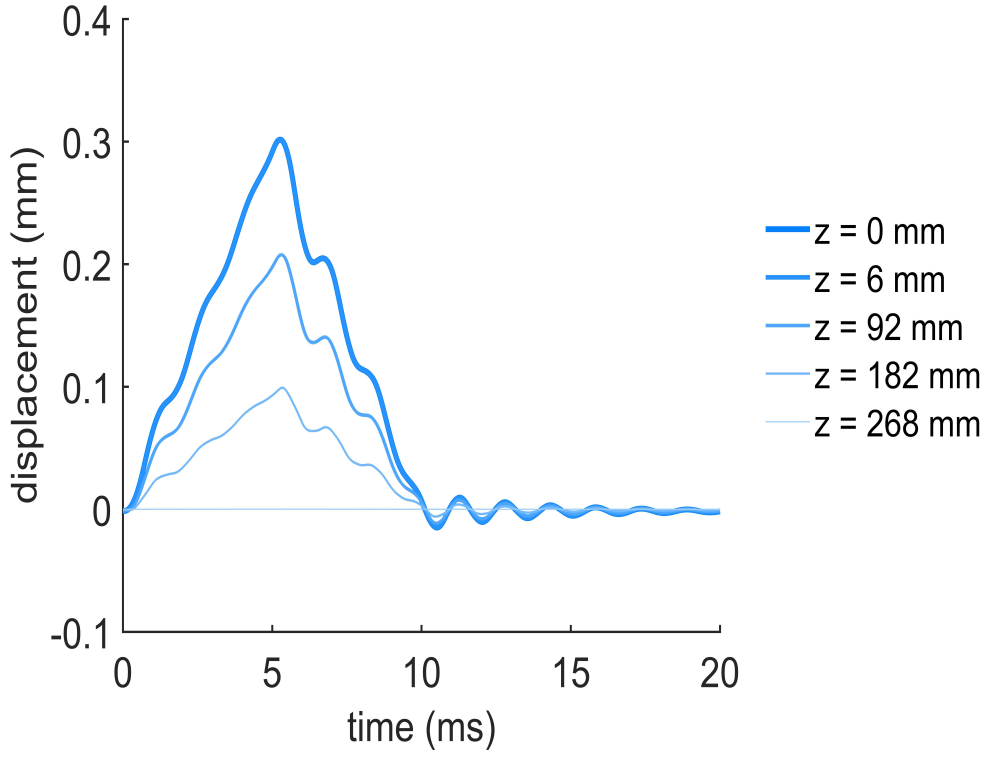

Figure 5.9: Displacement over time for the isosceles triangle load with $p = 1\,bar$ and $t = 10\,ms$ at different locations z.

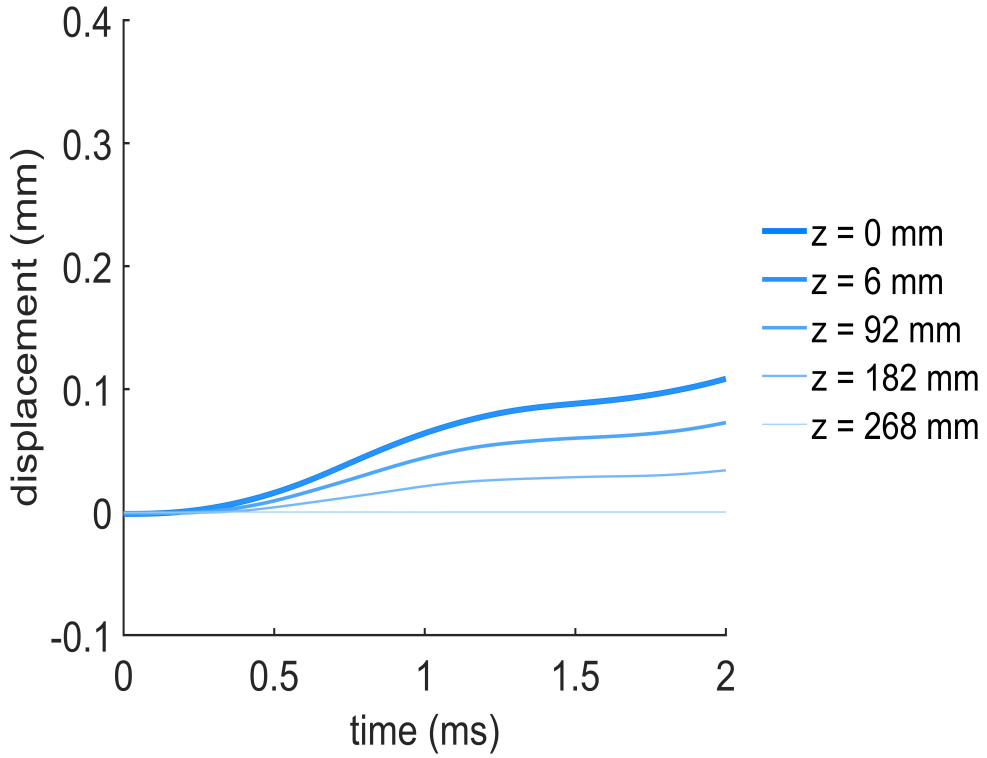

Figure 5.10: Displacement over time for the isosceles triangle load with $p = 1\,bar$ and $t = 10\,ms$ at different locations z.

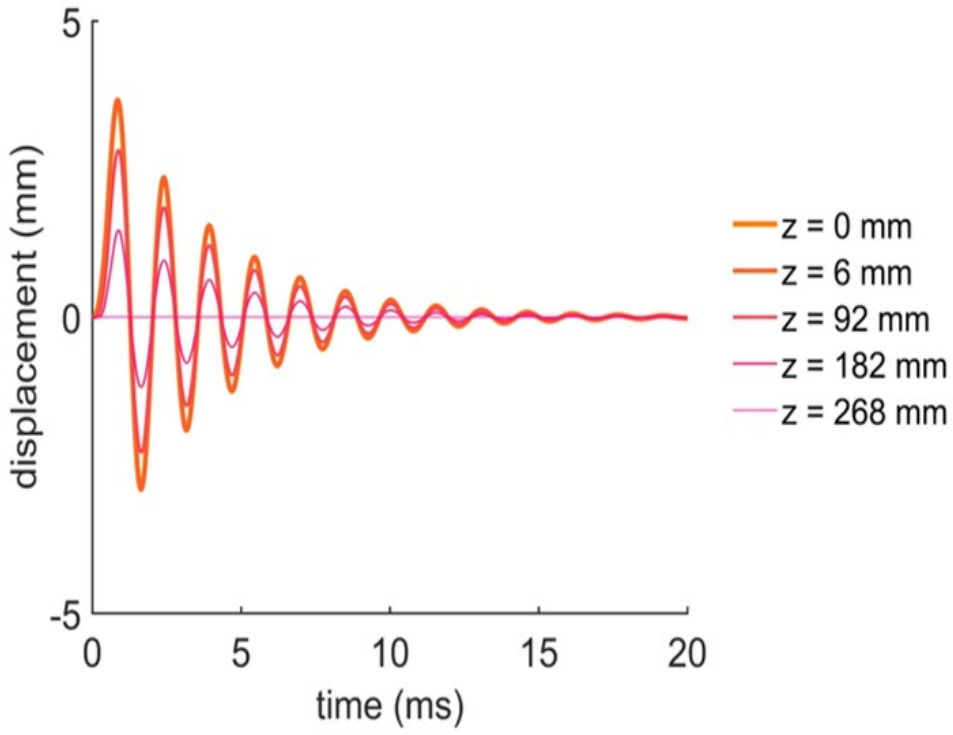

Figure 5.11: Displacement over time for the isosceles triangle load with $p = 10\,bar$ and $t = 1\,ms$ at different locations z.

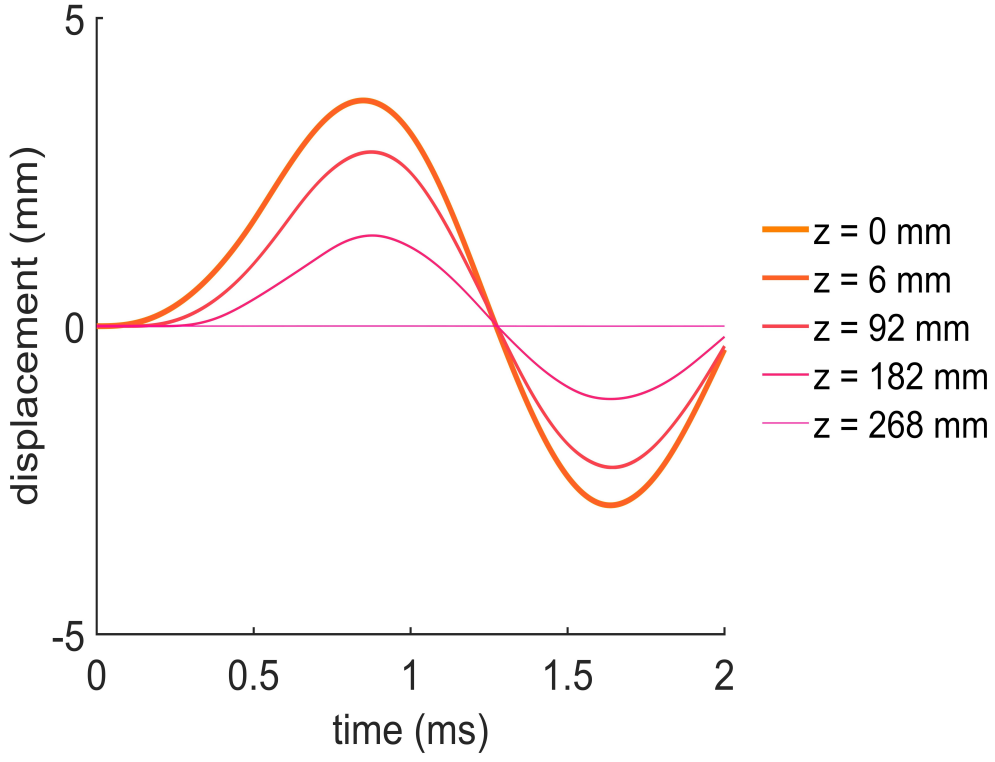

Figure 5.12: Displacement over time for the isosceles triangle load with $p = 10\,bar$ and $t = 1\,ms$ at different locations z.

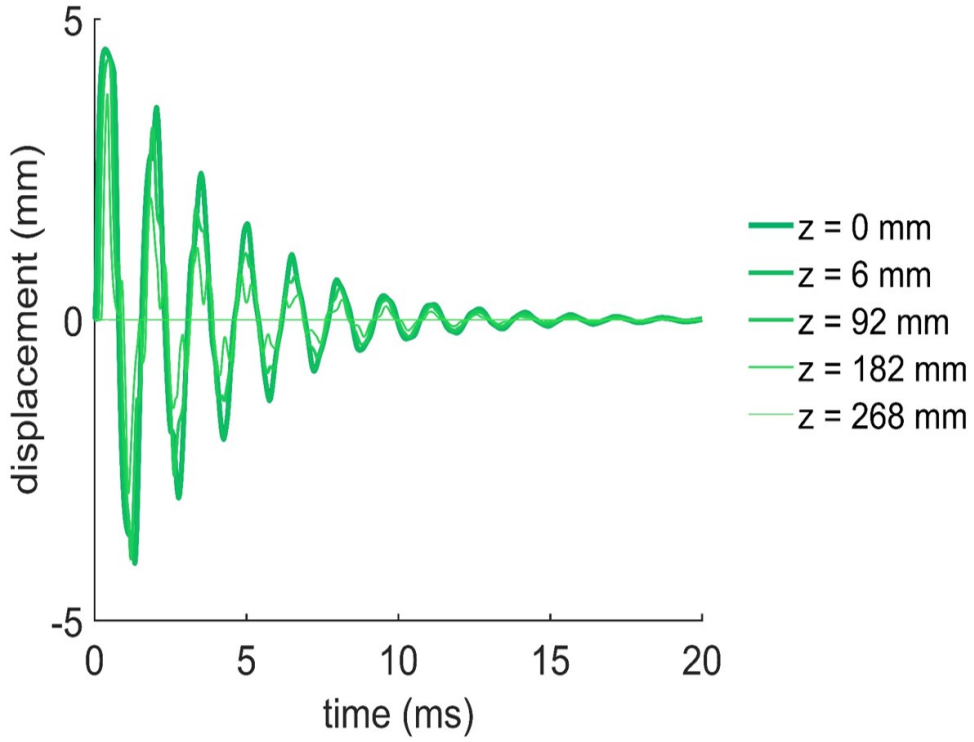

Figure 5.13: Displacement over time for the isosceles triangle load with $p = 100\,bar$ and $t = 0.1\,ms$ at different locations z.

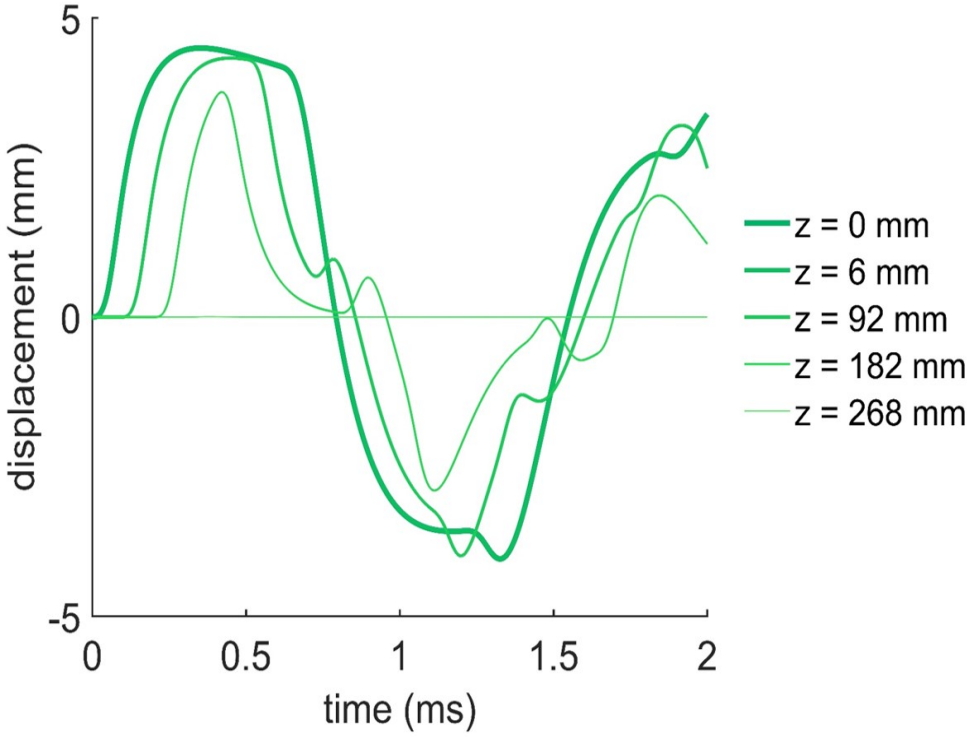

Figure 5.14: Displacement over time for the isosceles triangle load with $p = 100\,bar$ and $t = 0.1\,ms$ at different locations z.

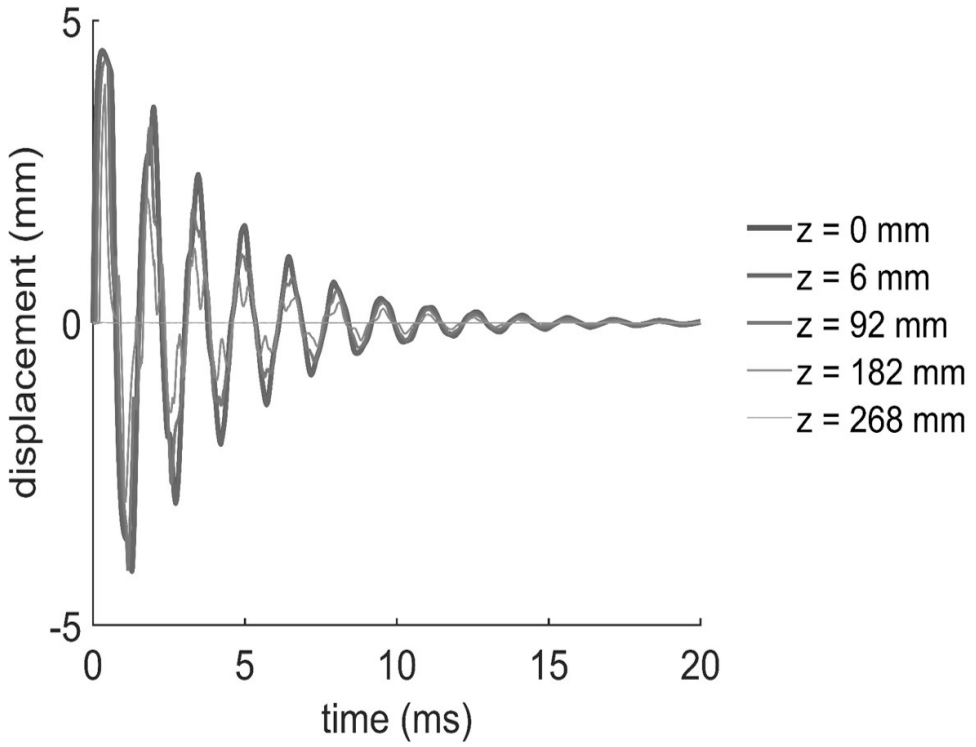

Figure 5.15: Displacement over time for the isosceles triangle load with $p = 1000\ bar$ and $t = 0.01\ ms$ at different locations z.

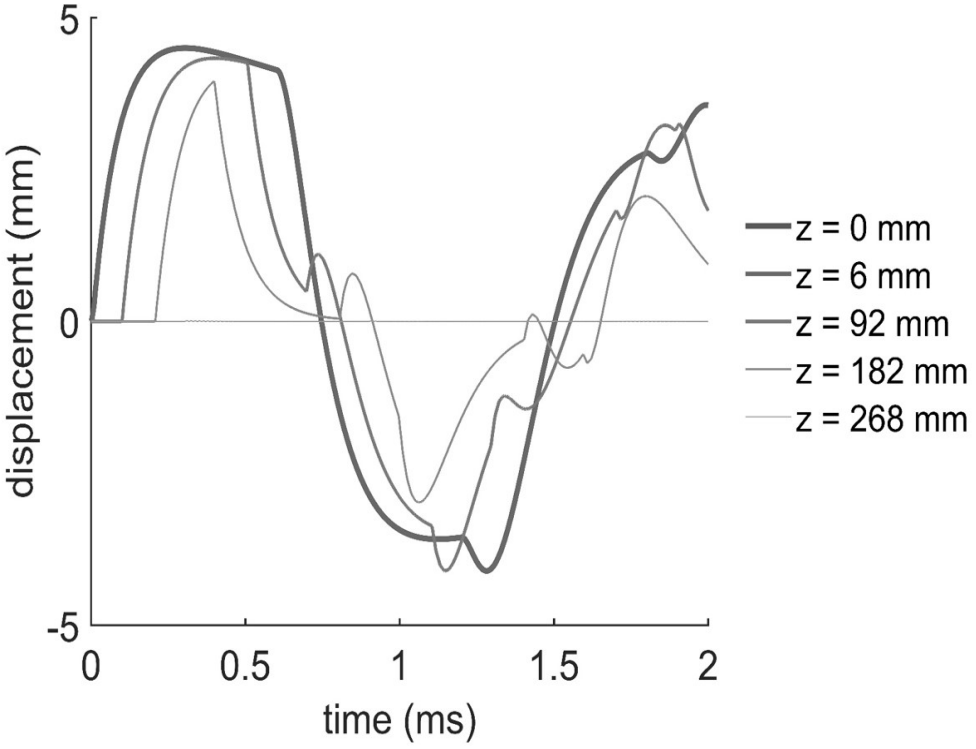

Figure 5.16: Displacement over time for the isosceles triangle load with $p = 1000\ bar$ and $t = 0.01\ ms$ at different locations z.

From the graphs above it is possible to see how for all four cases the deformation assumes the highest value at the free interface at $z = 0$, and then decreases with the increase of the thickness, until the last layer (back plywood L3); indeed, the location $z = 268\,mm$ corresponds to the middle of the last layer 3 and for all cases the deformation is zero due to the presence of the rigid wall that prevents any displacement.

In addition, the presence of a damping term is responsible of the decrease in the response. Notice that for all cases, it was chosen a value of damping $d = 10^5$.

Looking at the first curve, corresponding to $z = 0$, in darker blue in graph of Figure 5.9 (and Figure 5.10), the deformation is less than $0.2\,mm$, whereas for the other three cases it is less than $5\,mm$ for **case 2**, and close to $5\,mm$ for the last two.

Therefore, comparing all graphs in Figures 5.9-5.16 that show the deformations for the four different isosceles triangle loads, it is possible to notice that u is smaller in **case 1** which has the smallest value of pressure $p = 1\,bar$ and the highest duration time $t = 10\,ms$ than that of the other cases in which the pressure increases and the duration time decreases.

5.8 Conclusions

This chapter represents the answer to the second research question **Q2.** introduced at the beginning of the thesis. The purpose of this chapter was to apply the theory of waves propagation inside the material to the simplified layered structure presented in Chapter 2. As mentioned at the beginning, the first original idea was to express from a mathematical point of view the model of compression and distortion waves which propagate inside the layered material. Due to the global complexity of the problem, the initial 3D model was simplified to a 1D model where only compression waves propagated inside; this model was further simplified reducing the number of layers, even if it can easily be generalised to n-layers, as seen in Section 5.6. For the three-layered model, two cases were considered: the first one did not include any damping, whereas the second one considered a damping term d in the governing equation. Although the relationship between ω and k was much easier with no damping, however the presence of the term d in the governing equation made more realistic the model and, specially the process of waves propagation inside the structure. Four different loads have been considered for the 1D-damped three-layered model: the difference between the four impact loads concerned the values chosen for the duration times t and the pressures p. It was seen from the graphs in Section 5.7 that the deformation is smaller, for the case with the smallest value of p and the largest value of t (**case 1**), than the deformation obtained with a larger value of p and a smaller duration time t (the other cases). Furthermore, for all cases considered, the deformation decreases with the increase of the distance z from the free surface (at $z = 0$) until becoming zero in the back plywood.

Chapter 6

Conclusions

The propagation of waves in a layered material as consequence of an external impact was analysed in this thesis. The wave propagation phenomena at several interfaces were investigated, and consequently the theory of strain waves propagation was applied to a theoretical model.

This thesis concerned the wave impacts in the membrane LNG tanks which are subjected to sloshing impacts; when they are not completely filled, surface waves are generated and impact against the internal tank walls. The process of turning the natural gas into LNG (liquefied natural gas) has numerous advantages such as the resulting condensed liquid occupies a volume which is 600 smaller giving the chance to transport it in tanks over long distances by ships; in addition, the heat transfer is minimized and the cargo capacity is maximized by using cargo containment systems (CCSs).

As mentioned at the beginning, this project investigated the exact moment of the wave impact against a structure, namely when ELP1 took place and strain waves developed in the structure, whereas pressure waves travelled back in the liquid. Specifically, it focused on the physics of waves propagation as a consequence of an external impact. In order to provide an appropriate description of the physical phenomena and also a simplified theoretical model, the research questions **Q1.** and **Q2.** were formulated:

Q1. How do strain waves propagate through the structure upon a liquid impact?

Q2. How can the theory of the strain waves propagation be applied to a theoretical model?

Section 6.1 summarises and discusses the most important aspects of each chapter, whereas Section 6.2 provides some recommendations for future works.

6.1 Main Conclusions

Layered Structure Part

The model chosen for this project was the MarkIII CCS which is one of the most applied membrane CCSs. Membrane CCSs are generally used for large seagoing LNG carriers because the cargo capacity is maximized and the heat transfer is limited due to the insulation. The original configuration of the MarkIII was modified in order to have an easier configuration: interface-layer-interface-layer; the interfaces could separate two layers with the same or different material characteristics. There were two types of materials: plywood (top plywood L1, and back plywood L4) and reinforced poly-urethane foam (primary RPUF L2, and secondary RPUF L3). It was distinguished between impact area and out-of-impact area: the impact area was identified as the internal (layered) region initially affected, after a very small amount of time, by the direct impact, whereas the out-of-impact areas were the surrounding (layered) regions which felt the effects of the external load after a lightly larger amount of time. This distinction was considered essential because established the boundaries of the problem. Both these definitions agreed with the concept of *wave propagation*, that is to say, each region in a structure is not immediately affected by the external load but a certain amount of time is required before a *disturbance* modifies the current state of equilibrium. The external impact was considered as a disturbance that propagated inside the structure from the source located on the free surface. Furthermore, the concept of spreading area was also considered and defined as the region inside the structure where waves propagated; its extension depended on time (specifically, it increased over time). The spreading area shown in Chapter 2 considered an external force acting in one single point, and both its vertical and horizontal dimensions changed with time. As it was discussed later each variation of the external load caused a wave with a new geometry and a new spreading area.

Hydrodynamic Part

For a better understanding of the change in the external load, attention was focused on the hydrodynamic part. It concerned the external process, and represented the starting point of this project. When a liquid is involved in the impact against a solid body, then the analysis of the impact process becomes complicated: differently from a solid body the liquid is subjected to many physical phenomena that take place not only at the moment of the direct impact, but also before and after; they cause a change in the shape of the liquid mass. The basic elements of the impact loads are the ELPs (Elementary Loading Processes):

ELP1. Direct impact: the abrupt stop of the liquid when it directly impacts the structure;

ELP2. Building jet: the sharp turn of the liquid when it is forced along the structure;

ELP3. Compression of escaping or entrapping gas: the compression of the gas when it is escaping or entrapped.

The physical phenomena analysed in Chapter 4 were considered as a direct consequence of the impact of a liquid mass against a structure. The wave approaching the structure was continuously subjected to changes: before the impact the wave trough started increasing its velocity upwards as it got close to the wall, and the structure felt the pressure from outside; furthermore, instabilities were created due to the escaping gas which sheared the wave surface; the result was a distributed pressure over a larger surface area; as ELP1 took place, not only the loading area was affected by the direct impact of the crest, but also the region below was influenced by a load: the compressed gas pocket; the gas could not escape quickly enough and it was entrapped between the wave crest, the wave trough and the wall; after the direct impact more portions of the structure (the surrounding regions of the impact area) were involved because of the spreading of the wave crest along the wall surface. The direct impact represented a new condition for liquid and structure: both of them needed to re-adapt quickly to this new situation, and in order to decrease the discontinuity between liquid and wall, pressure waves and strain waves developed in the liquid and in the structure, respectively. The following figures show how different regions of the structure are involved in the changes of the liquid mass.

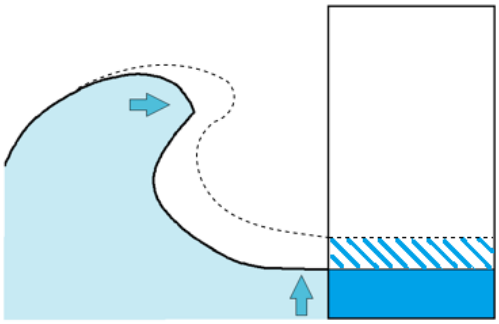

Figure 6.1: Before the impact: wave trough moving upward as the wave crest gets close to the wall.

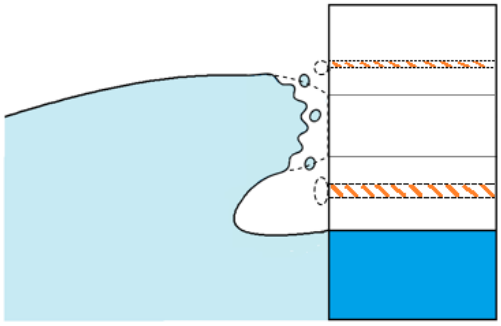

Figure 6.2: Before the impact: instabilities caused by the escaping gas distribute pressure over a large surface

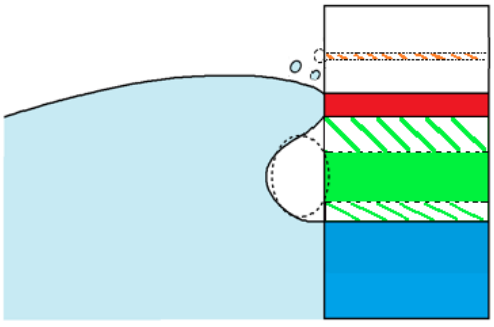

Figure 6.3: Moment of the impact: direct impact, instabilities and entrapped gas pocket.

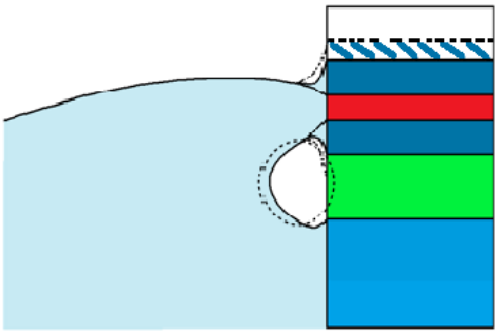

Figure 6.4: After the impact: Spreading of the wave crest and change in the gas pocket shape.

The external load changed in both space and time: as explained before, more portions of the surface of the model were involved in the contact with the liquid over time. Approximating the wave shape by a radius, $\overrightarrow{V_C(t)}$ expressed the velocity of the contact point C; actually there were two contact points moving with opposite velocities. This velocity decreased from ∞ to a specific value obtained at the critical time t_{cr}. Indeed, after t_{cr} the external process came to an end, meaning that the increase of the contact area and consequently the total force stopped at $t = t_{cr}$. Therefore, the external force depended on the contact area A and a pressure (pressure map) p which, in turn, depended on the space and time.

Waves Propagation Part

The propagation of the first wave took place immediately after ELP1; this first wave was assumed to be an incident compression spherical wave whose amplitude depended on the external load. At the first interface, the impinging of the first compression wave caused the generation of reflected and transmitted compression and distortion waves. The presence of distortion waves was justified from both a physical and mathematical point of view: physically, the passage of a compression wave is associated to both compression and shear, that is to say, if a small cube of material is in the path of a compression wave propagating in x-direction, then the cross-sectional areas perpendicular to x-direction are not modified, whereas those in the x-direction will be subjected to some changes; mathematically, if no distortion wave is assumed, then the boundary conditions at the interfaces are not satisfied at the same time. It was seen that compression waves were faster than distortion waves: in all layers $\beta_j \approx 0.63\,\alpha_j$, with $j = 1, 2, 3, 4$, and both compression and distortion velocities depended on the material characteristics. In the simplified structure, each incident wave generated both reflected and transmitted compression and distortion waves but it was only valid in the cases where the interfaces divided two elastic media; indeed, for the free interface (I0) no wave could be transmitted beyond the free surface, and for the last interface (I4) no wave could be transmitted in the rigid wall; thus, in these two situations only reflected compression and distortion waves were generated and they propagated back in the layer. Figure 6.5 shows the entire process of generation of new waves every time an incident (compression and distortion) wave meets an interface:

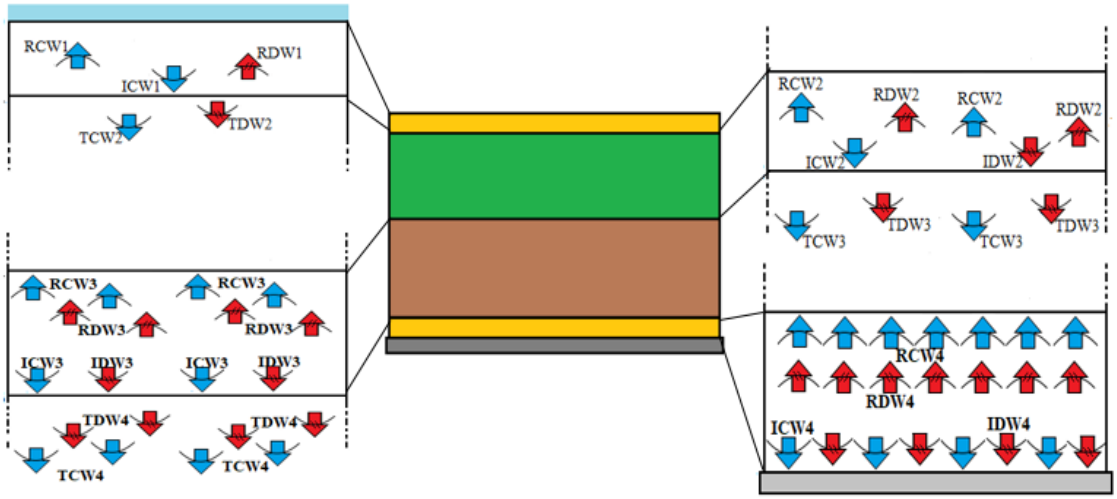

Figure 6.5: Generation of compression and distortion waves in all layers.

In order to understand what the relationship between propagation phenomena and time was, several G.W.P.P. models were taken into account. In the analysis of the global wave propagation phenomena, namely the incidence, reflection and transmission phenomena that occurred in the entire layered model, it was noticed that two conditions needed to be investigated:

C1 or C2 coincidence or distinction of wave propagation velocities α_j and β_j

C3 or C4 no change or decrease in the wave amplitudes

The distinction between compression and distortion velocities (condition **C2**) and the decrease in the wave amplitudes (condition **C4**) suggested a model as close as possible to the reality. As mentioned before, the propagation of a compression wave is a combination of shear and compression, and also numerically there is a difference between α and β values. Since after a certain amount of time, the internal process comes to an end, it is reasonable to assume a damping factor in the expressions of the waves. Furthermore, it was noticed that the easiest conditions to consider were **C1** ($\alpha_j = \beta_j$, with $j = 1, 2, 3, 4$) and **C3** ($A_i^{(j)} = A_r^{(j+1)} A_{tr}^{(j+1)}$), namely no distinction between compression and distortion waves, and no decrease in the reflected and transmitted wave amplitudes, that is to say, the process of waves propagation continued indefinitely. Models based on conditions **C1** and **C3** provide a model that is far from the reality. Figure 6.6 shows both compression and distortion waves in L1 and L2 assuming a decrease in the amplitudes, whereas Figure 6.7 shows only compression waves in L1 and L2 assuming no change in the amplitudes.

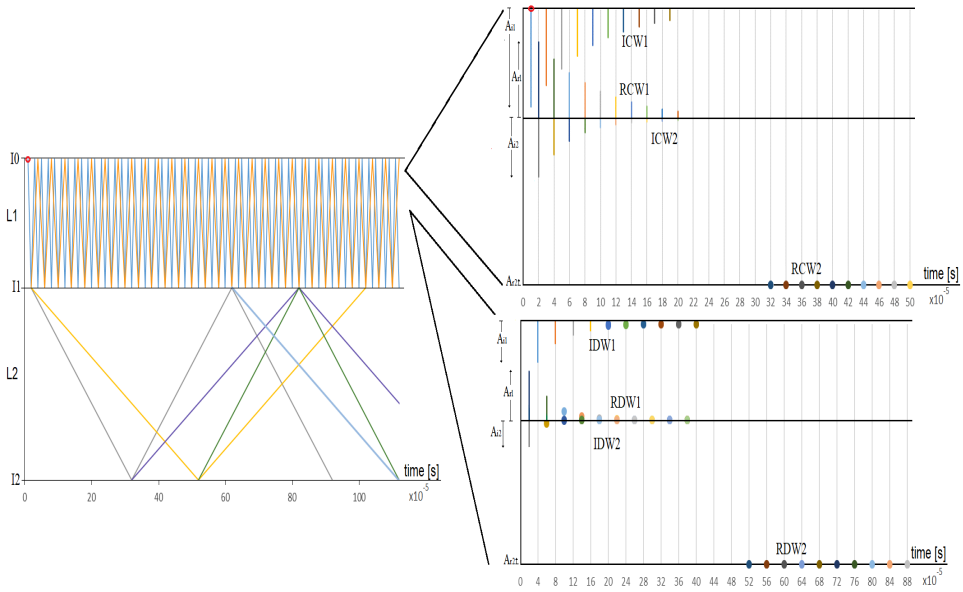

Figure 6.6: Final GWPP-model (L1 and L2) based on conditions C2 and C4.

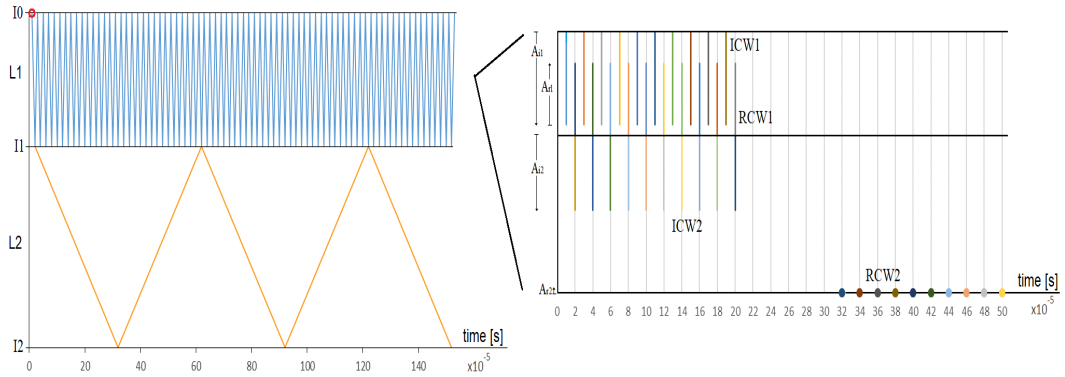

Figure 6.7: Final GWPP-model (L1 and L2) based on conditions C1 and C3.

As mentioned before, each change in the external load caused the generation and propagation of a new incident (compression) wave which, in turn, caused the generation of new propagation phenomena. Thus, if at the instant of time t_1 the corresponding force $F(t_1) = F_1$ generated an incident compression wave ICW_1, then at the next instant t_2 the corresponding force $F(t_2) = F_2$ generated a new incident compression wave ICW_2, and the same happened at the next instants. The following figures considered four instants of time, where t_1 corresponded to the instant when ELP1 took place, whereas t_n corresponded to the last instant of the process.

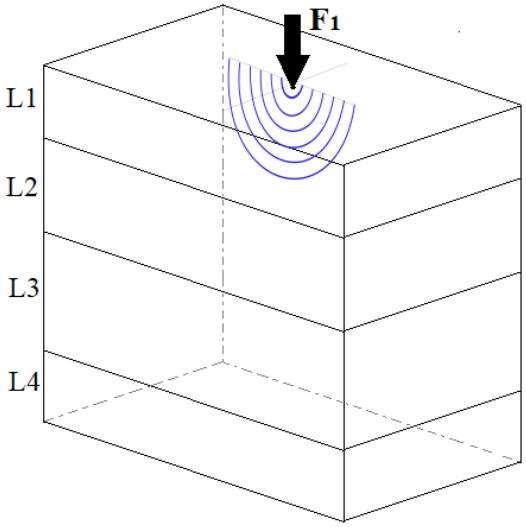

Figure 6.8: Propagation of waves inside the layered model due to the external force $F_1 = F(t_1)$.

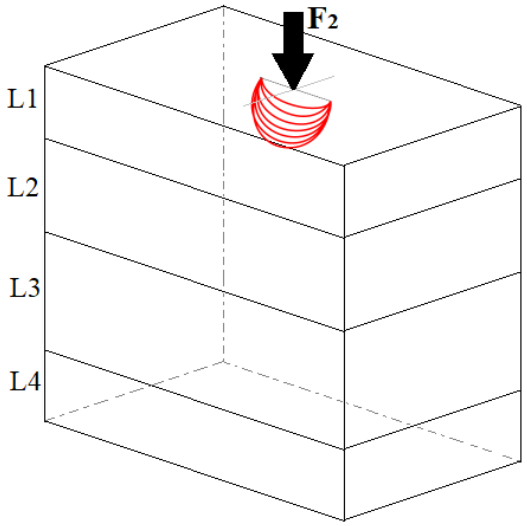

Figure 6.9: Propagation of waves inside the layered model due to the external force $F_2 = F(t_2)$.

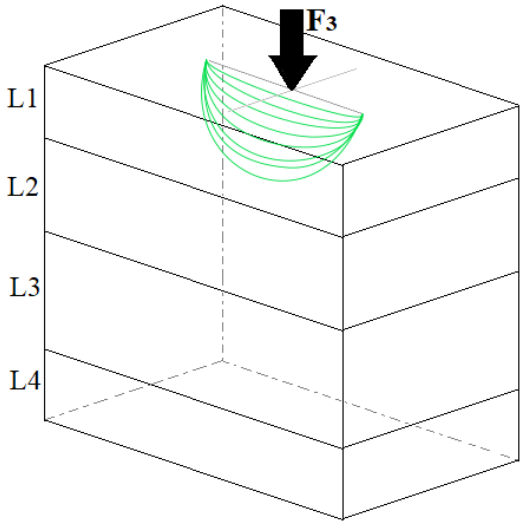

Figure 6.10: Propagation of waves inside the layered model due to the external force $F_3 = F(t_3)$.

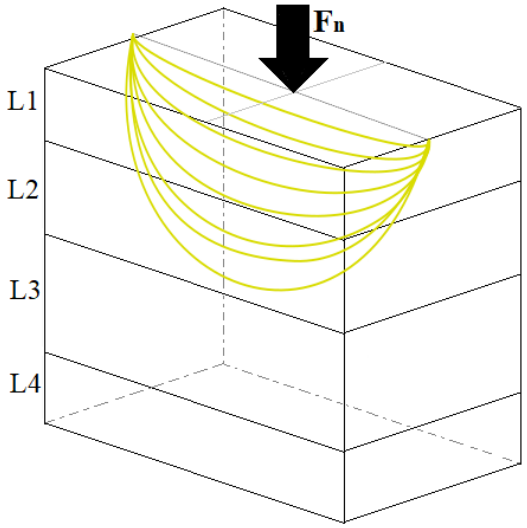

Figure 6.11: Propagation of waves inside the layered model due to the external force $F_n = F_f = F(t_f)$.

Therefore, a different spreading area corresponded at each external force; the main difference concerned the horizontal dimension which increased over time for a point load, and remained fixed for a distributed force. In order to describe the waves inside the material, potentials were associated to both compression and distortion waves. The number of potentials and, therefore, the number of waves increased at each interface. Each potential depended on the propagation velocity (α or β), the travelling direction, the wave frequency, and an amplitude which, in turn, depended on the external force. Both compression and distortion waves were assumed spher-

ical and the disturbance spread out radially from the source; the passage of the disturbance caused the displacement of the particles in the impact area: for a 3D case with a coordinate system (r, θ, z), the displacement occurred in all directions, whereas for a 2D-case the particles moved in $r-$ and $z-$ directions, and in 1D-case each particles moved only in $z-$ direction. These displacements were coupled each other and all of them involved both compression and distortion potentials.

In addition, it is important to say that the compression and distortion potentials Φ and Ψ, used for the first time in Section 4.2, were considered as a mathematical tool for expressing deformations and stresses as seen in the previously.

Mathematical Part

The mathematical part represented the last step of the project. The primary RPUF (L2) and the secondary RPUF (L3) that composed the simplified model introduced in Chapter 2 were combined together in one single layer and defined as L2. The final configuration of the theoretical model had three layers:

L1 Top plywood;

L2 Primary and Secondary RPUF;

L3 Back plywood.

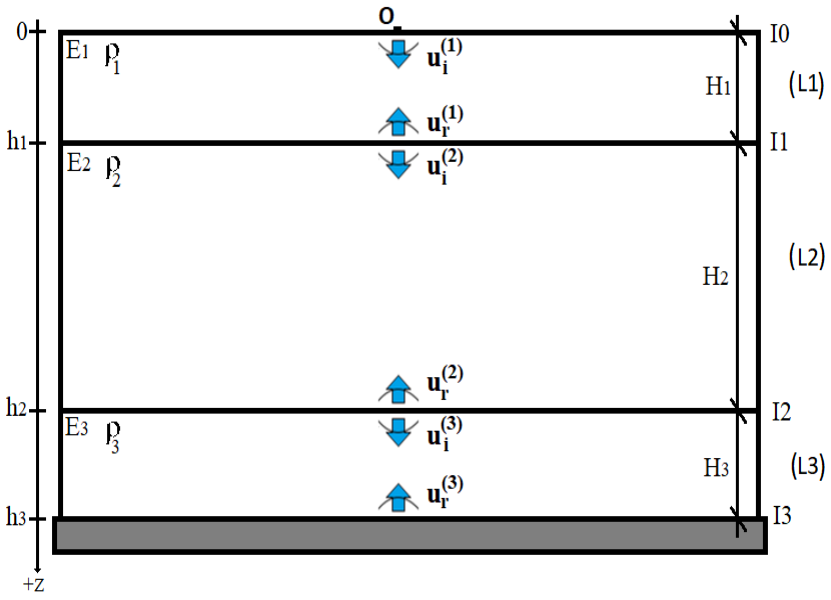

Figure 6.12: Three-layered model.

It was possible to join L2 and L3 because they had the same material characteristics.

Since the problem was simplified from the 3D case to the 1D case, the equations resulted simpler than the previous ones; instead of the compression and distortion potentials (Φ_j and Ψ_j), and the compression and distortion velocities (α_j and β_j), the deformations, elastic modulus and density were used. The propagation of distortion waves was neglected in the 1D case because they travel transversely to compression waves and from a mathematical point of view, it was seen that the general equation 4.4 only provided the wave equation for compression waves in 1D case.

In order to define the amplitudes, the boundary conditions at the interfaces were applied; it resulted in a system of six equations in six unknowns; written in matrix form; it resulted $S: MX = B$, where X and B were two vector columns (6x1), and M was the matrix of coefficients (6x6). It was noticed that each time a new layer was added between the first and the last ones, the same two boundary conditions needed to be added. Thus,

For a 3-layered material: M is a (6x6) matrix;

For a n-layered material : M is a ($2n$x$2n$) matrix.

It was decided to consider only three-layers instead of four as decided at the beginning because the four-layered case can easily obtained from the three-layered case and also it was easier to manage a matrix (6x6), instead of a matrix (8x8). Maintaining the same configuration, for each layer added between the first and the last one, two boundary conditions similar to **BC2** and **BC3** (or **BC4** and **BC5**) need to be included to the system of equations S. Notice that at the last interface (I3) the boundary condition guaranteed zero deformation due to the presence of the wall, whereas at the free interface (I0) it was assumed that the external force was the same as the internal force. The material characteristics (ρ_j, E_j) and the wave numbers k_j of each layer L_j appeared in the matrix M; therefore, the relationship between the wave number and the angular velocity depended on (ρ_j, E_j):

$$k_j = \omega\sqrt{\frac{\rho_j}{E_j}}$$

After finding the amplitudes by solving the system of equations S, the deformations for each layer were defined.

By adding a damping term in the governing equation, then the relationship between ω and k became:

$$k_j = \pm\sqrt{\frac{\rho_j}{E_j}\omega^2 - i\frac{d}{E_j}\omega}$$

Although the presence of damping made the process of waves propagation closer to the reality, the relationship between ω and k became more complicated and consequently, the corresponding expressions of A_j and B_j became more intricate than those shown in Appendix B.3.

Considering four different impact loads (all of them described by an isosceles triangle function, with different values of duration time and pressure) the deformations were calculated at different locations inside the model. It was seen that the deformations decreased with the increase of the distance from the free interface and in the last layer it resulted $u = 0$. Furthermore, comparing the internal and the external process, it is possible to state that the process of an impact wave against the free surface of a layered structure is relatively slow with respect to the internal process of waves propagation.

An the end, for the research question

Q1. How do strain waves propagate through the structure upon a liquid impact?

it is possible to conclude that an external load such as a wave impact which changes in space and time and represents the external process characterised by several physical phenomena, causes the generation of a first (compression) *strain wave* which propagates radially from the source, spreading the disturbance in the impact layered structure, and causing the generation of a complex system of reflected and transmitted compression and distortion waves at the several interfaces. Strain waves can be defined in terms of potentials which depend on the material characteristics of each layer. The model obtained from the study of the waves propagation is a 3D model, composed by four layers, having an external environment-interface-layer-interface-layer-interface-wall configuration, and where spherical compression and distortion waves propagate inside reducing their amplitude;

for the research question

Q2. How can the theory of the strain waves propagation be applied to a theoretical model?

it is possible to conclude that the simplified theoretical model obtained is a 1D model composed by three layers where compression plane waves propagate inside. The response is governed by

$$E_j \frac{\partial^2 u^{(j)}}{\partial z^2} = \rho_j \frac{\partial^2 u^{(j)}}{\partial t^2}$$

if no damping is involved, and by

$$E_j \frac{\partial^2 u^{(j)}}{\partial z^2} = \rho_j \frac{\partial^2 u^{(j)}}{\partial t^2} + d \frac{\partial u^{(j)}}{\partial t}$$

in the case of the presence of a damping term,

and where $u^{(j)} = A_j \, e^{i\omega t} e^{-izk_j} + B_j \, e^{i\omega t} e^{izk_j}$.

By choosing different isosceles triangle loads, the corresponding deformations that are obtained depend on the the duration time t and on the pressure p.

6.2 Recommendations

When the structure of this thesis was defined, the initial idea was to provide a layered theoretical model that could totally describe the physics of the waves propagation inside the layered structure. Many aspects of the problem were not immediately understood because it was a new topic. Starting from a 3D case, at the end, the layered structure was simplified to a 1D-model composed by three layers where compression plane waves were generated and could propagate inside as a consequence of an external impact. It was also seen that the three-layered model could be generalized to a n-layered model, if the same configuration was maintained, and considering two equations (boundary conditions) for each new added layer.

Differently from the 3D case in which the deformations occur in all directions, and the propagation of distortion waves need to be taken into account because a compression wave propagation is always a combination of shear and compression, the layered model in 1D case considers neither displacements in more than one direction nor distortion waves propagation, and for these reasons it not close to the reality. Considering a model in 2D or 3D, it can provide a more realistic behavior of the structure; in that case spherical compression and distortion waves (and the corresponding potentials) need to be used.

It was seen that the three-layered model can be generalised to a n-layered case (Section 5.6). An aspect that can be investigated is considering a model composed by a finite layer (top plywood) in contact with a semi-infinite layer (primary RPUF), and assume that the top plywood is composed by numerous sub-layers; with this configuration, only reflected waves generated at the interface between top plywood and primary RPUF need to be taken into account. As seen in the analysis of the global wave propagation phenomena in Section 4.5, the propagation times of both compression and distortion waves (t_α and t_β) are much smaller than those in the RPUF layers, and it means that more reflections will take place and more waves will be generated inside the top plywood. It could be interesting to investigate how the presence of sub-layers in the plywood affects the deformation of the structure since new (generated) reflected waves will make weaker the incident wave.

As already mentioned in the previous section, each change in the external process causes the propagation of a new incident (compression) wave which, in turn, generates a set of reflected and transmitted waves. This concept was discussed in Chapter 4 where four forces corresponding to four consecutive instants of time caused different shape geometries of the incident wave. Then, the solution needs to take into account all these contributions.

If the improvement of the theoretical model in 2D or 3D does not match with the physics, an alternative can be consider the following idea based on the *neural network* and shown in Figure 6.13:

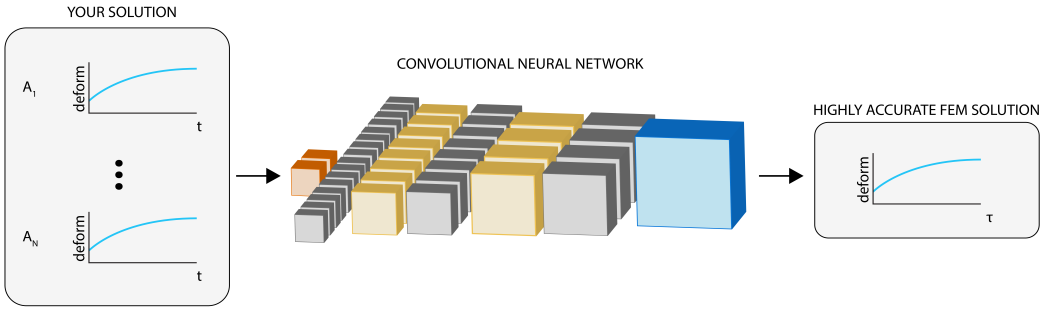

Figure 6.13: Neural Network, Complete Architecture. [12]

The idea is expressed as follows:

Training the neural network:

1. Construct highly accurate FEM solutions with several pre-defined profiles $F(t)$
2. Construct out solution, consisting of single non-interacting waves for specific instants of time t
3. Map our solution(s) (collection of single non-interacting waves) to the highly accurate FEM solution using a neural network

After training the neural network:

1. After the neural network is trained, the highly accurate FEM can be constructed with only our solutions and the trained neural network.

The idea of mapping an inaccurate solution (our solution with non-interacting waves) to an accurate solution (FEM where waves are interacting) is described in the following papers:

[Cohen 2010] Interactive fluid-particle simulation using translating Eulerian grids. [Macklin 2013] Position based fluids. [Prantl 2019] Generating Liquid Simulations with Deformation-aware Neural Networks. [Wiewel 2019] Latent Space Physics: Towards Learning the Temporal Evolution of Fluid Flow. [Xie 2018] tempogan: A temporally coherent, volumetric gan for super-resolution fluid flow. [Chu 2017] Data-driven synthesis of smoke flows with CNN-based feature descriptors. [Yang] Hybrid particle-grid modeling for multi-scale droplet/spray simulation. [Qui] Novel fluid detail enhancement based on multi-layer depth regression analysis and FLIP fluid simulation. [Halder] Neural network for multi-fidelity solver enhancement. [12] Halder Y. Multi-fidelity neural network for real-time fluid flow predictions.

Appendix A

A.1 Lame' Constants and Propagation Velocities

In order to prove that

$$\alpha = \sqrt{\frac{1}{\rho}\left(k + \frac{4}{3}G\right)} = \sqrt{\frac{\lambda + 2\mu}{\rho}}$$

$$\beta = \sqrt{\frac{G}{\rho}} = \sqrt{\frac{\mu}{\rho}}$$

It is possible to express the elastic modulus E and the Poisson's ratio ν as follows:

$$E = \frac{\mu(3\lambda + 2\mu)}{(\lambda + \mu)} \tag{A.1}$$

$$\nu = \frac{\lambda}{2(\lambda + \mu)} \tag{A.2}$$

Considering the relationship between elastic modulus E and shear modulus G

$$G = \frac{E}{2(1 + \nu)} \tag{A.3}$$

and substituting the equations A.1 and A.2 in equation A.4, it results:

$$G = \frac{E}{2(1+\nu)} = \frac{\frac{\mu(3\lambda+2\mu)}{(\lambda+\mu)}}{2\left(1 + \frac{\lambda}{2(\lambda+\mu)}\right)} = \frac{\frac{\mu(3\lambda+2\mu)}{\lambda+\mu}}{2\left(\frac{2\lambda+2\mu+\lambda}{2(\lambda+\mu)}\right)} = \frac{\mu(3\lambda+2\mu)}{(3\lambda+2\mu)} = \mu \tag{A.4}$$

In addition, the bulk modulus k, that is expressed as the ration between the applied pressure and the fractional change in volume, can be expressed by the following formula:

$$k = \lambda + \frac{2}{3}\mu \tag{A.5}$$

Therefore, it results:

$$\alpha = f(\rho, k, G) = \sqrt{\frac{1}{\rho}\left(k + \frac{4}{3}G\right)} = \sqrt{\frac{1}{\rho}\left(\lambda + \frac{2}{3}\mu + \frac{4}{3}\mu\right)} = \sqrt{\frac{\lambda + 2\mu}{\rho}} \tag{A.6}$$

$$\beta = f(\rho, G)) = \sqrt{\frac{G}{\rho}} = \sqrt{\frac{\mu}{\rho}} \tag{A.7}$$

In addition, the numerical values of the compression velocities α_j and distortion velocities β_j have been calculated by using the equations A.8, A.9 and A.10:

$$\lambda = \frac{E\nu}{(1+\nu)(1-2\nu)} \tag{A.8}$$

$$\mu = \frac{3}{2}(k - \lambda) \tag{A.9}$$

$$k = \frac{E}{3(1-2\nu)} \tag{A.10}$$

Equations A.8 and A.9 have been obtained from A.1 and A.2:

$$\left\{ \begin{array}{l} E = \frac{\mu(3\lambda+2\mu)}{(\lambda+\mu)} \\ \nu = \frac{\lambda}{2(\lambda+\mu)} \end{array} \right. ; \left\{ \begin{array}{l} E(\lambda+\mu) = \mu(3\lambda+2\mu) \\ 2\nu(\lambda+\mu) = \lambda \end{array} \right. ; \left\{ \begin{array}{l} E(\lambda+\mu) = \mu(3\lambda+2\mu) \\ 2\nu\lambda + 2\nu\mu = \lambda \end{array} \right.$$

$$\left\{ \begin{array}{l} E = \frac{\mu(3\lambda+2\mu)}{(\lambda+\mu)} \\ \nu = \frac{\lambda}{2(\lambda+\mu)} \end{array} \right. ; \left\{ \begin{array}{l} E(\lambda+\mu) = \mu(3\lambda+2\mu) \\ 2\nu(\lambda+\mu) = \lambda \end{array} \right. ; \left\{ \begin{array}{l} E(\lambda+\mu) = \mu(3\lambda+2\mu) \\ 2\nu\lambda + 2\nu\mu = \lambda \end{array} \right.$$

$$\left\{ \begin{array}{l} E(\lambda+\mu) = \mu(3\lambda+2\mu) \\ \lambda(-2\nu+1) = +2\nu\mu \end{array} \right. : \left\{ \begin{array}{l} E\left(\mu + \frac{2\nu\mu}{1-2\nu}\right) = \mu\left(3\frac{2\nu\mu}{1-2\nu} + 2\mu\right) \\ \lambda = \frac{2\nu\mu}{(1-2\nu)} \end{array} \right.$$

Thus,

$$E\mu\left(\frac{1-2\nu+2\nu}{1-2\nu}\right) = \mu\left(\frac{6\nu\mu + 2\mu - 4\mu\nu}{1-2\nu}\right); E = 2\mu + 2\nu\mu \rightarrow \frac{E}{2(1+\nu)} = \mu$$

$$\left\{ \begin{array}{l} \mu = \frac{E}{2(1+\nu)} \\ \lambda = \frac{2\nu}{1-2\nu} \cdot \frac{\epsilon}{2(1+\nu)} \end{array} \right. ; \left\{ \begin{array}{l} \lambda = \frac{E\nu}{(1+\nu)(1-2\nu)} \\ \mu = \frac{E}{2(1+\nu)} \end{array} \right.$$

Finally, since $k = \lambda + \frac{2}{3}\mu$, it results:

$$k = \frac{E\nu}{(1+\nu)(1-2\nu)} + \frac{2}{3}\frac{E}{2(1+\nu)} = \frac{E}{(1+\nu)}\left[\frac{\nu}{1-2\nu} + \frac{1}{3}\right]$$

$$k = \frac{E}{(1+)}\left[\frac{3\nu+1-2\nu}{3(1+2\nu)}\right] = \frac{E}{(1+\nu)}\left[\frac{1+\nu}{3(1-2\nu)}\right] = \frac{E}{3(1-2v)}$$

A.2 Numerical Values for Layers L_j

The following table shows the thickness and the calculated values of compression and distortion velocities and propagation-times for all layers:

Layers	H	α	β	t_α	t_β
	[m]	$[m/s]$	$[m/s]$	[s]	[s]
Top plywood	0.012	3670.625	2314.504	$0.327 \cdot 10^{-5}$	$0.518 \cdot 10^{-5}$
Primary RPUF	0.089	871.816	544.619	$10.2 \cdot 10^{-5}$	$16.3 \cdot 10^{-5}$
Secondary RPUF	0.160	871.816	544.619	$18.5 \cdot 10^{-5}$	$29.4 \cdot 10^{-5}$
Back Plywood	0.012	3670.625	2314.504	$0.327 \cdot 10^{-5}$	$0.518 \cdot 10^{-5}$

Table A.1: Space-Velocity-Time for each layer L_j

Calculating the ratios, it results:

$$\frac{H_2}{H_1} = 7.42 \qquad \frac{H_3}{H_1} = 13.33 \qquad \frac{H_4}{H_1} = 1.00$$

$$\frac{\alpha_2}{\alpha_1} = 0.2375 \qquad \frac{\alpha_3}{\alpha_1} = 0.2375 \qquad \frac{\alpha_4}{\alpha_1} = 1.00$$

$$\frac{t_{\alpha 2}}{t_{\alpha 1}} = 31.23 \qquad \frac{t_{\alpha 3}}{t_{\alpha 1}} = 56.14 \qquad \frac{t_{\alpha 4}}{t_{\alpha 1}} = 1.00$$

$$\frac{\beta_1}{\alpha_1} = 0.631 \quad \frac{\beta_2}{\alpha_1} = 0.148, \quad \frac{\beta_3}{\alpha_1} = 0.148 \quad \frac{\beta_4}{\alpha_1} = 0.631$$

$$\frac{t_{\beta 1}}{t_{\alpha 1}} = 1.585 \quad \frac{t_{\beta 2}}{t_{\alpha 1}} = 49.986 \quad \frac{t_{\beta 3}}{t_{\alpha 1}} = 89.863 \quad \frac{t_{\beta 4}}{t_{\alpha 1}} = 1.585$$

Thus, it results:

$$H_2 \simeq 7 \cdot H_1 \qquad H_3 \simeq 13 \cdot H_1 \qquad H_4 \simeq 1 \cdot H_1$$

$$\alpha_2 \simeq 0.25 \cdot \alpha_1 \qquad \alpha_3 \simeq 0.25 \cdot \alpha_1 \qquad \alpha_4 \simeq 1.00 \cdot \alpha_1$$

$$t_{\alpha_2} \simeq 30 \cdot t_{\alpha_1} \qquad t_{\alpha_3} \simeq 56 \cdot t_{\alpha_1} \qquad t_{\alpha_4} \simeq 1.00 \cdot t_{\alpha_1}$$

$$\beta_1 \simeq 0.6 \cdot \alpha_1 \quad \beta_2 \simeq 0.15 \cdot \alpha_1 \quad \beta_3 \simeq 1.15 \cdot \alpha_1 \quad \beta_4 \simeq 0.6 \cdot \alpha_1$$

$$t_{\beta_1} \simeq 2.0 \cdot t_{\alpha_1} \quad t_{\beta_2} \simeq 50 \cdot t_{\alpha_1} \quad t_{\beta_3} \simeq 90 \cdot t_{\alpha_1} \quad t_{\beta_4} \simeq 2.0 \cdot t_{\alpha_1}$$

A.3 Mathematical Demonstration of Situation 1.

Based on the situation shown in Figure 4.11, the expressions of the normal stress σ_{yy} and shear stress σ_{xy} are calculated as follows

$$\sigma_{yy} = \lambda(\frac{\partial q_1}{\partial x} + \frac{\partial q_2}{\partial x} + \frac{\partial w_1}{\partial y} + \frac{\partial w_2}{\partial y}) + 2\mu(\frac{\partial w_1}{\partial y} + \frac{\partial w_2}{\partial y})$$

$\frac{\partial q_1}{\partial x} = \cos\gamma_1 A_1 \cos(pt + f_1 x + g_1 y) f_1 = A_1 \cos(pt + f_1 x + g_1 y) \frac{p}{\alpha_1} \cos^2\gamma_1$

$\frac{\partial q_2}{\partial x} = \cos\gamma_2 A_2 \cos(pt + f_2 x - g_2 y + c_1) f_2 = A_2 \cos(pt + f_2 x - g_2 y + c_1) \frac{p}{\alpha_1} \cos^2\gamma_2$

$\frac{\partial w_1}{\partial y} = \sin\gamma_1 A_1 \cos(pt + f_1 x + g_1 y) g_1 = A_1 \cos(pt + f_1 x + g_1 y) \frac{p}{\alpha_1} \sin^2\gamma_1$

$\frac{\partial w_2}{\partial y} = -\sin\gamma_2 A_2 \cos(pt + f_2 x - g_2 y + c_1)(-g_2) = A_2 \cos(pt + f_2 x - g_2 y + c_1) \frac{p}{\alpha_1} \sin^2\gamma_2$

Substituting then, it results:

$$\sigma_{yy} = \frac{p}{\alpha_1}(\left[\lambda + 2\mu\sin^2\gamma_1\right] A_1 \cos(pt+f_1 x+g_1 y)+[\lambda+2\mu\sin^2\gamma_2]A_2\cos(pt+f_2 x-g_2 y+c_1)) \tag{A.11}$$

At the interface, $y = 0$ and $\sigma_{yy} = 0$. Then, equation A.11 becomes:

$$0 = \left[\lambda + 2\mu\sin^2\gamma_1\right] \frac{p}{\alpha_1} A_1 \cos(pt + f_1 x) + [\lambda + 2\mu\sin^2\gamma_2]\frac{p}{\alpha_1} A_2 \cos(pt + f_2 x + c_1) \tag{A.12}$$

$$\sigma_{xy} = \mu(\frac{\partial q_1}{\partial y} + \frac{\partial q_2}{\partial y} + \frac{\partial w_1}{\partial x} + \frac{\partial w_2}{\partial x})$$

$\frac{\partial q_1}{\partial y} = \cos\gamma_1 A_1 \cos(pt + f_1 x + g_1 y) g_1 = A_1 \cos(pt + f_1 x + g_1 y) \frac{p}{\alpha_1} \cos\gamma_1 \sin\gamma_1$

$\frac{\partial q_2}{\partial y} = \cos\gamma_2 A_2 \cos(pt+f_2 x-g_2 y+c_1)(-g_2) = -A_2 \cos(pt+f_2 x-g_2 y+c_1) \frac{p}{\alpha_1} \cos\gamma_2 \sin\gamma_2$

$\frac{\partial w_1}{\partial x} = \sin\gamma_1 A_1 \cos(pt + f_1 x + g_1 y) f_1 = A_1 \cos(pt + f_1 x + g_1 y) \frac{p}{\alpha_1} \sin\gamma_1 \cos\gamma_1$

$\frac{\partial w_2}{\partial x} = -\sin\gamma_2 A_2 \cos(pt+f_2 x-g_2 y+c_1) f_2 = -A_2 \cos(pt+f_2 x-g_2 y+c_1) \frac{p}{\alpha_1} sin\gamma_2 \cos\gamma_2$

Substituting then, it results:

$$\sigma_{xy} = \mu\frac{p}{\alpha_1}(A_1 \cos(pt+f_1 x+g_1 y)2\sin\gamma_1\cos\gamma_1 - A_2\cos(pt+f_2 x-g_2 y+c_1)(2\sin\gamma_2\cos\gamma_2));$$

(A.13)

At the interface, $y = 0$ and $\sigma_{xy} = 0$. Then, equation A.13 becomes:

$$0 = \mu(\frac{p}{\alpha_1} A_1 \cos(pt + f_1 x)\sin(2\gamma_1) - \frac{p}{\alpha_1} A_2 \cos(pt + f_2 x + c_1)\sin(2\gamma_2)) \tag{A.14}$$

Adding a second reflected wave, then the expressions of normal and shear stresses are modified by the presence of the following additional terms:

$$\lambda(\frac{\partial q_3}{\partial x} + \frac{\partial w_3}{\partial y}) + 2\mu(\frac{\partial w_3}{\partial y})$$

and

$$\mu(\frac{\partial q_3}{\partial y} + \frac{\partial w_3}{\partial x})$$

It results:

$\frac{\partial q_3}{\partial x} = \sin\gamma_3 A_3 \cos(pt + f_3 x - g_3 y + c_2)(f_3) = A_3 \cos(pt + f_3 x - g_3 y + c_2)\frac{p}{\beta_2}\cos\gamma_3 \sin\gamma_3$

$\frac{\partial w_3}{\partial y} = \cos\gamma_3 A_3 \cos(pt + f_3 x - g_3 y + c_2)(-g_3) = -A_3 \cos(pt + f_3 x - g_3 y + c_2)\frac{p}{\beta_2}\cos\gamma_3 \sin\gamma_3$

$\frac{\partial q_3}{\partial y} = \sin\gamma_3 A_3 \cos(pt + f_3 x - g_3 y + c_2)(-g_3) = -A_3 \cos(pt + f_3 x - g_3 y + c_2)\frac{p}{\beta_2}\sin^2(\gamma_3)$

$\frac{\partial w_3}{\partial y} = \cos\gamma_3 A_3 \cos(pt + f_3 x - g_3 y + c_2)(f_3) = A_3 \cos(pt + f_3 x - g_3 y + c_2)\frac{p}{\beta_2}\cos^2(\gamma_3)$

Substituting, then it results:

$$\begin{aligned}[\lambda\left(\tfrac{\partial q_3}{\partial x} + \tfrac{\partial w_3}{\partial y}\right) + 2\mu\left(\tfrac{\partial w_3}{\partial y}\right)\Big]_{y=0} &= \lambda\tfrac{p}{\beta_2}(A_3\cos(pt + f_3 x + c_2)\cos\gamma_3\sin\gamma_3 \\ -A_3\cos(pt + f_3 x + c_2)\cos\gamma_3\sin\gamma_3) &+ 2\mu\tfrac{p}{\beta_2}(-A_3\cos(pt + f_3 x + c_2)\cos\gamma_3\sin\gamma_3) \\ &= -2\mu\tfrac{p}{\beta_2}A_3\cos(pt + f_3 x + c_2)\cos\gamma_3\sin\gamma_3\end{aligned}$$

$$\begin{aligned}[\mu\left(\tfrac{\partial q_3}{\partial y} + \tfrac{\partial w_3}{\partial x}\right)]_{y=0} &= \mu\tfrac{p}{\beta_2}A_3(-\cos(pt + f_3 x + c_2)\sin^2\gamma_3 + \\ &+ \cos(pt + f_3 x + c_2)\cos^2\gamma_3) \\ &= \mu\tfrac{p}{\beta_2}A_3\cos(pt + f_3 x + c_2)(-\sin^2\gamma_3 + \cos^2\gamma_3)\end{aligned}$$

Equations A.12 and A.14 become:

$$\begin{aligned}\sigma_{yy} = 0 = \tfrac{A_1}{\alpha_1}\left[\lambda + 2\mu\sin^2\gamma_1\right]\cos(pt + f_1 x + g_1 y) + \\ [+\lambda + 2\mu\sin^2\gamma_2]\tfrac{A_2}{\alpha_1}\cos(pt + f_2 x - g_2 y + c_1) \\ -2\mu\tfrac{A_3}{\beta_2}\cos(pt + f_3 x + c_2)\cos\gamma_3\sin\gamma_3\end{aligned}$$

$$\begin{aligned}\sigma_{xy} = 0 = \tfrac{A_1}{\alpha_1}\cos(pt + f_1 x)\sin(2\gamma_1) - \tfrac{A_2}{\alpha_1}\cos(pt + f_2 x + c_1)\sin(2\gamma_2) \\ +\mu\tfrac{p}{\beta_2}A_3\cos(pt + f_3 x + c_2)(-\cos(2\gamma_3))\end{aligned}$$

Appendix B

B.1 Governing Equation

In order to obtain the governing equation 5.5, it was considered a section of the material as shown in the figure below;

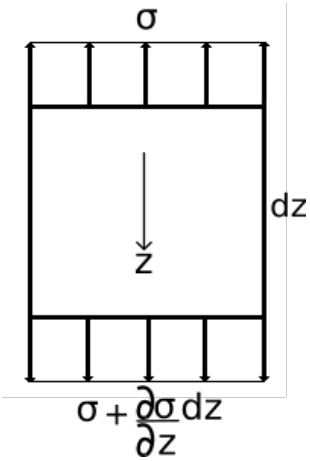

Figure B.1: Differential element.

Then, from the Newton II Law $\sum F + ma$, it results:

$$ma = (\rho V)\ddot{u} = \rho A dz \frac{\partial^2 u}{\partial^2 t}$$

$$\sum F = -\sigma A + \sigma A + \frac{\partial \sigma}{\partial z} A dz$$

Therefore,

$$-\sigma A + \sigma A + \frac{\partial \sigma}{\partial z} A dz = \rho A dz \frac{\partial^2 u}{\partial^2 t}$$

$$\frac{\partial \sigma}{\partial z} = \rho \frac{\partial^2 u}{\partial^2 t}$$

Since

$$\sigma = E\epsilon, \quad \epsilon = \frac{\partial u}{\partial z}$$

then, it results:

$$\frac{\partial}{\partial z}(E\frac{\partial u}{\partial z}) = \rho\frac{\partial^2 u}{\partial^2 t} \rightarrow E\frac{\partial^2 u}{\partial z^2} = \rho\frac{\partial^2 u}{\partial t^2}$$

B.2 Boundary Conditions for a 3-layered Model

The boundary conditions for the system of equations S are calculated as follows:

BC1: $F|_{z=0} = (\sigma e^{i\omega t})|_{z=0} = (\frac{\partial u_i^{(1)}}{\partial z} + \frac{\partial u_i^{(1)}}{\partial z})\Big|_{z=0}$

$$\sigma e^{i\omega t} = E_1 A_1 e^{i\omega t} e^{-ik_1 z}(-ik_1) + E_1 B_1 e^{i\omega t} e^{ikz}(ik_1);$$
$$(-ik_1 E_1 e^{-ik_1 z})A_1 + (ik_1 E_1 e^{ik_1 z})B_1 = \sigma;$$

at $z = 0$:

$$(-ik_1 E_1)A_1 + (ik_1 E_1)B_1 = \sigma$$

BC2: $E_1(\frac{\partial u_i^{(1)}}{\partial z} + \frac{\partial u_r^{(1)}}{\partial z})\Big|_{z=h_1} = E_2(\frac{\partial u_i^{(2)}}{\partial z} + \frac{\partial u_r^{(2)}}{\partial z})\Big|_{z=h_1}$

$$E_1(A_1 e^{i\omega t} e^{-ik_1 z}(-ik_1) + B_1 e^{i\omega t} e^{ik_1 z}(ik_1)) = E_2(A_2 e^{i\omega t} e^{-ik_2 z}(-ik_2) + B_2 e^{i\omega t} e^{ik_2 z}(ik_2));$$
$$(-E_1 k_1 e^{-ik_1 z})A_1 + (E_1 k_1 e^{ik_1 z})B_1 + (E_2 k_2 e^{-ik_2 z})A_2 + (-E_2 k_2 e^{ik_2 z}) = 0;$$

at $z = h_1$:

$$(-E_1 k_1 e^{-ik_1 h_1})A_1 + (E_1 k_1 e^{ik_1 h_1})B_1 + (E_2 k_2 e^{-ik_2 h_1})A_2 + (-E_2 k_2 e^{ik_2 h_1})B_2 = 0$$

BC3: $(\frac{\partial u_i^{(1)}}{\partial t} + \frac{\partial u_r^{(1)}}{\partial t})\Big|_{z=h_1} = (\frac{\partial u_i^{(2)}}{\partial t} + \frac{\partial u_r^{(2)}}{\partial t})\Big|_{z=h_1}$

$$A_1 e^{i\omega t} e^{-ik_1 z}(i\omega) + B_1 e^{i\omega t} e^{ik_1 z}(i\omega) = A_2 e^{i\omega t} e^{-ik_2 z}(i\omega) + B_2 e^{i\omega t} e^{ik_2 z}(i\omega);$$
$$(e^{-ik_1 z})A_1 + (e^{ik_1 z})B_1 + (-e^{-ik_2 z})A_2 + (-e^{ik_2 z})B_2 = 0;$$

at $z = h_1$:

$$(e^{-ik_1 h_1})A_1 + (e^{ik_1 h_1})B_1 + (-e^{-ik_2 h_1})A_2 + (-e^{ik_2 h_1})B_2 = 0$$

BC4: $E_2(\frac{\partial u_i^{(2)}}{\partial z} + \frac{\partial u_r^{(2)}}{\partial z})\Big|_{z=h_2} = E_3(\frac{\partial u_i^{(3)}}{\partial z} + \frac{\partial u_r^{(3)}}{\partial z})\Big|_{z=h_2}$

$$E_2(A_2 e^{i\omega t} e^{-ik_2 z}(-ik_2) + B_2 e^{i\omega t} e^{ik_2 z}(ik_2)) = E_3(A_3 e^{i\omega t} e^{-ik_3 z}(-ik_3) + B_3 e^{i\omega t} e^{ik_3 z}(ik_3));$$
$$(-E_2 k_2 e^{-ik_2 z})A_2 + (E_2 k_2 e^{ik_2 z})B_2 + (E_3 k_3 e^{-ik_3 z})A_3 + (-E_3 k_3 e^{ik_3 z})B_3 = 0;$$

at $z = h_2$:

$$(-E_2k_2e^{-ik_2h_2})A_2 + (E_2k_2e^{ik_2h_2})B_2 + (E_3k_3e^{-ik_3h_2})A_3 + (-E_3k_3e^{ik_3h_2})B_3 = 0$$

BC5: $(\frac{\partial u_i^{(2)}}{\partial t} + \frac{\partial u_r^{(2)}}{\partial t})\Big|_{z=h_2} = (\frac{\partial u_i^{(3)}}{\partial t} + \frac{\partial u_r^{(3)}}{\partial t})\Big|_{z=h_2}$

$$A_2e^{i\omega t}e^{-ik_2z}(i\omega) + B_2e^{i\omega t}e^{ik_2z}(i\omega) = A_3e^{i\omega t}e^{-ik_3z}(i\omega) + B_3e^{i\omega t}e^{ik_3z}(i\omega);$$
$$(e^{-ik_2z})A_2 + (e^{ik_2z})B_2 + (-e^{-ik_3z})A_3 + (-e^{ik_3z})B_3 = 0;$$

at $z = h_2$:

$$(e^{-ik_2h_2})A_2 + (e^{ik_2h_2})B_2 + (-e^{-ik_3h_2})A_3 + (-e^{ik_3h_2})B_3 = 0$$

BC6: $(u_i^{(3)} + u_r^{(3)})\Big|_{z=h_3} = 0|_{z=h_3}$

$$A_3e^{i\omega t}e^{-ik_3z} + B_3e^{i\omega t}e^{ik_3z} = 0;$$
$$A_3e^{-ik_3z} + B_3e^{ik_3z} = 0;$$

at $z = h_3$:

$$(e^{-ik_3h_3})A_3 + (e^{ik_3h_3})B_3 = 0$$

Combining all the boundary conditions, the system of equations S can be defined.

B.3 Theoretical Expressions of the Amplitudes

The determinant of (6x6) matrix M is:

$$\begin{aligned} det(A) = -2iE_1((E_2k_2 + E_3k_3)(E_1k_1 + E_2k_2)cos((k_1 - k_2)h_1 + (k_2 - k_3)h_2 + k_3h_3) \\ +(E_2k_2 - E_3k_3)(E_1k_1 - E_2k_2)cos((k_1 + k_2)h_1 + (-k_2 - k_3)h_2 + k_3h_3) \\ -(E_2k_2 - E_3k_3)(E_1k_1 + E_2k_2)cos((k_1 - k_2)h_1 + (k_2 + k_3)h_2 - k_3h_3) \\ -cos((k_1 + k_2)h_1 + (-k_2 + k_3)h_2 - k_3h_3)(E_2k_2 + E_3k_3)(E_1k_1 - E_2k_2))k_1 \end{aligned}$$

Substituting the numerical values of Table 5.1, and considering that $k_2 \approx 4\,k_1$ and $k_3 = k_1$:

$$det(A) = (1.14 \cdot 10^{25}i)k_1^3(1.23 \cdot 10^8 cos(0.98k_1) - 1.25 \cdot 10^8 cos(1.024k_1))$$

The theoretical values of the amplitudes A_j, B_j, with $j = 1, 2, 3$ in function of k_1 and σ are shown below:

$$A_1 = \frac{-5.62 \cdot 10^{-11}\mathrm{i}(5.33 \cdot 10^6\mathrm{e}^{1.024\mathrm{i}k_1} - 4.58 \cdot 10^6\mathrm{e}^{-0.98\mathrm{i}k_1} + 9.89 \cdot 10^6\mathrm{i}\sin(1.k_1))\,\sigma}{k_1\,(4.58 \cdot 10^6\cos(0.98\mathrm{k}_1) - 5.33 \cdot 10^6\cos(1.024k_1))}$$

$$B_1 = \frac{5.62 \cdot 10^{-11}\mathrm{i}(5.33 \cdot 10^6 \mathrm{e}^{1.024\mathrm{i}k_1} - 4.58 \cdot 10^6 \mathrm{e}^{-0.98\mathrm{i}k_1} + 9.89 \cdot 10^6 \mathrm{i}\sin(1.k_1))\,\sigma}{k_1\left(4.58 \cdot 10^6 \cos(0.98\mathrm{k}_1) - 5.33 \cdot 10^6 \cos(1.024k_1)\right)}$$

$$A_2 = \frac{-2.50 \cdot 10^{-7}\mathrm{i}\sigma\left(2309.\mathrm{e}^{1.06\mathrm{i}k_1} + 2141.\mathrm{e}^{0.36\mathrm{ik}1}\right)}{k_1\left(4.58 \cdot 10^6 \cos(0.976k_1) - 5.33 \cdot 10^6 \cos(1.02k_1)\right)}$$

$$B_2 = \frac{2.50 \cdot 10^{-7}\mathrm{i}\sigma\left(2309.\mathrm{e}^{1.06\mathrm{i}k_1} + 2141.\mathrm{e}^{0.36\mathrm{ik}1}\right)}{k_1\left(4.58 \cdot 10^6 \cos(0.976k_1) - 5.33 \cdot 10^6 \cos(1.02k_1)\right)}$$

$$A_3 = \frac{-0.000042\mathrm{i}\mathrm{e}^{0.27\mathrm{i}k_1}\sigma}{k_1\left(4.58 \cdot 10^6 \cos(0.98\mathrm{k}_1) - 5.33 \cdot 10^6 \cos(1.024k_1)\right)}$$

$$B_3 = \frac{0.000042\mathrm{i}\mathrm{e}^{0.27\mathrm{i}k_1}\sigma}{k_1\left(4.58 \cdot 10^6 \cos(0.98\mathrm{k}_1) - 5.33 \cdot 10^6 \cos(1.024k_1)\right)}$$

Bibliography

[1] BOGAERT, H. An experimental investigation of sloshing impact physics in membrane LNG tanks on floating structures. 2018. PhD Thesis. Delft University of Technology.

[2] GTT. MarkIII Containment Systems Building principle. GTT Training Session 2012.

[3] YUN, Young-Min et al. Structural Safety Assessment of Mark III Membrane Type Liquid Natural Gas Cargo Containment System under Ice Collision. Journal of Ocean Engineering and Technology, 2014, 28.2: 126-132.

[4] GUILCHER, P. M., et al. 2D simulations of breaking wave impacts on a flat rigid wall–part 1: influence of the wave shape. In: The Twenty-fourth International Ocean and Polar Engineering Conference. International Society of Offshore and Polar Engineers, 2014.

[5] VAN DER MEER, Deveraj, Gauthier, Anais, Jain, Utkarsh, Lohse, Detlef. A scaling-law approach to liquid impact. University of Twente. MULTIPHASE 2019, Ben Guerir, Morocco, October 14-16, 2019.

[6] LESSER, M. B. Analytic solution of liquid-drop impact problems. Proceedings of the Royal Society of London. A. Mathematical and Physical Sciences, 1981, 377.1770: 289-308.

[7] GTT. Liquid impact generator: creating wave shapes and pressure maps. SLING Meeting in CWI, Amsterdam, April 25, 2018.

[8] GRAFF, Karl F. Wave motion in elastic solids. Courier Corporation, 2012.

[9] COUTY, N. Dynamic response of the MarkIII CCS to fast loads. Technical Report, 03.09.2013.

[10] BORTFELD, R. Reflection and refraction of spherical compressional waves at arbitrary plane interfaces. Geophysical Prospecting, 2006, 10.4: 517-538.

[11] EWING, W. Maurice, et al. Elastic waves in layered media. 1957, New York-Toronto-London.